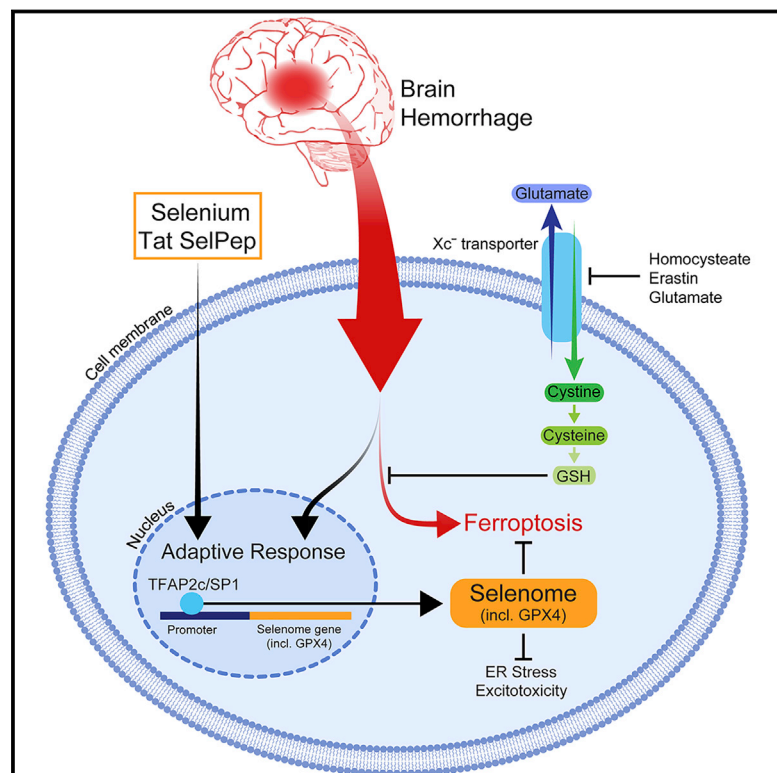


Selenium Drives a Transcriptional Adaptive Program to Block Ferroptosis and Treat Stroke

Graphical Abstract



Authors

Ishraq Alim, Joseph T. Caulfield, Yingxin Chen, ..., Botir T. Sagdullaev, Saravanan S. Karuppagounder, Rajiv R. Ratan

Correspondence

rrr2001@med.cornell.edu

In Brief

An adaptive response to ferroptotic stress is uncovered and leveraged to develop a neuroprotectant that reduces cell death and improves function after hemorrhagic stroke in mice.

Highlights

- Ferroptotic stimuli drive inadequate transcription of protective selenoproteins
- Selenium (Se) enhances adaptive transcription to protect cells from ferroptosis
- Se induces a protective selenome via DNA binding of TFAP2c and Sp1
- A selenocysteine-containing peptide, Tat SelPep, improves outcomes after stroke

Selenium Drives a Transcriptional Adaptive Program to Block Ferroptosis and Treat Stroke

Ishraq Alim,^{1,2} Joseph T. Caulfield,^{1,2} Yingxin Chen,^{1,2} Vivek Swarup,^{3,4,5} Daniel H. Geschwind,³ Elena Ivanova,^{1,2} Javier Seravalli,⁶ Youxi Ai,⁷ Lauren H. Sansing,⁷ Emma J. Ste.Marie,⁸ Robert J. Hondal,⁸ Sushmita Mukherjee,⁹ John W. Cave,^{1,2} Botir T. Sagdullaev,^{1,2} Saravanan S. Karuppagounder,^{1,2} and Rajiv R. Ratan^{1,2,10,*}

¹Sperling Center for Hemorrhagic Stroke Recovery, Burke Neurological Institute at Weill Cornell Medicine, White Plains, NY 10605, USA

²Feil Family Brain and Mind Research Institute, Weill Cornell Medicine, New York, NY 10065, USA

³Department of Neurology, David Geffen School of Medicine, University of California, Los Angeles, Los Angeles, CA 90095, USA

⁴Department of Neurobiology and Behavior, University of California, Irvine, Irvine, CA 92697, USA

⁵Institute for Memory Impairments and Neurological Disorders (UCI MIND), Irvine, CA 92697, USA

⁶Redox Biology Center and Department of Biochemistry, University of Nebraska, Lincoln, NE 68588, USA

⁷Department of Neurology, Yale University School of Medicine, New Haven, CT 06510, USA

⁸Department of Biochemistry, University of Vermont, Burlington, VT 05405, USA

⁹Department of Biochemistry, Weill Cornell Medicine, New York, NY 10065, USA

¹⁰Lead Contact

*Correspondence: rrr2001@med.cornell.edu

<https://doi.org/10.1016/j.cell.2019.03.032>

SUMMARY

Ferroptosis, a non-apoptotic form of programmed cell death, is triggered by oxidative stress in cancer, heat stress in plants, and hemorrhagic stroke. A homeostatic transcriptional response to ferroptotic stimuli is unknown. We show that neurons respond to ferroptotic stimuli by induction of selenoproteins, including antioxidant glutathione peroxidase 4 (GPX4). Pharmacological selenium (Se) augments GPX4 and other genes in this transcriptional program, the selenome, via coordinated activation of the transcription factors TFAP2c and Sp1 to protect neurons. Remarkably, a single dose of Se delivered into the brain drives antioxidant GPX4 expression, protects neurons, and improves behavior in a hemorrhagic stroke model. Altogether, we show that pharmacological Se supplementation effectively inhibits GPX4-dependent ferroptotic death as well as cell death induced by excitotoxicity or ER stress, which are GPX4 independent. Systemic administration of a brain-penetrant selenopeptide activates homeostatic transcription to inhibit cell death and improves function when delivered after hemorrhagic or ischemic stroke.

INTRODUCTION

Intracerebral hemorrhage (ICH; bleeding in the brain) is a stroke subtype associated with hypertension, cerebral amyloid angiopathy, arteriovenous malformations, and anticoagulant use. Despite the high morbidity and mortality of ICH (van Asch et al., 2010), there are no established treatments (Keep et al., 2012). Therapeutic strategies to limit secondary damage after ICH are of intense interest (Gurol and Greenberg, 2008). Secondary damage, including neuronal death, occurs hours to days following the

initial bleed (Brott et al., 1997) and is attributable to a host of factors from lysed blood, such as hemoglobin and the oxidized form of iron-rich heme (Huang et al., 2002).

Recent studies demonstrate that secondary cell death in ICH is not the result of random destruction of macromolecules by iron-catalyzed oxidants, but rather by ferroptosis, a non-apoptotic, programmed cell death pathway (Karuppagounder et al., 2016; Li et al., 2017; Zille et al., 2017). Ferroptosis is triggered by the enzymatic production of oxidant lipid species and can be blocked by selective lipid peroxidation inhibitors such as ferrostatin (Dixon et al., 2012; Khanna et al., 2003; Zille et al., 2017). In addition to ICH, ferroptosis operates in erastin and sulfasalazine-induced death of cancer cells (Dixon et al., 2012; Gout et al., 2001), heat stress in plants (Distéfano et al., 2017), ischemia-reperfusion injury (Friedmann Angeli et al., 2014), traumatic brain injury (Wenzel et al., 2017), and Parkinson's disease (Do Van et al., 2016).

In cortical neurons, ferroptosis induces transcriptional responses involving the activation of the leucine zipper transcription factor ATF4, and the upregulation of genes linked to cell death including, CHOP (a prodeath transcriptional activator), TRIB3 (a pseudokinase inhibitor of Akt), or CHAC1 (an enzyme that degrades glutathione; Karuppagounder et al., 2016; Lange et al., 2008). Germline deletion of ATF4 in neurons renders them resistant to homocysteic acid (HCA)-induced ferroptosis *in vitro*, and sensitivity to cell death can be reinstated by wild-type ATF4, but not ATF4 with the DNA binding domain mutated (Lange et al., 2008). Subsequent studies showed that iron chelators prevent ferroptosis in neurons induced by glutamate or hemin (used to model ICH *in vitro*) not by inhibiting Fenton chemistry but rather by targeting a family of iron-dependent enzymes, the hypoxia-inducible factor (HIF) prolyl hydroxylases, which are necessary for ATF4-dependent prodeath transcription (Karuppagounder et al., 2016). ATF4-dependent gene expression is observed in ferroptotic cancer cells induced by erastin, but the role of ATF4 in regulating ferroptotic death in cancer cells appears context dependent (Chen et al., 2017).

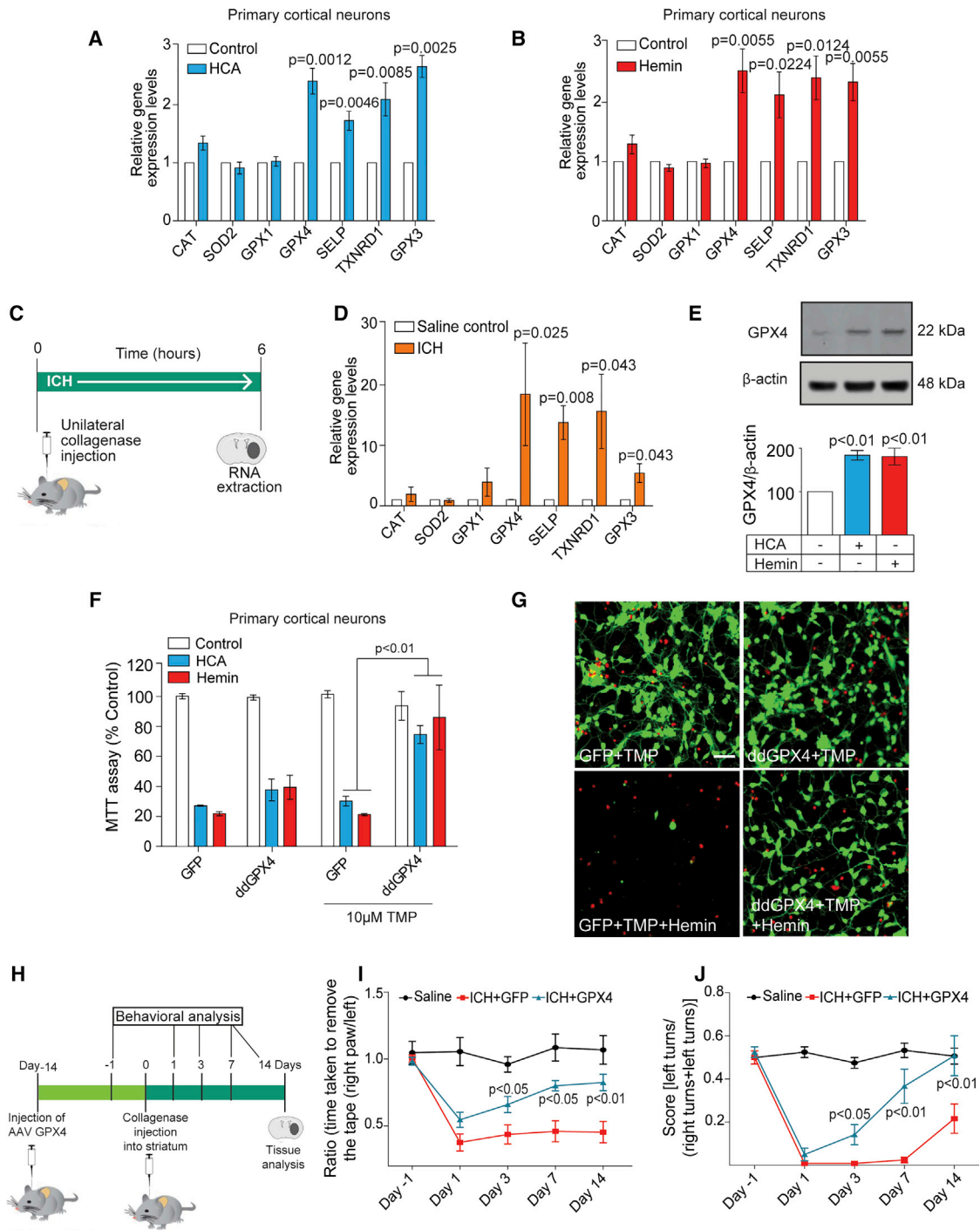


Figure 1. Ferroptotic Stimuli Increased Protective Selenoprotein mRNA Expression *In Vitro* and *In Vivo*

(A) qPCR showed that a cassette of selenoprotein mRNAs were induced 6 h after exposure to 5 mM HCA (a glutamate analog) but not a vehicle control. (n = 5, p < 0.01; t test; data shown in mean \pm SEM).

(B) qPCR showed that a cassette of selenoprotein mRNAs were induced after a 6 h exposure to 80 μ M hemin (n = 5, p < 0.05; t test; mean \pm SEM).

(C and D) Schematic of experimental paradigm for modeling ICH in mice (C). 6 h after collagenase injection, RNA was harvested from the ipsilateral striatum and qPCR revealed increases in selenoprotein mRNAs (D; n = 4; p < 0.05; t test; mean \pm SEM).

(E) Immunoblotting showed that ferroptotic stimuli induced GPX4 protein levels relative to β -actin (loading control), but they were unaffected by vehicle treatment (n = 4, p < 0.01; t test; mean \pm SEM).

(legend continued on next page)

The canonical tumor suppressor p53 has also been implicated as a transcriptional mediator of ferroptotic death (Jiang et al., 2015; Tarangelo et al., 2018; Wang et al., 2016; Xie et al., 2017). Specifically, p53 negatively regulates transcription of SLC7A11, the cystine-glutamate antiporter (X_c^-) (Jiang et al., 2015; Tarangelo et al., 2018). The ability of p53 to repress SLC7A11 and induce ferroptosis is consistent with prior observations that pharmacological inhibition of SLC7A11 also resulted in ferroptosis (e.g., via exposure to erastin, glutamate, HCA; Dixon et al., 2012). Indeed, *in vivo*, the tumor suppressive effects of an acetylation defective mutant of p53, which does not induce cell-cycle arrest, senescence, or apoptosis, can be overcome by forced expression of SLC7A11 (Jiang et al., 2015). Altogether, these findings suggest that p53 has multiple modes of tumor suppression including the activation of ferroptosis via suppression of SLC7A11 transcription. By contrast, p53-dependent transcription of p21^(waf1/cip1) (Tarangelo et al., 2018) or p53-dependent nuclear accumulation of DPP4 (Xie et al., 2017) appears to suppress ferroptosis via preservation of the redox balance, raising the possibility that p53 has multiple arms that lead to ferroptotic death or cell-cycle inhibition depending on levels of stress or damage. In addition to p53, the electrophile responsive transcription factor Nrf-2 can also suppress ferroptosis in tumor cells (Fan et al., 2017) or in neuronal cultures when activated selectively in glial cells (Haskew-Layton et al., 2010).

While SLC7A11 has been a logical focus of the transcriptional regulation of ferroptosis outlined above, recent studies have highlighted the central role that selenium plays in modulating ferroptotic death via its co-translational incorporation into selenocysteine in proteins such as glutathione peroxidase-4 (GPX4; Ingold et al., 2018). However, little is known about whether GPX4 and other selenoproteins are induced at a transcriptional level by ferroptotic stimuli and whether such a putative homeostatic adaptive response can be harnessed to limit ferroptosis in disease (Stoytcheva and Berry, 2009). Here, we show that selenoproteins, including GPX4, are induced at a transcriptional level as a frustrated adaptive response to ferroptotic stimuli *in vitro* and *in vivo* in the nervous system. Unexpectedly, supraphysiological levels of selenium drive this transcriptional response, the selenome, via TFAP2c and Sp1 to prevent ferroptosis and ferroptosis-independent modes of cell death. Delivery of selenium directly into the cerebral ventricle or systemically via brain penetrant, selenocysteine peptides activates the adaptive transcriptional response to ferroptosis and improves functional recovery following stroke.

RESULTS

Ferroptotic Stresses and ICH Drive a Frustrated Adaptive Response Involving Selenoproteins

In order to elucidate novel strategies to halt ICH-induced neuronal injury, we focused on ferroptosis in neurons. Ferroptosis is a distinct form of cell death that is caspase independent, mediated by lipid peroxidation, regulated by GPX4, and is non-cell autonomous and highly synchronized (Dixon et al., 2012; Friedmann Angeli et al., 2014; Kagan et al., 2017; Linkermann et al., 2014; Poursaitidis et al., 2017; Yang et al., 2014). ICH-induced cell death occurs by ferroptosis (Karuppagounder et al., 2016; Li et al., 2017; Zille et al., 2017). Indeed, increases in lipoxygenases or lipid peroxidation can be observed in mice or humans after ICH (Li et al., 2017; Karuppagounder et al., 2018), and canonical ferroptosis inhibitors protect against ICH *in vivo* or in response to hemin *in vitro* (Li et al., 2017; Zille et al., 2017). We also found that ICH *in vivo* induces terminal deoxynucleotidyl transferase dUTP nick end labeling (TUNEL) labeling indicative of endonucleolytic cleavage of DNA, another feature of ferroptosis (Friedmann Angeli et al., 2014; Figure S1A), and lysis of the plasma membrane occurs synchronously after exposure to hemin *in vitro* as has been demonstrated in some ferroptotic paradigms (Linkermann et al., 2014; Poursaitidis et al., 2017; Figure S1B).

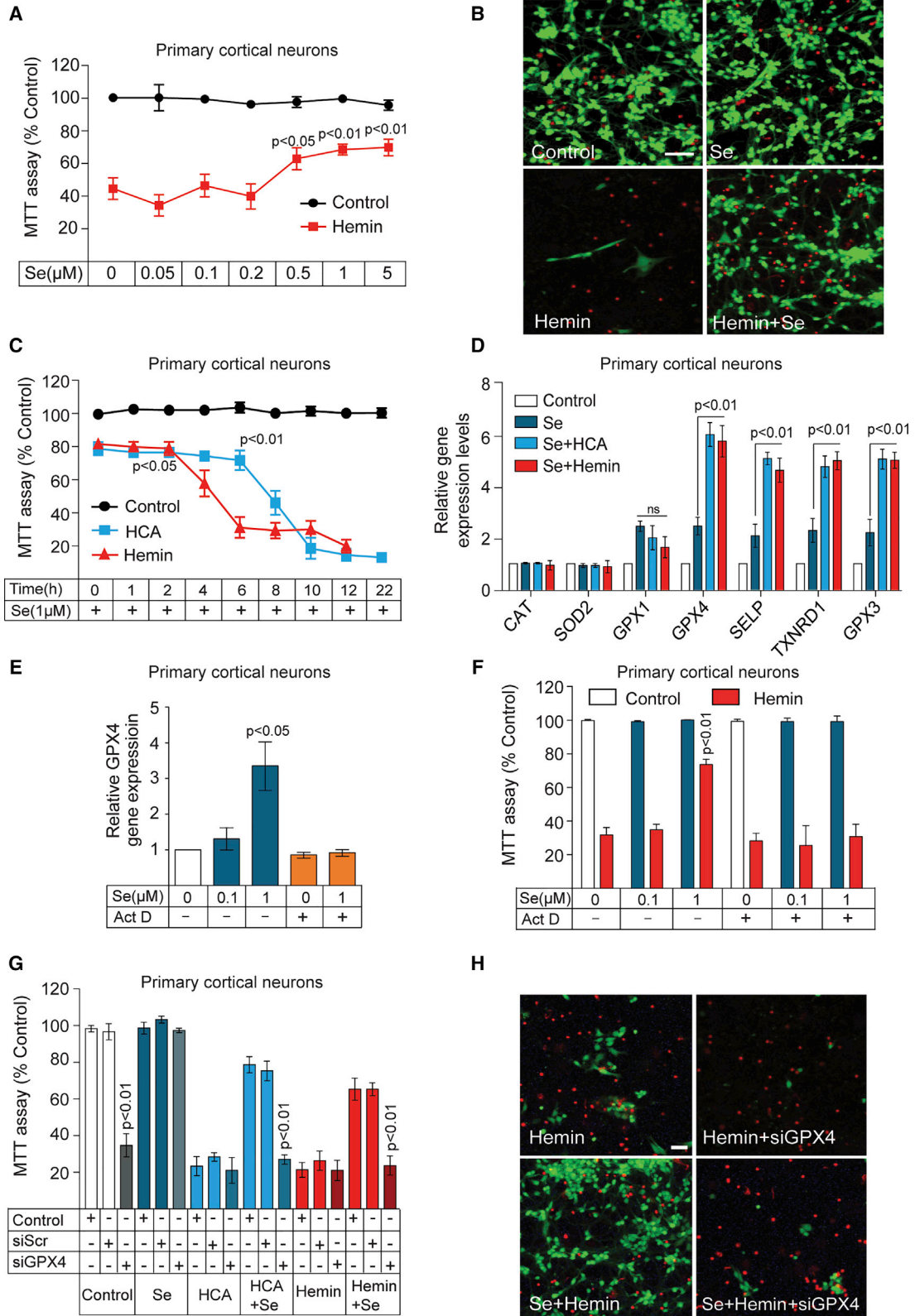
To define an adaptive transcriptional response to ferroptosis, we probed changes in mRNA levels of antioxidant enzymes known to neutralize reactive lipids including GPX4 in primary neurons using a glutamate-induced cell death paradigm now recognized as ferroptosis (Ratan et al., 1994a; Zille et al., 2019) or an *in vitro* model of ICH involving hemin, which also leads to ferroptosis (Karuppagounder et al., 2016; Zille et al., 2017). As expected, the expression of canonical anti-oxidant enzymes such as superoxide dismutase (SOD2) and catalase were not induced in either paradigm (Figures 1A and 1B). Rather, within 6 h of exposure to HCA (homocysteate, a glutamate analog) or hemin (the oxidized form of heme used to model ICH *in vitro*), we found increased expression of several selenium-containing antioxidant enzymes, including glutathione peroxidase 4 (GPX4), thioredoxin reductase 1 (TXNRD1), glutathione peroxidase 3 (GPX3), and selenoprotein P (SelP) (Figures 1A and 1B). The expression of these selenoenzymes was also induced *in vivo* in the striatum ipsilateral to the lesion in a murine model of human ICH (Figures 1C and 1D).

As ferroptotic cell death occurs extensively in the *in vitro* and *in vivo* paradigms examined, the induction of selenoprotein gene expression in our model systems is likely an inadequate attempt of the cell to protect itself. To investigate this possibility,

(F) Cell viability was not increased in HCA-exposed neurons infected with an adenovirus encoding a GFP (control \pm 10 μ M trimethoprim [TMP]) but was increased in neurons infected with an adenovirus encoding GPX4 with a destabilization domain (ddGPX4) treated with 10 μ M of TMP ($n = 5$; $p < 0.01$; t test; mean \pm SEM). (G) Live(green)/Dead (red) imaging of primary cortical neurons infected with adenovirus encoding GFP (control, 10 μ M TMP), or an adenovirus encoding GPX4 with an attached destabilization domain (ddGPX4, 10 μ M TMP) 24 h after exposure to 80 μ M hemin or vehicle control ($n = 5$ independent cultures). Scale bar, 50 μ m.

(H–J) Forced expression of GPX4 but not a GFP control into neurons *in vivo* 2 weeks prior to ICH induced behavioral recovery in mice (H). (I and J) Forced expression of GPX4 significantly enhanced performance on the tape removal task (a measure of sensory neglect, $n = 16$; $p < 0.05$; ANOVA; mean \pm SEM) or the corner test (a measure of spatial neglect, $n = 16$; $p < 0.05$; ANOVA; mean \pm SEM) up to 14 days post-ICH in mice.

See also Figure S1.



(legend on next page)

we manipulated GPX4 levels, since this enzyme can neutralize oxidized lipids and inhibit ferroptosis in non-neural cell types (Yang et al., 2014). Following HCA or hemin treatment of cortical neurons, induction of GPX4 message and protein is observed by 4–8 h (Figures 1A, 1B, 1E, and S1C). To verify that GPX4 is protective, we reversibly destabilized GPX4 protein levels (Iwamoto et al., 2010). In this experiment, neurons expressed a destabilized form of GPX4 (ddGPX4) at a low steady-state until trimethoprim (TMP, 10 μ M) was added to rapidly stabilize GPX4 protein levels (within 1 h; Figure S1D). TMP-mediated stabilization of GPX4 protected neurons when added up to 4 or 8 h after hemin or HCA addition, respectively (Figures 1F, 1G, and S1E). Steady-state levels of GPX4 from neurons with adenovirus-mediated transduction of either ddGPX4 or GFP were not increased. Moreover, neither the addition of TMP alone nor ddGPX4 expression without TMP had a protective effect (Figure 1F). These studies show that GPX4 induction is part of an adaptive response within neurons to ferroptotic stimuli, and that increasing GPX4 levels above those that are induced by ferroptotic stimuli well after insult onset is sufficient to protect neurons.

To address whether ICH leads to ferroptotic death of neurons *in vivo*, we drove neuron-specific expression of GPX4 in the intact mouse brain. GPX4 is a known regulator of ferroptosis in multiple cell types, and we tested whether forced expression in neurons could reduce cell death and behavioral impairment after ICH. Accordingly, we injected an AAV8 viral vector encoding GPX4 under control of the synapsin 1 promoter into the striatum. This protocol resulted in predominantly neuronal transduction in the mediolateral striatum with expected increases in GPX4 expression (Figure S1F; Kügler et al., 2003). Forced GPX4 expression 2 weeks prior to ICH lead to reductions in cell death (as measured by Fluoro-jade staining; Figure S1G) and nearly complete functional recovery after ICH by 14 days in tests of sensory or spatial neglect (Figures 1H–1J). Beneficial effects were observed without any effect on hematoma size arguing against the possibility that GPX4 inhibits collagenase-induced brain bleeding (Figure S1H). GPX4 is thus sufficient to prevent cell death following ICH and, with recent data implicating reactive lipids in ICH (Karuppagounder et al., 2018), provides additional evidence that ICH-induced neuronal loss is due to ferroptosis.

Se Drives a Protective Transcriptional Response Involving GPX4

Selenium is an essential micronutrient required for synthesis of the amino acid selenocysteine (Hatfield and Gladyshev, 2002), which is a critical feature of GPX4 and other selenoenzymes since it provides greater resistance to oxidative inactivation than enzymes that contain cysteine alone (Ingold et al., 2018; Snider et al., 2013). Sodium selenite (SeO_3^{2-} , hereafter referred to as Se) is used frequently to deliver selenium to cells in culture. Selenite is taken up into the cell and is used to load selenocysteine co-translationally (Hatfield and Gladyshev, 2002; Turanov et al., 2009, 2011). Accordingly, we tested whether Se treatment could provide neuroprotection. We found that Se addition dose-dependently inhibited ferroptosis induced by hemin or HCA (Figures 2A, 2B, S1I, and S1J) and could be added hours after HCA or hemin exposure and still protect neurons (Figures 2C).

The ability of selenium to load selenocysteine co-translationally predicted that selenium supplementation would protect via translational mechanisms (Hatfield and Gladyshev, 2002; Turanov et al., 2011). Unexpectedly, we found that Se treatment increased transcription of several selenoprotein genes, including GPX4 (Figures 2D and S1K; GPX4 protein Figure S1L). Moreover, the transcriptional inhibitor, actinomycin-D, abrogated Se-induced protection from hemin-induced ferroptosis (Figures 2E and 2F). Together, these unexpected findings indicate that Se can augment an adaptive transcriptional response to neuronal ferroptotic stresses and that transcription is critical for Se to prevent death.

To address whether transcriptional induction of GPX4 is necessary for the protective effects of Se, we reduced expression of GPX4 in cortical neurons using small interfering RNAs (siRNAs) targeting three distinct GPX4 exons in separate experiments (Figures S2A and S2B). Since reducing GPX4 expression levels alone leads to neuronal cell death within 12–16 h (Figures 2G and S2E), cultures were supplemented with 50 μ M of N-acetylcysteine (NAC), a glutathione enhancing agent, to maintain survival with reduced expression of GPX4 (Figures S2A and S2B). 50 μ M NAC protected GPX4-depleted neurons without affecting GPX4 expression (Figures S2A and S2C) and without affecting sensitivity to ferroptosis (Figures S2D). Exposure of cultured neurons to hemin or HCA resulted in cell death, whereas

Figure 2. Sodium Selenite Induced Essential Selenoprotein Transcription to Protect Neurons from Cell Death

- (A) Concentration response of Se-induced changes in viability 16 h after exposure of primary cortical neurons to 80 μ M hemin ($n = 8$; $p < 0.05$; t test; data shown in mean \pm SEM)
- (B) Live(green)/Dead(red) assay of primary cortical neurons exposed to hemin (80 μ M, 16 h) in the presence and absence of protective concentrations of Se (1 μ M, $n = 3$ independent cultures). Scale bar, 75 μ m.
- (C) 1 μ M Se preserved cortical neuron viability when added well after exposure to hemin (80 μ M) or the glutamate analog, HCA (5 mM). ($n = 5$; $p < 0.05$; t test; mean \pm SEM).
- (D) Protective concentrations of Se (1 μ M) augmented induction of GPX4 and other selenoprotein mRNAs in primary cortical neurons (as measured by qPCR). Addition of protective concentrations of Se (1 μ M) \pm 5 mM HCA or 80 μ M hemin have additive effects on GPX4 and other selenoproteins ($n = 5$; $p < 0.01$; ANOVA; mean \pm SEM).
- (E and F) A non-selective transcription inhibitor actinomycin-D (2 μ g/mL) abrogated Se-induced increases in GPX4 mRNA in primary cortical neurons; (E; $n = 4$; $p < 0.05$; t test; mean \pm SEM) and protection from hemin-induced toxicity (F; $n = 3$; $p < 0.01$; t test; mean \pm SEM).
- (G) Reduction of GPX4 levels via short interfering RNAs abrogated Se (1 μ M)-induced protection from HCA (5 mM) or hemin (80 μ M) in primary cortical neurons (1 μ M; $n = 4$; $p < 0.01$; ANOVA; mean \pm SEM) as measured by (3-(4,5-dimethylthiazol-2-yl)-2,5-diphenyltetrazolium bromide (MTT) reduction.
- (H) Live(green)/Dead (red) assay of primary cortical neurons showed that Se-induced protection from hemin (80 μ M) or HCA (5 mM) was abrogated by reduction in GPX4 levels. Scale bar, 50 μ m ($n = 3$ independent cultures).

See also Figures S1, S2, and S3.

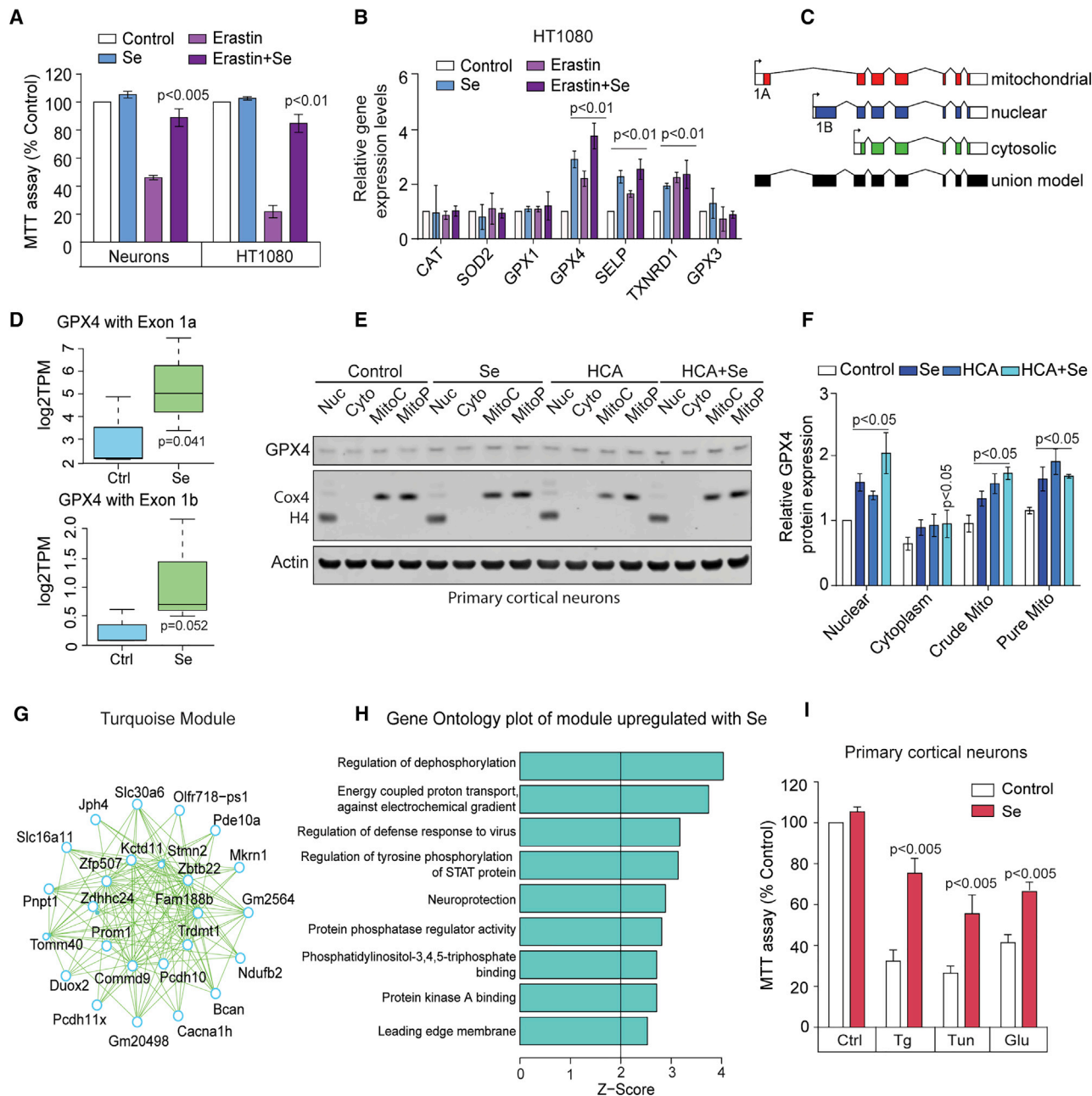


Figure 3. Se-Induced Selenoprotein mRNA Induction and Protection Extended to Ferroptosis in Cancer Cells and Involved a Broad Connectome Capable of Interdicting GPX4-Dependent and GPX4-Independent Cell Death Pathways

(A) Se (1 μ M) treatment prevented erastin-induced death in HT1080 fibrosarcoma cells and primary cortical neurons (5 μ M erastin; n = 4; p < 0.05; t test; data shown in mean \pm SEM).

(B) Protective concentrations of Se (1 μ M) induce GPX4 mRNA in HT1080 fibrosarcoma cells (n = 4; p < 0.01; t test; mean \pm SEM).

(C) A schematic diagram of transcriptional variants of GPX4 involving regulation from distinct promoters associated with distinct exons.

(D) Change in RNA levels of mitochondrial targeted GPX4 transcript variant (with exon 1a) and nuclear targeted GPX4 transcript variant (with exon 1b) after unbiased RNA sequencing analysis 6 h after Se (1 μ M) treatment in neurons (n = 4; false discover rate [FDR] < 0.05; box and whisker plot).

(E and F) GPX4 protein levels in fractionated nuclear, cytoplasmic, and mitochondrial (crude and pure) compartments from neurons after 8 h treatment with vehicle or Se (1 μ M) plus the glutamate analog HCA (5 mM). Nuclear fractions were verified by presence of Histone H4 (H4), and the crude and pure mitochondrial fractions were verified by the presence of cytochrome oxidase IV (Cox4). (F) Quantification of GPX4 protein levels in subcellular fractions normalized to actin loading control (n = 3; p < 0.01; ANOVA; mean \pm SEM).

(G and H) Supervised weighted gene correlation network analysis (WGCNA) revealed multiple modules of co-expressed genes including a “turquoise” model. Genes of note in this module are Fam188b, which has been shown to negatively regulate p53 and cell death in cancer cells and Trdmt1, an arginine

(legend continued on next page)

co-treatment with Se protected against ferroptosis except in cells where GPX4 levels were reduced (Figures 2G, 2H, and S2E). Similarly, death induced by ferroptosis inducer and GPX4 inhibitor, RSL3 could not be overcome by Se addition (Figures S3A, Fin56, and S3B). Collectively, these results demonstrate that GPX4 induction is necessary for Se-dependent protection against hemin and HCA-induced ferroptosis.

Se Prevents Erastin-Induced Ferroptosis in Cancer Cells and Excitotoxicity and Endoplasmic Reticulum Stress-Induced Death in Neurons

Ferroptosis was originally identified as a mechanism by which the chemotherapeutic agent, erastin, induced death in KRAS mutant cancer cells (Yagoda et al., 2007). These seminal studies showed that toxicity by erastin, like glutamate or HCA in cortical neurons, is mediated via inhibition of the X_c^- transporter (Zille et al., 2019). Pharmacological or molecular blockade of the X_c^- transporter leads to cellular cystine starvation, depletion of the antioxidant glutathione, and lipid peroxide-induced ferroptosis (Dixon et al., 2012; Ratan et al., 1994a; Yang et al., 2014). Consistent with our findings that Se can block ferroptosis in neurons, we found that Se (1 μ M) could abrogate erastin-mediated ferroptotic cell death in both in human HT-1080 fibrosarcoma cells and mouse primary cortical neurons (Figures 3A and S3C). Of note, Se also abrogated FIN56-induced ferroptotic death in cortical neurons, an agent that can inhibit squalene synthetase and deplete coenzyme Q (Figure S3B). Moreover, Se-induced expression of several selenoprotein mRNAs in erastin-treated cancer cells and neurons (Figures 3B and S3D). Together, these studies demonstrate that Se can augment a transcriptional stress response induced by ferroptotic stimuli in transformed and non-transformed cells to prevent cell death.

The ability of Se to protect multiple cell types from diverse inducers of ferroptotic stress led us to evaluate downstream pathways driven by Se exposure in primary neurons. RNA sequencing (RNA-seq) analysis of neurons exposed to the protective dose of Se showed robust upregulation and downregulation of many genes (238 differentially expressed genes). Our bioinformatics program uses an exon union model that scans reads across all exons, and together are designated as “full length.” Using the exon union model, full-length GPX4 was not differentially expressed between the control and selenium groups. However, consistent with our qPCR data, which used primers from exon 1a (Figures 3C and S3E), we found that expression of the GPX4 transcript that includes exon 1a was as significantly induced in the RNA-seq analysis by selenium (Figure 3D). The start codon for the mitochondrial form of GPX4, including the mitochondrial targeting sequence is present in exon 1a (Figure 3C). As expected from this analysis, we found an extranuclear increase in GPX4 protein in a pattern consistent with mitochondrial localization in neuroblasts exposed to selenium (Figure S3G). Subcellular frac-

tionation studies confirmed a significant increase in GPX4 protein in the mitochondrial fraction of Se-treated neurons (Figures 3E and 3F).

In addition to mitochondrial GPX4, analysis of exon 1b (nuclear form of GPX4) showed it was also significantly induced by Se alone or Se plus a ferroptotic stimulus (Figures 3D and S3F). As expected, immunofluorescence confirmed a significant increase in nuclear GPX4 staining (Figure S3G). These increases in nuclear GPX4 were validated using immunoblotting of the nuclear fraction of control and Se-treated neurons (Figures 3E and 3F). Altogether, these data support the notion that nuclear or mitochondrial GPX4 could mediate protection from ferroptosis induced by pharmacological selenium.

To organize the RNA-seq data into biologically coherent networks, we applied a supervised weighted gene-coexpression network analysis (WGCNA; Zhang and Horvath, 2005) to define networks of genes that are co-regulated with the significantly induced mitochondrial form of GPX4 (exon 1a). This analysis revealed several gene ontology networks that were significantly upregulated (Figures 3G and 3H, Table S1; e.g., neuroprotection or regulation of defense response to virus) and significantly downregulated (Figure S4A; Table S2; e.g., ATP metabolism or transcription factor coactivator activity). The findings are consistent with the hypothesis that GPX4 is co-regulated with programs involved in stress response and neuroprotection.

Unsupervised WGCNA identified modules that were upregulated (Figures S4B–S4D, royal blue and dark red, downregulated module, blue, and S4E) containing genes associated with protection from endoplasmic reticulum (ER) stress. These included EIF3c, a component required for cap-independent translation (IRES mediated) under conditions of ER stress (Spriggs et al., 2008), and Git1, an inhibitor of the IP3 receptor (Figure S4F; Kiviluoto et al., 2013; Ruiz et al., 2009; Zhang et al., 2009). Git1 would be expected to diminish ER stress by inhibiting calcium release from the ER. Moreover, Selenoprotein K (SelK), a selenoprotein involved in ER-associated degradation of misfolded glycosylated proteins (Lee et al., 2015), was also induced by Se (Figure S1K). Accordingly, we found Se significantly inhibited ER-stress-induced death induced by thapsigargin or tunicamycin (Figure 3I). Of note, forced expression of GPX4 had no effect on ER-stress-induced death, which indicates that genes other than GPX4 within the selenome mediate this protection (Figure S4G).

We also noted upregulation of genes that could provide resistance to excitotoxicity: NAPB, Nsmf, NMUR1, as well as Parp11, which is involved in NMDA receptor regulation and DNA repair (Figures S4C, S4D, and S4F; Iwai et al., 2008; Scarpa et al., 2013; Spilker et al., 2016; Wang et al., 2013). Accordingly, Se protected against excitotoxicity in mature neuronal cultures (Figure 3I), and like ER stress, is not sensitive to forced expression of GPX4 (Figure S4H). These findings indicate that Se-induced

methyltransferase that can post-translationally modify histones and tRNAs. (H) Gene ontology (GO) analysis of turquoise module, which was the most upregulated module by Se according to supervised (WGCNA) analysis reveals upregulation of a host of biologically clustered genes including energy metabolism and neuroprotection.

(I) Se (1 μ M) protects against endoplasmic reticulum (ER) stress-induced cell death (e.g., Thapsigargin or tunicamycin) or excitotoxicity in cortical neurons (n = 4; p < 0.05; t test; mean \pm SEM).

See also Figures S3 and S4.

neuroprotection is mediated by the activation of more than one gene within the selenome besides GPX4.

Se Drives the Transcriptional Activators TFAP2c and Sp1 to Upregulate GPX4

Our findings showed that Se can induce a transcriptional response that can prevent ferroptosis, ER-stress-induced death, or excitotoxicity *in vitro*. Since the data established a direct link between Se-induced GPX4 transcription and protection from neuronal ferroptosis (Figure 2), we next examined the GPX4 promoter and upstream region to better understand how GPX4 (and possibly other genes in the protective selenome) is induced by Se (Figure S5A). Transcriptional assays using a transiently transfected reporter construct containing the 4-kb region upstream of the GPX4 translation start site showed significant induction of GPX4 promoter activity in neurons exposed to protective Se concentrations. Targeted deletions of this upstream region revealed that the $-1,189$ and $-1,467$ bp sub-region was critical for Se-induced promoter activity (Figures 4A and S5B). Analysis of this critical sub-region identified five motifs with similarity to transcription factor AP-2 family binding sites (5'-GCCNNN(NN)GGC-3'; Figure 4B; Williamson et al., 1996). Mutation of three of these motifs blocked Se-induced GPX4 promoter activity (Figure 4C). The TFAP-2 family is highly conserved in mice and humans and is represented by five isoforms (TFAP2a-e; Eckert et al., 2005). Since TFAP2c was the only isoform whose expression we detected in mouse primary neurons (Figures S5C, S5D, and S5H), we focused on this isoform. Chromatin immunoprecipitation (ChIP) assays showed that Se exposure significantly increased TFAP2c occupancy on the Se-responsive region of the GPX4 (Figures 4D and S5I). TFAP2c binding to the upstream region was significantly stronger at 4 versus 6 h post-Se treatment (Figure 4D). As GPX4 expression levels are elevated longer than 4 h following Se exposure, additional transcription factors likely sustain the activation of GPX4 transcription. TFAP2c binding overlaps with Sp1 in other gene promoters (Orso et al., 2010;

Yang et al., 1995), and our lab previously showed that Sp1 DNA binding is significantly induced by ferroptotic oxidative stress (Ryu et al., 2003). Thus, we examined whether Se exposure induced Sp1 binding to the Se-responsive region of the GPX4 promoter. ChIP studies showed that Se exposure induced Sp1 occupancy of this region, but unlike TFAP2c, this occupancy was significantly greater at 6 versus 4 h post-Se treatment (Figures 4E, 4F, S5G, S5I, Sp1 protein expression, S5E, and S5F). To confirm that the Se-responsive region of GPX4 could mediate TFAP2c and Sp1-dependent regulation, human TFAP2c or Sp1 were overexpressed with either a wild-type GPX4 reporter or a mutant reporter lacking the TFAP2c binding sites. These studies showed that TFAP2c and Sp1 activated only the wild-type reporter, which suggests that TFAP2c and Sp1 act via the same DNA binding site(s) or closely adjacent sites (Figures 4G and 4H). In addition, overexpression of TFAP2c or Sp1 drove mRNA expression for several genes induced by ferroptotic stimuli alone and protected neurons from hemin or HCA-induced ferroptosis (Figures 4I, 4J, S5K, and S5L). By contrast, overexpression of an Sp1 protein with a zinc-finger DNA binding domain deletion (mSp1) did not induce expression of ferroptotic-stress response genes or provide protection from HCA (Figures 4I, 4J, S5J, and S5M). Overexpression of the Sp1 mutant protein also reduced protection mediated by Se in primary neurons or HT1080 fibrosarcoma cells (Figures 4J, 4K, and S5N). Together, these findings show that Se provides protection from ferroptosis, at least in part, by activating gene expression regulated by TFAP2c and Sp1.

Intracerebroventricular Injection of Se Drives Sp1 and GPX4 Expression in Neurons and Improves Functional Recovery

To address whether Se can block ferroptotic death via transcriptional regulation of the selenome following ICH *in vivo*, we examined the protective effects of Se in a mouse model of ICH. Injections in uninjured mice showed that an optimal Se concentration

Figure 4. Se-Induced Expression of GPX4 and Other Selenome RNAs Was Mediated by the Transcriptional Activators TFAP2c and Sp1

- (A) Identification of TFAP2c response element in the GPX4 non-coding region responsible for Se-induced upregulation. Regions of the 4,000 bp proximal promoter region of the GPX4 gene via distinct promoter-luciferase reporters are identified (left of schematic). Luciferase activity measurements of designated promoter-reporter constructs in hippocampal neuroblasts (HT22) were treated with Se ($1 \mu\text{M}$; $n = 4$; $p < 0.05$; t test; data shown as mean \pm SEM) (right of schematic).
- (B) The region $-1,467$ to $-1,189$ bp upstream of the translational start site of the GPX4 gene was essential for Se-induced promoter-reporter induction. This region contained 5 TFAP2c consensus binding sites, which could be driven in cortical neurons by TFAP2c or Sp1. Arrows indicate 5' to 3'.
- (C) Mutations in the TFAP2c sites in the promoter of GPX4 abrogated induction by Se ($1 \mu\text{M}$). Note significant reductions in luciferase activity of the GPX4 promoter with mutations of 1, 4, and 5 G/C to A/T mutant TFAP2c sites ($-1,467$ to $-1,189$ bp) as compared to the wild-type (control) promoter treated with Se ($1 \mu\text{M}$) \pm 5 mM HCA ($n = 4$; $p < 0.05$; t test; mean \pm SEM).
- (D and E) Chromatin immunoprecipitation using specific antibodies showed the kinetics of binding of TFAP2c (D) or Sp1 (E) to the GPX4 promoter ($-1,467$ to $-1,189$) 4 or 6 h after protective Se ($1 \mu\text{M}$) exposure in the presence a ferroptotic stimulus in neurons. ($n = 4$; $p < 0.01$; ANOVA; mean \pm SEM).
- (F) Schematic of kinetics of transcription factor binding to the GPX4 promoter after ferroptotic stimulus. Protective Se augments the amplitude of this response (shown in D and E).
- (G and H) Forced expression TFAP2c (G) or wild-type Sp1 (H) drove a wild-type GPX4 ($-1,467$ to $-1,189$ bp) promoter-luciferase reporter (GPX4-luc), but not a reporter with the AP2 response elements mutated (mGPX4; $n = 4$; $p < 0.01$; t test; mean \pm SEM). As expected, a DNA binding mutant of Sp1 (H) did not activate transcription of the GPX4 gene. These findings suggest that TFAP2c and Sp1 are binding to similar AP2 sites in the GPX4 promoter.
- (I) Forced TFAP2c or Sp1 drove expression of selenoprotein mRNAs but not SOD2 mRNA in primary cortical neurons. As expected, expression of a construct with the DNA binding domain of Sp1 mutated does not induce expression of any RNAs ($n = 5$; $p < 0.05$; ANOVA; mean \pm SEM).
- (J and K) Forced expression of Sp1 in primary cortical neurons (J) or HT1080 fibrosarcoma cells (K) protected against glutamate (J) or erastin. Forced expression of a DNA binding mutant of Sp1 abrogated the protection from HCA-induced ferroptosis in neurons (J) or erastin-induced ferroptosis in HT1080 fibrosarcoma cells (K) by Se ($1 \mu\text{M}$) ($n = 4$; $p < 0.05$; ANOVA; mean \pm SEM).

See also Figure S5.

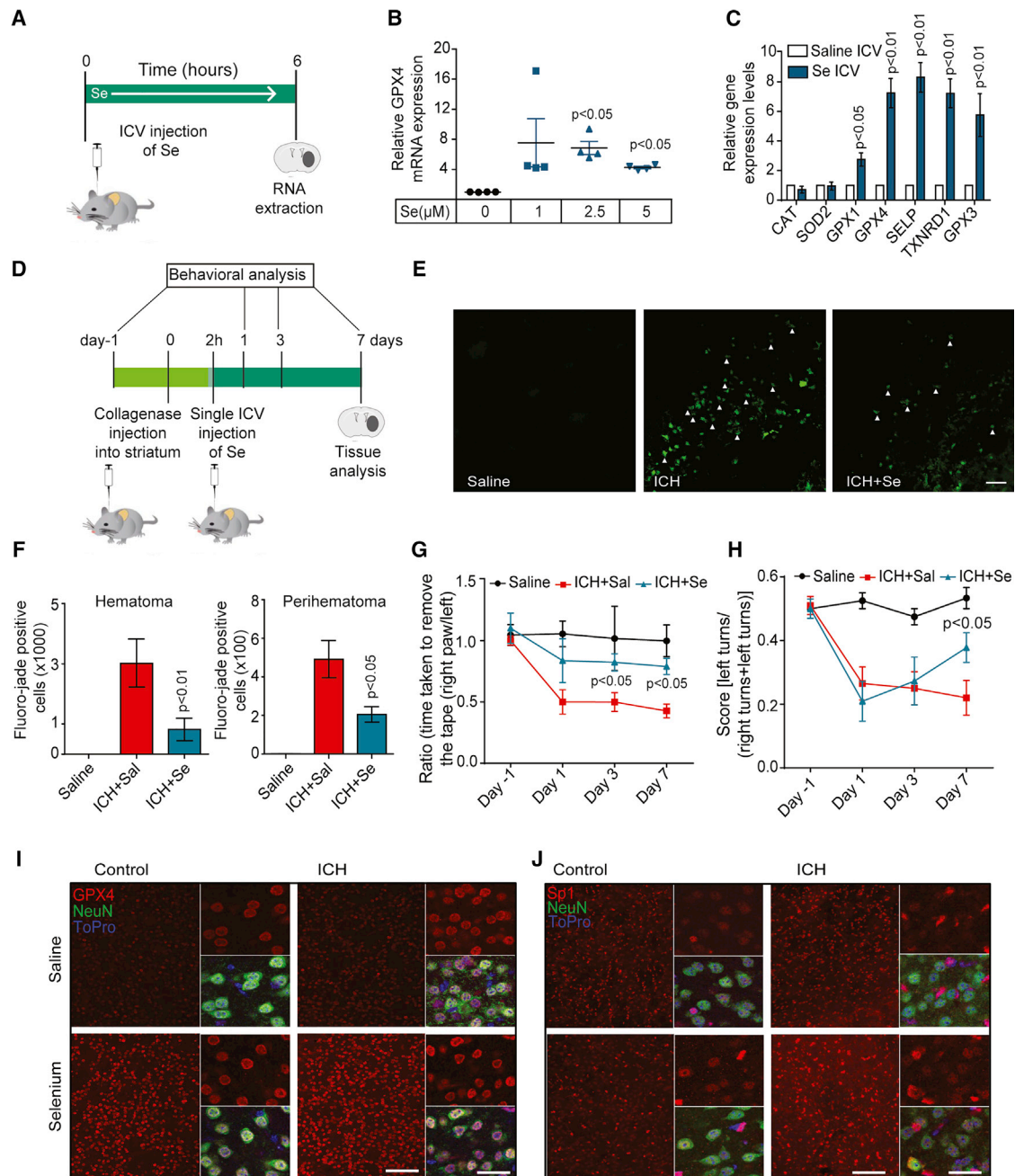


Figure 5. Intracerebroventricular Injection of Se (2.5 μ M)-Induced Transcription of GPX4 and Other Selenoprotein mRNAs Reduced Cell Death and Improved Recovery following Hemorrhagic Stroke in Mice

(A and B) GPX4 mRNA was increased ipsilateral to hemorrhagic stroke 6 h following ICV injection (A) of 2.5 and 5 μ M Se (B; $n = 4$; $p < 0.05$; t test; scatterplot indicates mean \pm SEM).

(C) ICV injection of 2.5 μ M Se induced a cassette of selenoprotein mRNAs but not catalase or SOD2 mRNAs in the ipsilateral striatum ($n = 4$; $p < 0.05$; t test; mean \pm SEM).

(D–H) A single ICV injection of 2.5 μ M Se given 2 h after ICH (schematic, D) reduced cell death at 7 days post-injury. (E) Arrows point to Fluoro-jade positive cells. (F) Quantitation of Fluoro-jade positive cells in the hematoma and perihematoma region ($n = 12$; $p < 0.05$ t test; mean \pm SEM). ICV injection of Se improved behavior as monitored by a tape removal task (G, $n = 16$; $p < 0.05$; ANOVA; mean \pm SEM; day 7 Se improves outcome by 72% \pm 5%) or a corner task (H; $n = 16$; $p < 0.05$; ANOVA; mean \pm SEM; day 7 Se improves outcome by 54% \pm 7%).

(I and J) Immunofluorescence of neurons (NeuN; green) or GPX4 (red) in contralateral and ipsilateral striatum sections obtained from vehicle-treated (control) mouse striatum or Se-treated mice ICH striatum 7 days after hemorrhagic stroke showed augmentation of ICH-induced increases in neuronal GPX4 after a single

(legend continued on next page)

for inducing selenoprotein expression was 2.5 μM (Figures 5A–5C). Of note, despite the parabolic response of selenoprotein mRNAs to injected Se, we noted no toxicity or death in mice at any concentration tested. Intracerebroventricular (ICV) injection 2 h after striatal ICH resulted in diminished cell death (Figures 5D–5F; measured by Fluoro-jade staining) and improved functional recovery at 7 days using a measure of spatial neglect (the corner task), and at 3 and 7 days with a measure of sensory neglect (the tape removal task; Figures 5G and 5H; Hua et al., 2002; Karuppagounder et al., 2016). The reduced cell death and functional improvement is not due to Se inhibiting collagenase activity, as ICH sizes were not affected by treatment (Figure S6A). Measurements of tissue selenium levels using mass spectrometry showed that the pharmacological dose of Se we used to generate transcriptional and neuroprotective effects is associated with significant increases in cellular selenium and did not represent a form of nutrient rescue in response to stress-induced selenium depletion (Figures S6B and S6C). Immunofluorescence verified that Sp1 and GPX4 protein levels are increased in neurons up to 7 days following Se injection (Figures 5I, 5J, and S6D–S6F, immunoblot validation of GPX4 protein levels 24 h after ICH; Figure S6G).

Selenium's ability to drive transcriptional expression of GPX4 (and possibly other genes comprising the selenome) to inhibit ferroptosis *in vivo* makes it an attractive potential therapeutic strategy for ICH. However, ICV injection of selenium presents several challenges as a therapeutic strategy. First, ICV injection requires insertion of a catheter or needle into the human brain (Ding et al., 2015; Fam et al., 2017), which not only creates risk of infection but also is invasive, and could delay treatment. Second, and more important, *in vitro*, Se addition to cultured neurons shows a parabolic dose response with a narrow therapeutic window raising concerns about toxicity if doses are not titrated within a narrow range (Figure 6A). To overcome these challenges, we developed a peptide strategy designed to allow induction of GPX4 and other genes of the selenome with systemic administration. The peptide contains a transduction domain from the HIV-Tat protein, which is capable of delivering covalently attached cargoes across the BBB into cells of the CNS (Aarts et al., 2002; Cook et al., 2012; Hill et al., 2012; Schwarze et al., 1999). To deliver selenium into cells, we created a Tat-linked SelP Peptide (Tat SelPep) that was composed of the Tat peptide attached to amino acids from the C terminus of SelP, which included selenocysteine. Full-length SelP is the only selenoprotein that contains a domain containing multiple selenocysteine residues and circulates in the body to distribute selenium (Burk and Hill, 2005).

Exposure of cortical neurons to Tat SelPep (containing UKUNLN from SelP), but not Tat Cys (containing 2 cysteine residues without any selenocysteines), or Tat alone lead to concentration-dependent protection from hemin-induced ferroptosis with an EC_{50} of 156 nM, or HCA-induced ferroptosis with an EC_{50} of 91 nM. Tat Cys did not result in significant protection until

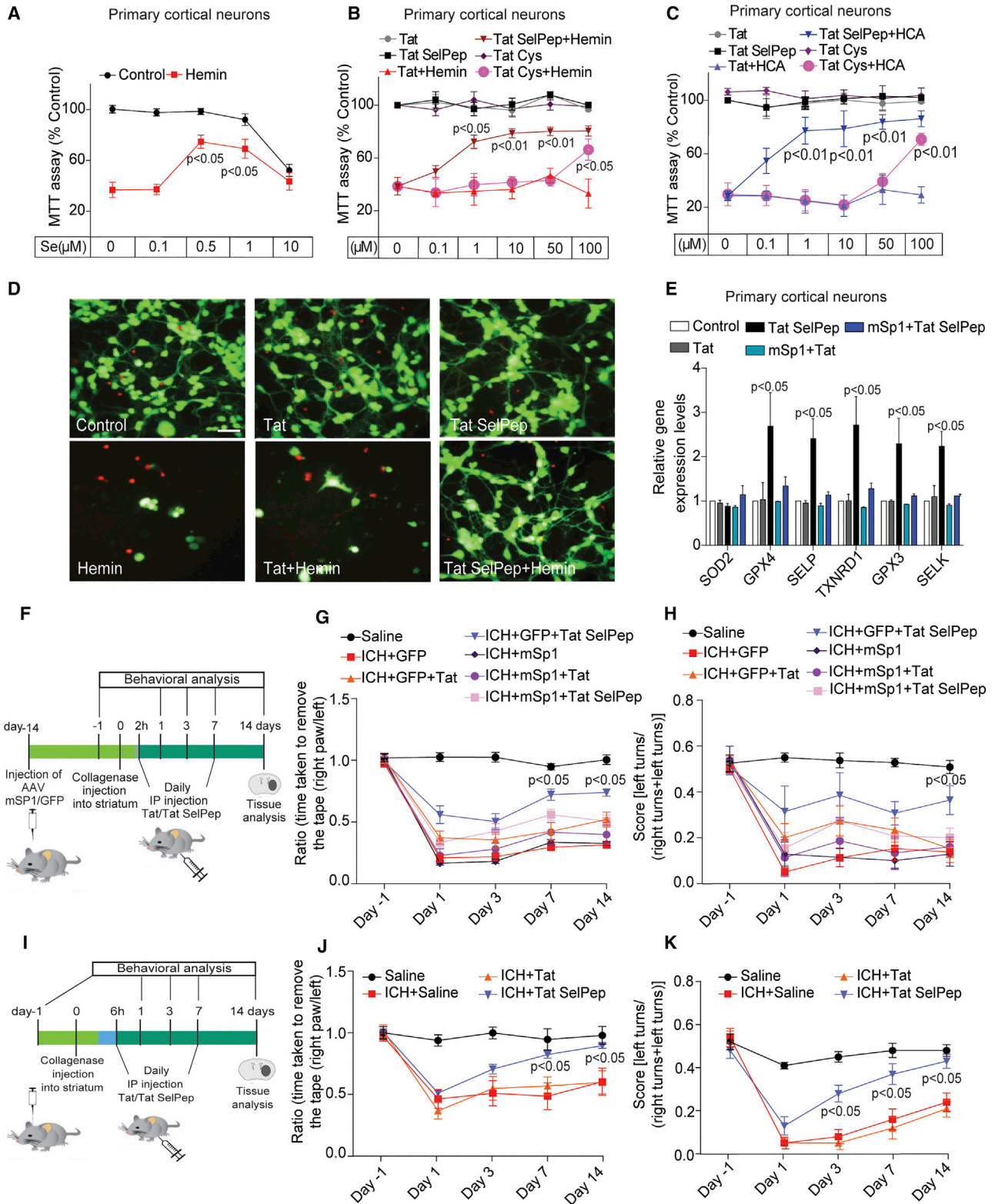
a concentration of 100 μM , which was more than 100-fold less potent than Tat SelPep (Figures 6B and 6C). Single-cell analysis of cell viability and death confirmed that Tat SelPep prevented hemin-induced ferroptosis and completely preserved cell bodies and neurites of neurons (Figures 6D and S7A). Additionally, these studies show that unlike Se exposure, Tat SelPep has a wide therapeutic window with no apparent toxicity over more than a three orders of magnitude increase in concentration (Figures 6B and 6C), suggesting that the Tat SelPep peptide is as effective as Se supplementation but is more potent and less toxic.

To verify that Tat SelPep drives GPX4 expression and other genes of the selenome *in vitro*, we monitored select candidate RNAs by qPCR. As expected, Tat SelPep (delivered at an optimally protective dose of 1 μM) induced significant increases in GPX4, SelP, TXNRD1, GPX3, and SelK (Figure 6E). Of note, transcriptional induction of these genes by Tat SelPep was abrogated by forced expression of mutant Sp1 (Figure 6E), consistent with our model that Tat SelPep and Se are affecting neurons by inducing a similar Sp1-dependent transcriptional pathway.

Altogether, these mechanistic and cell biological data *in vitro* predicted that systemic delivery of Tat SelPep given after ICH should drive GPX4 expression, abrogate ferroptotic death, and stimulate functional recovery in mice. As a first step, we used GPX4 expression in distinct organs as a biomarker to define a dose of Tat SelPep capable of significantly inducing GPX4 mRNA expression in multiple organs including the brain. Intraperitoneal administration of 12 $\mu\text{g/g}$ of Tat SelPep but not 12 $\mu\text{g/g}$ of Tat alone induced significant expression of GPX4 in heart, liver, striatum (brain), and cortex (brain; Figure S7B). Accordingly, we examined the effect of this dose of Tat SelPep on cell death and behavioral outcomes when delivered 2 h post-injury (Figure S7C). Delivery of Tat SelPep but not Tat alone reduced cell death (as measured by Fluoro-jade staining) and improved sensory and spatial neglect beginning at day 3 for sensory neglect, and reaching statistical significance for both tasks by day 14 following injury (Figures S7C–S7G). Our model predicts that Tat SelPep's effects should be interdicted by specific inhibitors of transcription of GPX4 and other genes in the selenome. As our data show that Sp1 mediates Se-induced expression of GPX4, we assessed the necessity for Sp1 in driving expression of GPX4 and other genes induced by Tat SelPep *in vivo* by employing an AAV8 vector encoding a dominant-negative, mutant Sp1 (lacking a functional DNA binding domain) under control of the synapsin 1 promoter (Figures 6F). As expected, inhibition of Sp1 activity, completely abrogated the beneficial effects of Tat SelPep in the collagenase-induced ICH model (Figures 6G, 6H, S7H, and S7I). These findings are consistent with a scheme where pharmacological selenium can drive the activation of a transcriptional pathway, which is sustained by Sp1, and leads to the upregulation of anti-ferroptotic GPX4, as well as other genes involved in stress adaptation.

To establish whether Tat SelPep can improve functional recovery with a larger therapeutic window, we used a treatment

ICV injection of Se (2.5 μM ; n = 3 individual animals). Scale bar, 100 μM ; insets, 25 μM (I). Immunofluorescence of neurons (NeuN; green) or Sp1 (red) staining following in sections obtained from vehicle (control) mouse striatum or Se striatum 7 days after ICH and/or Se (2.5 μM ; n = 3 individual animals) injection. Scale bar, 100 μM ; insets, 25 μM (J). See also Figure S6.



(legend on next page)

paradigm similar to that described above but extended the timing of treatment to 6 h (Figure 6I). Remarkably, we found that even administration of Tat SelPep 6 h after onset of ICH could enhance behavioral recovery (Figures 6J, 6K, S7J, and S7K).

Intraperitoneal Injection of Tat SelPep Reduces Infarct Volume following Focal Ischemia

Since we observed that pharmacological selenium was protective against GPX4-dependent and -independent insults *in vitro* including excitotoxicity, we next performed experiments to evaluate whether Tat SelPep could be protective *in vivo* in a rodent model of ischemic stroke where ferroptotic pathways have been implicated (Dixon et al., 2012; Yigitkanli et al., 2013). A filament suture was used to occlude the middle cerebral artery for 45 min, and after 2 h of reperfusion, a single dose of Tat SelPep (12 μ g/g), Tat (12 μ g/g), or vehicle alone was delivered via intraperitoneal injection (Figure 7A). Tat SelPep but not Tat alone significantly reduced infarct volume ($n = 16$; $p < 0.05$; ANOVA; mean \pm SEM; Tat SelPep reduced infarct volume by $49.2\% \pm 3.79\%$ compared to saline) with a clinically relevant therapeutic window (Figures 7B and 7C; Aarts et al., 2002; Cook et al., 2012; Hill et al., 2012). Prior studies have highlighted the role that 12/15 lipoxygenase and its lipid metabolites play in ischemic stroke raising the possibility that GPX4-dependent and -independent mechanisms are responsible for Tat SelPep-mediated neuroprotection from ischemia (Yigitkanli et al., 2013; Pekcec et al., 2013).

Our *in vivo* findings are consistent with a model in which Tat SelPep is driving a TFAP2c and Sp1-dependent homeostatic transcriptional response to counteract reactive lipids and cell death in rodent models of hemorrhagic or ischemic stroke to improve significant functional recovery with a clinically relevant window post-treatment.

DISCUSSION

While selenium was discovered over 200 years ago (Berzelius, 1818), only recent data have established its indispensability for the function of prosurvival proteins, specifically GPX4, associ-

ated with ferroptosis (Ingold et al., 2018). Our findings extend this essential *physiological* perspective on selenium biology to suggest that *pharmacological* selenium supplementation, even in the absence of nutritional deficiency (Figures 2D, 5C, and 6E), has an unexpected ability to drive adaptive transcription to counter ferroptosis (and other stresses) and protect neurons. Knowledge of how to drive GPX4 expression pharmacologically in the brain and other organs has clear therapeutic implications for hemorrhagic stroke, and possibly other CNS and non-CNS conditions associated with ferroptotic death (e.g., Parkinson's disease and liver ischemia; Bellinger et al., 2011; Friedmann-Angeli et al., 2014; Hauser et al., 2013). It may also have implications for diseases associated with ER stress (e.g., ALS; Saxena et al., 2009) and excitotoxicity (e.g., ischemia; Goldberg and Choi, 1993; Sattler et al., 1999; Dixon et al., 2012; Yigitkanli et al., 2013).

The ability of GPX4 and other selenoproteins to be selectively induced by ferroptotic stimuli suggests that the stress-induced increase in the transcription of a number of putative, "antioxidant" selenoproteins is an adaptive homeostatic, but insufficient response to prevent cell death in the face of ferroptotic insults. As Se supplementation has been previously shown to load selenocysteine proteins co-translationally (Ingold et al., 2018; Rafferty et al., 1998; Rusolo et al., 2013), we examined the effect of Se supplementation on this response. As expected, Se supplementation led to protection in the face of ferroptotic insults. What was unexpected was that Se supplementation could drive transcription of a host of selenoproteins. Detailed promoter analysis of the anti-ferroptotic gene, GPX4, identified TFAP2c and Sp1 as driving transcription in response to ferroptotic stimuli or Se supplementation. A model emerges that TFAP2c and Sp1 sense pharmacological changes in cellular "selenium" or selenocysteine and act sequentially to activate GPX4 transcription and a cassette of other genes that form a selenome. It is formally possible that increases in selenoprotein levels represent a way for cells to compensate for increased free and potentially toxic selenium, or selenocysteine, by increasing its incorporation into selenoproteins, where its redox reactivity can be homeostatically controlled. It also suggests that the set point for GPX4 levels in any cell could be set via transcriptional regulation

Figure 6. Tat SelPep (SelP Domain Peptide Linked to a Tat Transduction Domain) Possessed a Wider Therapeutic Window *In Vitro* Than Se, and Systemic SelPep Treatment Improved Functional Outcomes following ICH via an Sp1-Dependent Pathway with a Therapeutic Window of at Least 6 h

(A) Concentration response of Se-induced protection from hemin (80 μ M)-induced death. At 10 μ M Se, toxicity was observed in the presence and absence of hemin ($n = 5$; $p < 0.05$; t test; data shown in mean \pm SEM).
(B and C) Concentration response of Tat SelPep-induced protection from hemin- (80 μ M, B) or HCA- (5 mM, C) induced death. Parallel experiments with Tat Cys (where selenocysteines are mutated to cysteine) showed that Tat Cys is far less potent than Tat SelPep ($n = 5$; $p < 0.05$; ANOVA; mean \pm SEM).
(D) Live(green)/Dead (red) assay of neurons 16 h after vehicle (control) or hemin (80 μ M) treatment with Tat SelPep (1 μ M; $n = 3$ independent cultures) or a Tat control only (1 μ M, $n = 3$). Scale bar, 50 μ m.
(E) Protective concentrations of Tat SelPep (1 μ M), like Se, induced selenoprotein mRNAs in primary cortical neurons in an Sp1-dependent manner. ($n = 5$; $p < 0.05$; ANOVA; mean \pm SEM).
(F–H) Tat SelPep enhances recovery when delivered 2 h after hemorrhagic stroke onset in a Sp1-dependent manner. (F) Experimental paradigm involving infection with AAV8 constructs encoding mutant Sp1 or GFP two weeks prior to induction of ICH into the mouse striatum. 2 h following ICH, Tat SelPep (12 μ g/g), Tat (12 μ g/g), or vehicle alone were delivered intraperitoneally and tape removal (G) or the corner test (H) were performed ($n = 16$; $p < 0.05$; ANOVA; mean \pm SEM).
(I–K) Experimental paradigm for evaluating Tat SelPep delivered after stroke onset in treating ICH (I). ICH was followed by an intraperitoneal injection of Tat (12 μ g/g) or Tat SelPep (12 μ g/g) 6 h later and then every day for 7 days post-injury. Tat SelPep but not Tat alone reduces sensory neglect (J, tape removal task, $n = 16$; $p < 0.05$; ANOVA; mean \pm SEM; day 14 Tat SelPep improves outcome by $96\% \pm 5\%$) and spatial neglect (K, corner task, $n = 16$; $p < 0.05$; ANOVA; mean \pm SEM; day 14 Tat SelPep improves outcome by $95\% \pm 7\%$) 14 days after ICH.
See also Figure S7.

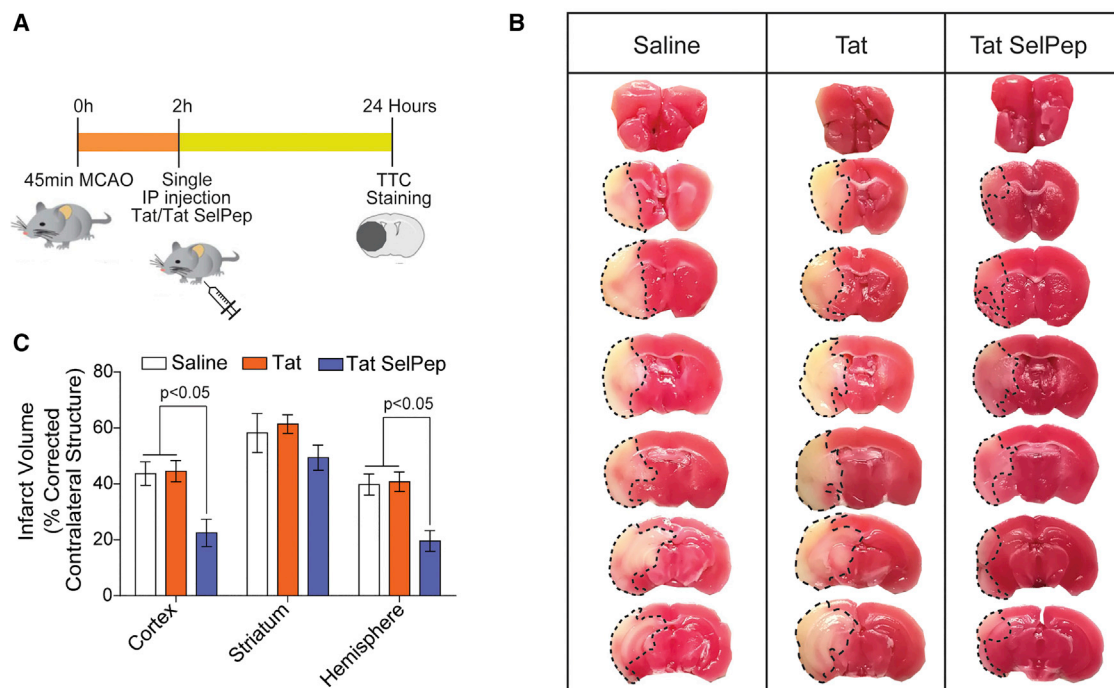


Figure 7. Tat SelPep Reduces Infarct Volume following Acute Ischemic Stroke with a Therapeutic Window of at Least 2 h

(A–C) Tat SelPep (12 μ g/g) but not Tat (12 μ g/g) control, reduced infarct volume in a model of ischemic stroke. (A) Middle cerebral artery occlusion (MCAO) in one hemisphere for 45 min. Saline, Tat, or Tat SelPep were given via intraperitoneal injection 2 h after MCAO occlusion. (B) Representative images of TTC staining in brain sections at 24 h post-injury. Infarction area is indicated in white color with black outline. (C) Infarct volume measured in cortex, striatum, and whole hemisphere (cortex+striatum), corrected by contralateral structure. Tat SelPep showed significant reduction in infarct volume in cortex and whole hemisphere compared to saline and Tat controls ($n = 12$; $p < 0.05$; ANOVA; mean \pm SEM; Tat SelPep reduced infarct volume by $49.2\% \pm 3.79\%$ compared to saline).

by selenium availability, implying that the sensitivity to ferroptotic stimuli in any tissue, including cancer cells (Dixon et al., 2012; Viswanathan et al., 2017), could be determined by the amount of free selenium (or selenocysteine) that is delivered into the cell.

The ability of Se or TFAP2c/Sp1 to drive a cassette of genes raises the possibility that these genes are activated as part of a coordinated stress response to compensate for ferroptotic or other stresses (e.g., ER stress and excitotoxicity). Se-induced significant changes in the expression of 238 genes including the mitochondrial and nuclear forms of GPX4 (Figures 3 and S4). Expression of mitochondrial and nuclear GPX4 isoforms are driven by distinct promoters and could have distinct roles in regulating signaling in distinct death paradigms as previously suggested (Hauser et al., 2013; Savaskan et al., 2007a, 2007b). A recent study from our lab demonstrated that nuclear ALOX5 mediates cell death following ICH (Karuppagounder et al., 2018) raising the possibility that nuclear GPX4 is the necessary isoform induced by Se to counteract lipid peroxidation and prevent cell death seen in ICH. Of course, other lipoxygenase (ALOX12 and 15) with distinct subcellular localizations have been implicated in ischemic stroke (Dixon et al., 2012; Yigitkanli et al., 2013) suggesting that depending on the clinical condition that GPX4 may mediate protection from distinct subcellular sites.

Nutritional selenium is preferentially targeted to the brain and testes (in men) under conditions where selenium is rate limiting

in the body (Brown and Burk, 1973; Schomburg and Schweizer, 2009). Indeed, removal of the testes in male mice that are genetically deficient in selenoprotein enzymes abrogates neurodevelopmental and neurodegenerative effects of selenium deficiency (Pitts et al., 2015). To overcome the nutritional targeting of selenium in the whole body to achieve pharmacological levels of Se in the brain, we injected Se directly into the ventricular system and found elevated GPX4 message specifically in this organ and reduced ferroptotic death and improved functional recovery following ICH in mice (Figure 5). However, we found that Se supplementation *in vitro* and *in vivo* has a parabolic dose response curve, raising concerns not only about the mode of delivery, but the ultimate safety of this approach. To overcome this challenge, we developed a peptide (Tat SelPep), which possesses a Tat transduction domain linked to six amino acids in the C-terminal domain of SelP. This peptide not only possesses a wide therapeutic window *in vitro* and *in vivo*, but also can induce GPX4 expression in a number of organs that were tested including the brain, heart, and liver (Figures 6 and S7B). *In vivo* studies showed that the salutary effects of Tat SelPep are inhibited by forced expression of a dominant-negative Sp1, consistent with the notion that Tat SelPep, like Se, drives transcription of GPX4 via a Sp1-mediated pathway (Figure 6). The ability to drive expression of the GPX4 and other genes of the selenome in any organ of the body offers a host of potential therapeutic opportunities for conditions where GPX4 deficiency is associated with

cell death or dysfunction (Stockwell et al., 2017). Moreover, it offers a way to supplement Se in the whole body with less concern for toxicity (Burk and Hill, 2015; Jones et al., 2017). Our studies also suggest that agents that disarm transcription of GPX4 and other genes of the selenome might be a mechanism to potentiate tumor kill in response to ferroptosis inducers such as erastin (Dixon et al., 2012; Yang et al., 2014; Yu et al., 2015). Overall, these studies describe a novel transcriptional mode of regulation for Se in controlling cell death *in vitro* and *in vivo* with potentially broad nutritional (Jones et al., 2017) and therapeutic implications.

STAR★METHODS

Detailed methods are provided in the online version of this paper and include the following:

- KEY RESOURCES TABLE
- CONTACT FOR REAGENT AND RESOURCE SHARING
- EXPERIMENTAL MODEL AND SUBJECT DETAILS
 - Animal Models
 - Immature primary cortical neuronal cultures
 - Mature primary cortical neuronal cultures
 - Cultured cell lines
- METHOD DETAILS
 - Collagenase-induced mouse model of ICH
 - Stereotaxic administration of adeno-associated viral vectors into the striatum
 - Behavioral analysis
 - Experimental ischemic model (filament MCAO method)
 - Immunocytochemistry
 - Fluoro-jade Staining
 - Hematoma Volume Measurement
 - Quantitative real-time PCR
 - *In vitro* ICH model
 - *In vitro* model of ferroptosis in neurons
 - *In vitro* model of excitotoxicity
 - *In vitro* model of ER stress-induced death
 - *In vitro* cell death time-lapse measurements
 - Chromatin immunoprecipitation
 - Plasmid amplification
 - Response Element Screening
 - Cell based luciferase Assays
 - Use of adenovirus infection for modulating gene expression
 - siRNA to reduce levels of target genes
 - Protein extraction and immunoblotting
 - RNA Sequencing and Weighted Gene Co-Expression Network Analysis
 - Inductively coupled plasma mass spectrometry
 - HIV-Tat Peptide Synthesis for Drug Delivery
- QUANTIFICATION AND STATISTICAL ANALYSIS
- DATA AND SOFTWARE AVAILABILITY

SUPPLEMENTAL INFORMATION

Supplemental Information can be found online at <https://doi.org/10.1016/j.cell.2019.03.032>.

ACKNOWLEDGMENTS

We would like to thank V. Gladyshev (Harvard), H. Kornblum (UCLA), L. Greene (Columbia), and J. Baraban (Johns Hopkins) for constructive comments to the project and manuscript. We thank L. Gross and A. Kumar for assistance with editing. We thank L.M. Gerber and Z. Chen (Weill-Cornell) for assistance with statistical analysis. We thank R. Weigel and M. Kulak (U. Iowa) for the generous gift of their TFAP2c virus. We thank D. Spitz (U. Iowa) for generously sharing his GPX4-L virus. We thank the Microscopy and Image Analysis Core of Weill Cornell Medicine for use of their equipment. We thank S. Agger for graphical abstract design. This work was funded with support from the Dr. Miriam and Sheldon G. Adelson Medical Research Foundation, the Burke Foundation, the Sperling Center for Hemorrhagic Stroke Recovery at the Burke Medical Research Institute, the Laster Program in Peptide Therapeutics, and the NIH (grant P01 NIA AG014930, project 1, to R.R.R.). B.T.S. thanks the NIH (R01-EY026576). D.H.G. thanks the NIH (5R01 MH110927, 5R01 MH109912, 5U01 MH105991, and 5R01 MH100027), and V.S. thanks the Larry L. Hillblom Foundation (Postdoctoral Fellowship).

AUTHOR CONTRIBUTIONS

I.A. and R.R.R. conceived and designed the research. I.A. performed most of the experiments with the help of S.S.K., J.T.C., and Y.C. E.I., I.A., and B.T.S. conducted immunofluorescence experiments. Y.C. and S.S.K. conducted *in vivo* surgeries. V.S. and D.H.G. conducted and analyzed RNA-seq data. J.S. measured element content using ICP-MS experiments and analysis. R.J.H. and E.J.S.M. provided input and technical assistance in the synthesis of the peptides. S.M. and I.A. performed the time-lapse imaging. J.W.C. helped in preparation of the manuscript. R.R.R. wrote the manuscript with help from I.A. All authors discussed the results and commented on the manuscript.

DECLARATION OF INTERESTS

D.H.G. is a paid consultant to Ovid Therapeutics. R.R.R., I.A., and S.S.K. have a pending US non-provisional patent for selenium-based therapies, filed: May 2, 2018, serial number: US20180327456A1. The authors declare no other competing financial interests related to this work.

Received: April 20, 2018

Revised: January 29, 2019

Accepted: March 13, 2019

Published: May 2, 2019

REFERENCES

- Aarts, M., Liu, Y., Liu, L., Besshoh, S., Arundine, M., Gurd, J.W., Wang, Y.T., Salter, M.W., and Tymianski, M. (2002). Treatment of ischemic brain damage by perturbing NMDA receptor- PSD-95 protein interactions. *Science* 298, 846–850.
- Bellinger, F.P., Bellinger, M.T., Seale, L.A., Takemoto, A.S., Raman, A.V., Miki, T., Manning-Boğ, A.B., Berry, M.J., White, L.R., and Ross, G.W. (2011). Glutathione Peroxidase 4 is associated with Neuromelanin in Substantia Nigra and Dystrophic Axons in Putamen of Parkinson's brain. *Mol. Neurodegener.* 6, 8.
- Berzelius, J.J. (1818). Undersökning af en ny Mineral-kropp, funnen i de ore-nare sorterna af det i Falun tillverkade svaflet. *Afhandlingar i fysik, kemi och mineralogi* 6, 42.
- Bodhankar, S., Chen, Y., Lapato, A., Dotson, A.L., Wang, J., Vandenbark, A.A., Saugstad, J.A., and Offner, H. (2015). PD-L1 Monoclonal Antibody Treats Ischemic Stroke by Controlling Central Nervous System Inflammation. *Stroke* 46, 2926–2934.
- Brott, T., Broderick, J., Kothari, R., Barsan, W., Tomsick, T., Sauerbeck, L., Spilker, J., Dulzner, J., and Khoury, J. (1997). Early hemorrhage growth in patients with intracerebral hemorrhage. *Stroke* 28, 1–5.
- Brown, D.G., and Burk, R.F. (1973). Selenium retention in tissues and sperm of rats fed a Torula yeast diet. *J. Nutr.* 103, 102–108.

- Burk, R.F., and Hill, K.E. (2005). Selenoprotein P: an extracellular protein with unique physical characteristics and a role in selenium homeostasis. *Annu. Rev. Nutr.* *25*, 215–235.
- Burk, R.F., and Hill, K.E. (2015). Regulation of Selenium Metabolism and Transport. *Annu. Rev. Nutr.* *35*, 109–134.
- Chen, D., Fan, Z., Rauh, M., Buchfelder, M., Eyupoglu, I.Y., and Savaskan, N. (2017). ATF4 promotes angiogenesis and neuronal cell death and confers ferroptosis in a xCT-dependent manner. *Oncogene* *36*, 5593–5608.
- Cook, D.J., Teves, L., and Tymianski, M. (2012). Treatment of stroke with a PSD-95 inhibitor in the gyrencephalic primate brain. *Nature* *483*, 213–217.
- Ding, D., Przybylowski, C.J., Starke, R.M., Sterling Street, R., Tyree, A.E., Webster Crowley, R., and Liu, K.C. (2015). A minimally invasive anterior skull base approach for evacuation of a basal ganglia hemorrhage. *J. Clin. Neurosci.* *22*, 1816–1819.
- Distéfano, A.M., Martin, M.V., Córdoba, J.P., Bellido, A.M., D'Ippólito, S., Colman, S.L., Soto, D., Roldán, J.A., Bartoli, C.G., Zabaleta, E.J., et al. (2017). Heat stress induces ferroptosis-like cell death in plants. *J. Cell Biol.* *216*, 463–476.
- Dixon, S.J., Lemberg, K.M., Lamprecht, M.R., Skouta, R., Zaitsev, E.M., Gleason, C.E., Patel, D.N., Bauer, A.J., Cantley, A.M., Yang, W.S., et al. (2012). Ferroptosis: an iron-dependent form of nonapoptotic cell death. *Cell* *149*, 1060–1072.
- Do Van, B., Gouel, F., Jonneaux, A., Timmerman, K., Gelé, P., Pétrault, M., Bastide, M., Laloux, C., Moreau, C., Bordet, R., et al. (2016). Ferroptosis, a newly characterized form of cell death in Parkinson's disease that is regulated by PKC. *Neurobiol. Dis.* *94*, 169–178.
- Dobin, A., Davis, C.A., Schlesinger, F., Drenkow, J., Zaleski, C., Jha, S., Batut, P., Chaisson, M., and Gingeras, T.R. (2013). STAR: ultrafast universal RNA-seq aligner. *Bioinformatics* *29*, 15–21.
- Eckert, D., Buhl, S., Weber, S., Jäger, R., and Schorle, H. (2005). The AP-2 family of transcription factors. *Genome Biol.* *6*, 246.
- Fam, M.D., Hanley, D., Stadnik, A., Zeineddine, H.A., Girard, R., Jesselson, M., Cao, Y., Money, L., McBee, N., Bistran-Hall, A.J., et al. (2017). Surgical Performance in Minimally Invasive Surgery Plus Recombinant Tissue Plasminogen Activator for Intracerebral Hemorrhage Evacuation Phase III Clinical Trial. *Neurosurgery* *81*, 860–866.
- Fan, Z., Wirth, A.K., Chen, D., Wruck, C.J., Rauh, M., Buchfelder, M., and Savaskan, N. (2017). Nrf2-Keap1 pathway promotes cell proliferation and diminishes ferroptosis. *Oncogenesis* *6*, e371.
- Friedmann Angeli, J.P., Schneider, M., Proneth, B., Tyurina, Y.Y., Tyurin, V.A., Hammond, V.J., Herbach, N., Aichler, M., Walch, A., Eggenhofer, E., et al. (2014). Inactivation of the ferroptosis regulator Gpx4 triggers acute renal failure in mice. *Nat. Cell Biol.* *16*, 1180–1191.
- Goldberg, M.P., and Choi, D.W. (1993). Combined oxygen and glucose deprivation in cortical cell culture: calcium-dependent and calcium-independent mechanisms of neuronal injury. *J. Neurosci.* *13*, 3510–3524.
- Gout, P.W., Buckley, A.R., Simms, C.R., and Bruchofsky, N. (2001). Sulfasalazine, a potent suppressor of lymphoma growth by inhibition of the x(c)-cystine transporter: a new action for an old drug. *Leukemia* *15*, 1633–1640.
- Grossetete, M., and Rosenberg, G.A. (2008). Tissue inhibitor of matrix metalloproteinases-3 (TIMP-3) lacks involvement in bacterial collagenase-induced intracerebral hemorrhage in mouse. *Acta Neurochir. Suppl. (Wien)* *105*, 89–93.
- Guroi, M.E., and Greenberg, S.M. (2008). Management of intracerebral hemorrhage. *Curr. Atheroscler. Rep.* *10*, 324–331.
- Han, Y., Albericio, F., and Barany, G. (1997). Occurrence and Minimization of Cysteine Racemization during Stepwise Solid-Phase Peptide Synthesis(1),(2). *J. Org. Chem.* *62*, 4307–4312.
- Harris, K.M., Flemer, S., Jr., and Hondal, R.J. (2007). Studies on deprotection of cysteine and selenocysteine side-chain protecting groups. *J. Pept. Sci.* *13*, 81–93.
- Haskew-Layton, R.E., Payappilly, J.B., Smirnova, N.A., Ma, T.C., Chan, K.K., Murphy, T.H., Guo, H., Langley, B., Sultana, R., Butterfield, D.A., et al. (2010). Controlled enzymatic production of astrocytic hydrogen peroxide protects neurons from oxidative stress via an Nrf2-independent pathway. *Proc. Natl. Acad. Sci. USA* *107*, 17385–17390.
- Hatfield, D.L., and Gladyshev, V.N. (2002). How selenium has altered our understanding of the genetic code. *Mol. Cell. Biol.* *22*, 3565–3576.
- Hauser, D.N., Dukes, A.A., Mortimer, A.D., and Hastings, T.G. (2013). Dopamine quinone modifies and decreases the abundance of the mitochondrial selenoprotein glutathione peroxidase 4. *Free Radic. Biol. Med.* *65*, 419–427.
- Hill, M.D., Martin, R.H., Mikulis, D., Wong, J.H., Silver, F.L., Terbrugge, K.G., Milot, G., Clark, W.M., Macdonald, R.L., Kelly, M.E., et al.; ENACT trial investigators (2012). Safety and efficacy of NA-1 in patients with iatrogenic stroke after endovascular aneurysm repair (ENACT): a phase 2, randomised, double-blind, placebo-controlled trial. *Lancet Neurol.* *11*, 942–950.
- Hondal, R.J., and Raines, R.T. (2002). Semisynthesis of proteins containing selenocysteine. *Methods Enzymol.* *347*, 70–83.
- Hua, Y., Schallert, T., Keep, R.F., Wu, J., Hoff, J.T., and Xi, G. (2002). Behavioral tests after intracerebral hemorrhage in the rat. *Stroke* *33*, 2478–2484.
- Huang, F.P., Xi, G., Keep, R.F., Hua, Y., Nemoianu, A., and Hoff, J.T. (2002). Brain edema after experimental intracerebral hemorrhage: role of hemoglobin degradation products. *J. Neurosurg.* *96*, 287–293.
- Ingold, I., Berndt, C., Schmitt, S., Doll, S., Poschmann, G., Buday, K., Roveri, A., Peng, X., Porto Freitas, F., Seibt, T., et al. (2018). Selenium Utilization by GPX4 Is Required to Prevent Hydroperoxide-Induced Ferroptosis. *Cell* *172*, 409–422.
- Iwai, T., Iinuma, Y., Kodani, R., and Oka, J. (2008). Neuromedin U inhibits inflammation-mediated memory impairment and neuronal cell-death in rodents. *Neurosci. Res.* *61*, 113–119.
- Iwamoto, M., Björklund, T., Lundberg, C., Kirik, D., and Wandless, T.J. (2010). A general chemical method to regulate protein stability in the mammalian central nervous system. *Chem. Biol.* *17*, 981–988.
- Jiang, L., Kon, N., Li, T., Wang, S.J., Su, T., Hibshoosh, H., Baer, R., and Gu, W. (2015). Ferroptosis as a p53-mediated activity during tumour suppression. *Nature* *520*, 57–62.
- Jones, G.D., Droz, B., Greve, P., Gottschalk, P., Poffett, D., McGrath, S.P., Seneviratne, S.I., Smith, P., and Winkel, L.H. (2017). Selenium deficiency risk predicted to increase under future climate change. *Proc. Natl. Acad. Sci. USA* *114*, 2848–2853.
- Kagan, V.E., Mao, G., Qu, F., Angeli, J.P., Doll, S., Croix, C.S., Dar, H.H., Liu, B., Tyurin, V.A., Ritov, V.B., et al. (2017). Oxidized arachidonic and adrenic PES navigate cells to ferroptosis. *Nat. Chem. Biol.* *13*, 81–90.
- Kaiser, E., Colescott, R.L., Bossinger, C.D., and Cook, P.I. (1970). Color test for detection of free terminal amino groups in the solid-phase synthesis of peptides. *Anal. Biochem.* *34*, 595–598.
- Karuppagounder, S.S., Alim, I., Khim, S.J., Bourassa, M.W., Sleiman, S.F., John, R., Thinnas, C.C., Yeh, T.L., Demetriades, M., Neitemeier, S., et al. (2016). Therapeutic targeting of oxygen-sensing prolyl hydroxylases abrogates ATF4-dependent neuronal death and improves outcomes after brain hemorrhage in several rodent models. *Sci. Transl. Med.* *8*, 328ra29.
- Karuppagounder, S.S., Alin, L., Chen, Y., Brand, D., Bourassa, M.W., Dietrich, K., Wilkinson, C.M., Nadeau, C.A., Kumar, A., Perry, S., et al. (2018). N-acetylcysteine targets 5 lipoxygenase-derived, toxic lipids and can synergize with prostaglandin E₂ to inhibit ferroptosis and improve outcomes following hemorrhagic stroke in mice. *Ann. Neurol.* *84*, 854–872.
- Keep, R.F., Hua, Y., and Xi, G. (2012). Intracerebral haemorrhage: mechanisms of injury and therapeutic targets. *Lancet Neurol.* *11*, 720–731.
- Khanna, S., Roy, S., Ryu, H., Bahadduri, P., Swaan, P.W., Ratan, R.R., and Sen, C.K. (2003). Molecular basis of vitamin E action: tocotrienol modulates 12-lipoxygenase, a key mediator of glutamate-induced neurodegeneration. *J. Biol. Chem.* *278*, 43508–43515.
- Kiviluoto, S., Vervliet, T., Ivanova, H., Decuyper, J.P., De Smedt, H., Missiaen, L., Bultynck, G., and Parys, J.B. (2013). Regulation of inositol 1,4,5-trisphosphate receptors during endoplasmic reticulum stress. *Biochim. Biophys. Acta* *1833*, 1612–1624.

- Kügler, S., Kilic, E., and Bähr, M. (2003). Human synapsin 1 gene promoter confers highly neuron-specific long-term transgene expression from an adenoviral vector in the adult rat brain depending on the transduced area. *Gene Ther.* *10*, 337–347.
- Kulak, M.V., Cyr, A.R., Woodfield, G.W., Bogachek, M., Spanheimer, P.M., Li, T., Price, D.H., Domann, F.E., and Weigel, R.J. (2013). Transcriptional regulation of the GPX1 gene by TFAP2C and aberrant CpG methylation in human breast cancer. *Oncogene* *32*, 4043–4051.
- Lai, J.C., and Clark, J.B. (1979). Preparation of synaptic and nonsynaptic mitochondria from mammalian brain. *Methods Enzymol.* *55*, 51–60.
- Lange, P.S., Chavez, J.C., Pinto, J.T., Coppola, G., Sun, C.W., Townes, T.M., Geschwind, D.H., and Ratan, R.R. (2008). ATF4 is an oxidative stress-inducible, prodeath transcription factor in neurons in vitro and in vivo. *J. Exp. Med.* *205*, 1227–1242.
- Lee, Y.H., Williams, S.C., Baer, M., Sterneck, E., Gonzalez, F.J., and Johnson, P.F. (1997). The ability of C/EBP beta but not C/EBP alpha to synergize with an Sp1 protein is specified by the leucine zipper and activation domain. *Mol. Cell Biol.* *17*, 2038–2047.
- Lee, J.H., Park, K.J., Jang, J.K., Jeon, Y.H., Ko, K.Y., Kwon, J.H., Lee, S.R., and Kim, I.Y. (2015). Selenoprotein S-dependent Selenoprotein K Binding to p97(VCP) Protein Is Essential for Endoplasmic Reticulum-associated Degradation. *J. Biol. Chem.* *290*, 29941–29952.
- Li, Q., Han, X., Lan, X., Gao, Y., Wan, J., Durham, F., Cheng, T., Yang, J., Wang, Z., Jiang, C., et al. (2017). Inhibition of neuronal ferroptosis protects hemorrhagic brain. *JCI Insight* *2*, e90777.
- Linkermann, A., Skouta, R., Himmerkus, N., Mulay, S.R., Dewitz, C., De Zen, F., Prokai, A., Zuchriegel, G., Krombach, F., Welz, P.S., et al. (2014). Synchronized renal tubular cell death involves ferroptosis. *Proc. Natl. Acad. Sci. USA* *111*, 16836–16841.
- Orso, F., Corà, D., Ubezio, B., Provero, P., Caselle, M., and Taverna, D. (2010). Identification of functional TFAP2A and SP1 binding sites in new TFAP2A-modulated genes. *BMC Genomics* *11*, 355.
- Parikhshak, N.N., Swarup, V., Belgard, T.G., Irimia, M., Ramaswami, G., Gandal, M.J., Hartl, C., Leppa, V., Ubieta, L.T., Huang, J., et al. (2016). Genome-wide changes in lncRNA, splicing, and regional gene expression patterns in autism. *Nature* *540*, 423–427.
- Patro, R., Duggal, G., Love, M.I., Irizarry, R.A., and Kingsford, C. (2017). Salmon provides fast and bias-aware quantification of transcript expression. *Nat. Methods* *14*, 417–419.
- Pekcec, A., Yigitkanli, K., Jung, J.E., Pallast, S., Xing, C., Antipenko, A., Minchenko, M., Nikolov, D.B., Holman, T.R., Lo, E.H., and van Leyen, K. (2013). Following experimental stroke, the recovering brain is vulnerable to lipoxigenase-dependent semaphorin signaling. *FASEB J.* *27*, 437–445.
- Pitts, M.W., Kremer, P.M., Hashimoto, A.C., Torres, D.J., Byrns, C.N., Williams, C.S., and Berry, M.J. (2015). Competition between the Brain and Testes under Selenium-Compromised Conditions: Insight into Sex Differences in Selenium Metabolism and Risk of Neurodevelopmental Disease. *J. Neurosci.* *35*, 15326–15338.
- Poursaitidis, I., Wang, X., Crighton, T., Labuschagne, C., Mason, D., Cramer, S.L., Triplett, K., Roy, R., Pardo, O.E., Seckl, M.J., et al. (2017). Oncogene-Selective Sensitivity to Synchronous Cell Death following Modulation of the Amino Acid Nutrient Cystine. *Cell Rep.* *18*, 2547–2556.
- Rafferty, T.S., McKenzie, R.C., Hunter, J.A., Howie, A.F., Arthur, J.R., Nicol, F., and Beckett, G.J. (1998). Differential expression of selenoproteins by human skin cells and protection by selenium from UVB-radiation-induced cell death. *Biochem. J.* *332*, 231–236.
- Ratan, R.R., Murphy, T.H., and Baraban, J.M. (1994a). Macromolecular synthesis inhibitors prevent oxidative stress-induced apoptosis in embryonic cortical neurons by shunting cysteine from protein synthesis to glutathione. *J. Neurosci.* *14*, 4385–4392.
- Ratan, R.R., Murphy, T.H., and Baraban, J.M. (1994b). Oxidative stress induces apoptosis in embryonic cortical neurons. *J. Neurochem.* *62*, 376–379.
- Ruiz, A., Matute, C., and Alberdi, E. (2009). Endoplasmic reticulum Ca(2+) release through ryanodine and IP(3) receptors contributes to neuronal excitotoxicity. *Cell Calcium* *46*, 273–281.
- Rusolo, F., Pucci, B., Colonna, G., Capone, F., Guerriero, E., Milone, M.R., Nazzaro, M., Volpe, M.G., Di Bernardo, G., Castello, G., and Costantini, S. (2013). Evaluation of selenite effects on selenoproteins and cytokinome in human hepatoma cell lines. *Molecules* *18*, 2549–2562.
- Ryu, H., Lee, J., Zaman, K., Kubilis, J., Ferrante, R.J., Ross, B.D., Neve, R., and Ratan, R.R. (2003). Sp1 and Sp3 are oxidative stress-inducible, antideath transcription factors in cortical neurons. *J. Neurosci.* *23*, 3597–3606.
- Sattler, R., Xiong, Z., Lu, W.Y., Hafner, M., MacDonald, J.F., and Tymianski, M. (1999). Specific coupling of NMDA receptor activation to nitric oxide neurotoxicity by PSD-95 protein. *Science* *284*, 1845–1848.
- Savaskan, N.E., Borchert, A., Bräuer, A.U., and Kuhn, H. (2007a). Role for glutathione peroxidase-4 in brain development and neuronal apoptosis: specific induction of enzyme expression in reactive astrocytes following brain injury. *Free Radic. Biol. Med.* *43*, 191–201.
- Savaskan, N.E., Ufer, C., Kühn, H., and Borchert, A. (2007b). Molecular biology of glutathione peroxidase 4: from genomic structure to developmental expression and neural function. *Biol. Chem.* *388*, 1007–1017.
- Saxena, S., Cabuy, E., and Caroni, P. (2009). A role for motoneuron subtype-selective ER stress in disease manifestations of FALS mice. *Nat. Neurosci.* *12*, 627–636.
- Scarpa, E.S., Fabrizio, G., and Di Girolamo, M. (2013). A role of intracellular mono-ADP-ribosylation in cancer biology. *FEBS J.* *280*, 3551–3562.
- Schallert, T., Fleming, S.M., Leasure, J.L., Tillerson, J.L., and Bland, S.T. (2000). CNS plasticity and assessment of forelimb sensorimotor outcome in unilateral rat models of stroke, cortical ablation, parkinsonism and spinal cord injury. *Neuropharmacology* *39*, 777–787.
- Schomburg, L., and Schweizer, U. (2009). Hierarchical regulation of selenoprotein expression and sex-specific effects of selenium. *Biochim. Biophys. Acta* *1790*, 1453–1462.
- Schroll, A.L., Hondal, R.J., and Flemer, S., Jr. (2012). 2,2'-Dithiobis(5-nitropyridine) (DTNP) as an effective and gentle deprotectant for common cysteine protecting groups. *J. Pept. Sci.* *18*, 1–9.
- Schwarze, S.R., Ho, A., Vocero-Akbani, A., and Dowdy, S.F. (1999). In vivo protein transduction: delivery of a biologically active protein into the mouse. *Science* *285*, 1569–1572.
- Snider, G.W., Ruggles, E., Khan, N., and Hondal, R.J. (2013). Selenocysteine confers resistance to inactivation by oxidation in thioredoxin reductase: comparison of selenium and sulfur enzymes. *Biochemistry* *52*, 5472–5481.
- Spilker, C., Nullmeier, S., Grochowska, K.M., Schumacher, A., Butnaru, I., Macharadze, T., Gomes, G.M., Yuanxiang, P., Bayraktar, G., Rodenstein, C., et al. (2016). A Jacob/Nsmf Gene Knockout Results in Hippocampal Dysplasia and Impaired BDNF Signaling in Dendritogenesis. *PLoS Genet.* *12*, e1005907.
- Spriggs, K.A., Stoneley, M., Bushell, M., and Willis, A.E. (2008). Re-programming of translation following cell stress allows IRES-mediated translation to predominate. *Biol. Cell* *100*, 27–38.
- Stockwell, B.R., Friedmann Angeli, J.P., Bayir, H., Bush, A.I., Conrad, M., Dixon, S.J., Fulda, S., Gascón, S., Hatzios, S.K., Kagan, V.E., et al. (2017). Ferroptosis: A Regulated Cell Death Nexus Linking Metabolism, Redox Biology, and Disease. *Cell* *171*, 273–285.
- Stoytcheva, Z.R., and Berry, M.J. (2009). Transcriptional regulation of mammalian selenoprotein expression. *Biochim. Biophys. Acta* *1790*, 1429–1440.
- Tang, J., Liu, J., Zhou, C., Alexander, J.S., Nanda, A., Granger, D.N., and Zhang, J.H. (2004). Mmp-9 deficiency enhances collagenase-induced intracerebral hemorrhage and brain injury in mutant mice. *J. Cereb. Blood Flow Metab.* *24*, 1133–1145.
- Tarangelo, A., Magtanong, L., Biegging-Rolett, K.T., Li, Y., Ye, J., Attardi, L.D., and Dixon, S.J. (2018). p53 Suppresses Metabolic Stress-Induced Ferroptosis in Cancer Cells. *Cell Rep.* *22*, 569–575.
- Turanov, A.A., Lobanov, A.V., Fomenko, D.E., Morrison, H.G., Sogin, M.L., Klobutcher, L.A., Hatfield, D.L., and Gladyshev, V.N. (2009). Genetic code

- supports targeted insertion of two amino acids by one codon. *Science* 323, 259–261.
- Turanov, A.A., Xu, X.M., Carlson, B.A., Yoo, M.H., Gladyshev, V.N., and Hatfield, D.L. (2011). Biosynthesis of selenocysteine, the 21st amino acid in the genetic code, and a novel pathway for cysteine biosynthesis. *Adv. Nutr.* 2, 122–128.
- van Asch, C.J., Luitse, M.J., Rinkel, G.J., van der Tweel, I., Algra, A., and Klijn, C.J. (2010). Incidence, case fatality, and functional outcome of intracerebral haemorrhage over time, according to age, sex, and ethnic origin: a systematic review and meta-analysis. *Lancet Neurol.* 9, 167–176.
- Viswanathan, V.S., Ryan, M.J., Dhruv, H.D., Gill, S., Eichhoff, O.M., Seashore-Ludlow, B., Kaffenberger, S.D., Eaton, J.K., Shimada, K., Aguirre, A.J., et al. (2017). Dependency of a therapy-resistant state of cancer cells on a lipid peroxidase pathway. *Nature* 547, 453–457.
- Wang, Z., Wei, X., Liu, K., Zhang, X., Yang, F., Zhang, H., He, Y., Zhu, T., Li, F., Shi, W., et al. (2013). NOX2 deficiency ameliorates cerebral injury through reduction of complexin II-mediated glutamate excitotoxicity in experimental stroke. *Free Radic. Biol. Med.* 65, 942–951.
- Wang, S.J., Li, D., Ou, Y., Jiang, L., Chen, Y., Zhao, Y., and Gu, W. (2016). Acetylation Is Crucial for p53-Mediated Ferroptosis and Tumor Suppression. *Cell Rep.* 17, 366–373.
- Wenzel, S.E., Tyurina, Y.Y., Zhao, J., St Croix, C.M., Dar, H.H., Mao, G., Tyurin, V.A., Anthonymuthu, T.S., Kapralov, A.A., Amoscato, A.A., et al. (2017). PEBP1 Wardens Ferroptosis by Enabling Lipoygenase Generation of Lipid Death Signals. *Cell* 171, 628–641.
- Williamson, J.A., Boshier, J.M., Skinner, A., Sheer, D., Williams, T., and Hurst, H.C. (1996). Chromosomal mapping of the human and mouse homologues of two new members of the AP-2 family of transcription factors. *Genomics* 35, 262–264.
- Xie, Y., Zhu, S., Song, X., Sun, X., Fan, Y., Liu, J., Zhong, M., Yuan, H., Zhang, L., Billiar, T.R., et al. (2017). The Tumor Suppressor p53 Limits Ferroptosis by Blocking DPP4 Activity. *Cell Rep.* 20, 1692–1704.
- Yagoda, N., von Rechenberg, M., Zaganjor, E., Bauer, A.J., Yang, W.S., Fridman, D.J., Wolpaw, A.J., Smukste, I., Peltier, J.M., Boniface, J.J., et al. (2007). RAS-RAF-MEK-dependent oxidative cell death involving voltage-dependent anion channels. *Nature* 447, 864–868.
- Yang, X., Fyodorov, D., and Deneris, E.S. (1995). Transcriptional analysis of acetylcholine receptor alpha 3 gene promoter motifs that bind Sp1 and AP2. *J. Biol. Chem.* 270, 8514–8520.
- Yang, W.S., SriRamaratnam, R., Welsch, M.E., Shimada, K., Skouta, R., Viswanathan, V.S., Cheah, J.H., Clemons, P.A., Shamji, A.F., Clish, C.B., et al. (2014). Regulation of ferroptotic cancer cell death by GPX4. *Cell* 156, 317–331.
- Yigitkanli, K., Pekcec, A., Karatas, H., Pallast, S., Mandeville, E., Joshi, N., Smirnova, N., Gazaryan, I., Ratan, R.R., Witztum, J.L., et al. (2013). Inhibition of 12/15-lipoxygenase as therapeutic strategy to treat stroke. *Ann. Neurol.* 73, 129–135.
- Yu, Y., Xie, Y., Cao, L., Yang, L., Yang, M., Lotze, M.T., Zeh, H.J., Kang, R., and Tang, D. (2015). The ferroptosis inducer erastin enhances sensitivity of acute myeloid leukemia cells to chemotherapeutic agents. *Mol. Cell. Oncol.* 2, e1054549.
- Zambon, A.C., Gaj, S., Ho, I., Hanspers, K., Vranizan, K., Evelo, C.T., Conklin, B.R., Pico, A.R., and Salomonis, N. (2012). GO-Elite: a flexible solution for pathway and ontology over-representation. *Bioinformatics* 28, 2209–2210.
- Zhang, B., and Horvath, S. (2005). A general framework for weighted gene co-expression network analysis. *Stat. Appl. Genet. Mol. Biol.* 4, e17.
- Zhang, S., Hisatsune, C., Matsu-Ura, T., and Mikoshiba, K. (2009). G-protein-coupled receptor kinase-interacting proteins inhibit apoptosis by inositol 1,4,5-triphosphate receptor-mediated Ca²⁺ signal regulation. *J. Biol. Chem.* 284, 29158–29169.
- Zille, M., Karuppagounder, S.S., Chen, Y., Gough, P.J., Bertin, J., Finger, J., Milner, T.A., Jonas, E.A., and Ratan, R.R. (2017). Neuronal Death After Hemorrhagic Stroke In Vitro and In Vivo Shares Features of Ferroptosis and Necroptosis. *Stroke* 48, 1033–1043.
- Zille, M., Kumar, A., Kundu, N., Bourassa, M.W., Wong, V.S.C., Willis, D., Karuppagounder, S.S., and Ratan, R.R. (2019). Ferroptosis in neurons and cancer cells is similar but differentially regulated by histone deacetylase inhibitors. *eNeuro* 6. Published online February 15, 2019. <https://doi.org/10.1523/ENEURO.0263-18.2019>.

STAR★METHODS

KEY RESOURCES TABLE

REAGENT or RESOURCE	SOURCE	IDENTIFIER
Antibodies		
Rabbit anti-GPX4 (Immunofluorescence)	Lifespan Biosciences	Cat#LS-B14362
Rabbit anti-GPX4 (Immunoblot)	Lifespan Biosciences	Cat#LS-B1596; RRID:AB_2263528
Rabbit anti-Sp1	EMD Millipore	Cat#07-645; RRID:AB_310773
Mouse anti-NeuN	EMD Millipore	Cat#MAB377; RRID:AB_2298772
Mouse anti-TFAP2c	Santa Cruz	Cat#SC12762; RRID:AB_667770
Rabbit IgG	Santa Cruz	Cat#SC2027; RRID:AB_737197
Mouse anti-TFAP2d	Abcam	Cat#ab169153
Rabbit anti-TFAP2a	Cell Signaling Technology	Cat#3208; RRID:AB_2056341
Rabbit anti-Histone H3	Cell Signaling Technology	Cat#4499; RRID:AB_10544537
Mouse anti-Histone H3	Cell Signaling Technology	Cat#3638; RRID:AB_1642229
Mouse anti-Histone H4	Cell Signaling Technology	Cat#2935; RRID:AB_1147658
Rabbit anti-COX 4	Cell Signaling Technology	Cat#4850; RRID:AB_2085424
Bacterial and Virus Strains		
DH5 α	Invitrogen	Cat#18265-017
High efficiency 5 α E.coli	New England Bioscience	Cat#C29871
Adenoviral ddGPX4	This paper/viraquest	N/A
Adenoviral Sp1	Ryu et al., 2003	N/A
Adenoviral mutant Sp1	This paper/viraquest	N/A
Adenovirus GPX4-L	D. Spitz/Viraquest	N/A
Adenovirus CAT	This paper/viraquest	N/A
Adenovirus SOD2	This paper/viraquest	N/A
Adenovirus TFAP2c	Kulak et al., 2013	N/A
AAV8-eGFP	Vector Biolabs	Cat# 7061
AAV8-CMV Null	Vector Biolabs	Cat# 7077
AAV8-esyn-GPX4	This paper/Vector Biolabs	N/A
AAV8-esyn-mSp1 (mutant Sp1)	This paper/Vector Biolabs	N/A
Chemicals, Peptides, and Recombinant Proteins		
Sodium Selenite	Sigma Aldrich	Cat#S5261
Collagenase Type VII-S	Sigma Aldrich	Cat#C2399
ToPro-3 Iodide (642/661)	Invitrogen	Cat#T3605
Fluoro Jade B	EMD Millipore	Cat#AG 310
MK801	Sigma Aldrich	Cat#M107
Hemin	Sigma Aldrich	Cat#H9039
Actinomycin-D	Sigma Aldrich	Cat#A1410
L-homocysteic acid	Sigma Aldrich	Cat#H9633
Erastin	Selleck Chemicals	Cat#S7424
Trimethoprim (TMP)	Sigma Aldrich	Cat#T7883
N-acetyl-cysteine	Sigma Aldrich	Cat#A7250
FIN56	Sigma Aldrich	Cat#SML1740
Nonidet P40 Substitute	Affymetrix	Cat#9002-93-1
Thapsigargin	Sigma Aldrich	Cat#T9033
Tunicamycin	Sigma Aldrich	Cat# T-7765
1-hydroxy-7-azabenzotriazole (HOAt)	Advanced ChemTech	Cat# RC8208

(Continued on next page)

Continued

REAGENT or RESOURCE	SOURCE	IDENTIFIER
2-Chlorotriyl chloride resin	Advanced ChemTech	Cat#SC5055
Z-VAD-FMK	Enzo Life Sciences	Cat#AXL-260-020-M001
RSL3	Cayman Chemical	Cat#19288
Triisopropylsilane (98%)	Acros Organics	Cat#214920500
<i>N,N'</i> -diisopropylcarbodiimide	Chem-Implex Int'l	Cat#00110
1-[Bis(dimethylamino)methylene]-1 <i>H</i> -1,2,3-triazolo[4,5- <i>b</i>]pyridinium 3-oxid hexafluorophosphate (HATU)	Oakwood Chemical	Cat#023926
Tat (GRKKRRQRRRPQ)	Schwarze et al., 1999	N/A
Tat-SelPep (GRKKRRQRRRPQKUNLN)	This paper	N/A
Tat-Cys (GRKKRRQRRRPQCKCNLN)	This paper	N/A
NdeI	New England Biosciences	Cat#R0111S
BamHI	New England Biosciences	Cat#R0136S
HindIII	New England Biosciences	Cat#R0104S
XBal	New England Biosciences	Cat#R0145T
Critical Commercial Assays		
EZ-Magna ChIP Assay Kit	Millipore	Cat# 17-408
NucleoSpin RNA II Kit	Clontech	Cat#740955-250
TaqMan RNA to Ct 1-step kit	Applied Biosystems	Cat#4392656
MTT Assay Kit	Promega	Cat#G4100
Live/Dead Assay Kit	Thermo Fisher Scientific	Cat#L3224
Dual Luciferase Assay Kit	Promega	Cat#E1980
DeadEnd Fluorometric TUNEL system	Promega	Cat#G3250
MiRNeasy Kit	QIAGEN	Cat#217004
RiboZero Gold Kit	Illumina	Cat#MRZG1234
Quant-iT PicoGreen Assay	Life Technologies	Cat#p7589
Qiaquick Gel Extraction Kit	QIAGEN	Cat#28704
Quick T4 DNA Ligase Kit	New England Biolabs	Cat#M2200
Fast Ion Plasmid Maxi Kit	IBI Scientific	Cat# IB47125
Deposited Data		
RNA Sequencing of primary cortical neurons treated with selenium and HCA	This paper	https://www.ncbi.nlm.nih.gov/geo/ , GEO: GSE126787
Raw western blots, WGCNA data, time lapse cell death videos, TUNEL staining, additional siRNA data, Z-VAD-FMK data and behavior scatterplots.	This paper	https://www.mendeley.com/ ; https://doi.org/10.17632/2jsgwzh3zz.1
Experimental Models: Cell Lines		
Mouse: HT22 Neuroblast Cell Line	EMD Millipore	Cat#SCC129
Human: HT1080 Fibrosarcoma Cell Line	ATCC	Cat#CCL-121
Experimental Models: Organisms/Strains		
CD1 Pregnant mice (15 days into pregnancy)	Charles River	N/A
Male C57BL/6 Mice	Charles River	N/A
Oligonucleotides		
Complete list of primers and oligonucleotides used can be found in Table S3	This Paper	N/A
Recombinant DNA		
GPX4 promoter reporter (−1 to −4000 bp)	This paper/viraquest	N/A
GPX4 promoter reporter (−1763 to −1189 bp)	This paper/viraquest	N/A
GPX4 promoter reporter (−1763 to −1189 bp) binding mutations	This paper/viraquest	N/A
pTK-renilla plasmid	Promega	Cat#E2261

(Continued on next page)

Continued

REAGENT or RESOURCE	SOURCE	IDENTIFIER
Software and Algorithms		
Prism 6	Graphpad	https://www.graphpad.com/
Axiovision Software	Carl Zeiss	https://www.zeiss.com/
ImageJ	NIH	https://imagej.nih.gov/ij/
Image Studio ver. 5.2	LI-COR	https://www.licor.com/
rna-STAR	Dobin et al., 2013	https://github.com/alexdobin/STAR
Salmon	Patro et al., 2017	https://salmon.readthedocs.io/en/latest/index.html
Go Elite	Zambon et al., 2012	http://www.genmapp.org/go_elite/
Zen Black/Blue	Carl Zeiss	https://www.zeiss.com/
Other		
Fetal Bovine Serum (FBS)	Life Technologies	Cat#16140-071
Horse Serum	Life Technologies	Cat#26050-088
Penicillin-Streptomycin	Thermo Fisher Scientific	Cat# 15140122
GS21	MTI-Globalstem	Cat#GSM-3100
MEM Non-essential amino acids	Thermo Fisher Scientific	Cat#11140050

CONTACT FOR REAGENT AND RESOURCE SHARING

Further information and requests for resources and reagents should be directed to and will be fulfilled by the lead contact, Dr. Rajiv R. Ratan (rrr2001@med.cornell.edu).

EXPERIMENTAL MODEL AND SUBJECT DETAILS

Animal Models

All mice and procedures were approved by the Institutional Animal Care and Use Committee of Weill Cornell Medical College and were in accordance with the guidelines established by the National Institutes of Health (NIH) and Animal Research: Reporting of *In Vivo* Experiments (ARRIVE). All mice were housed in a pathogen-free facility on a 12-hour light/dark cycle from 6am to 6pm and provided *ad libitum* access to food and water. Animals used in *in vivo* studies were 8-10 week old Male C57BL/6 mice (Charles River). Primary neuronal cultures were obtained from embryonic day 15 pups (mixed gender) from 8-12 week old pregnant Female CD1 mice (Charles River). Animals used for *in vivo* and *in vitro* experiments were all healthy prior to experiments and had not been used for previous procedures or drug treatments.

Immature primary cortical neuronal cultures

Primary cortical neurons were obtained from embryonic (E15) CD1 mice (mixed gender) under sterile conditions. Cortices were dissected, washed in PBS, homogenized in papain (Worthington Biochemical) for 20 min in a 37°C waterbath. Cells were plated in minimum essential medium containing 10% fetal bovine serum (FBS; Life Technologies), 5% horse serum (Life Technologies), and 1% penicillin/streptomycin (Thermo Fisher Scientific) in 96-well plates, 6-well plates, or 10-cm dishes coated with poly-D-lysine (PDL; Sigma Aldrich). Neurons were maintained at 37°C with 5% CO₂ for 24 hours after plating prior to experiments. Cells were validated as neurons from visual morphology and positive expression of neuronal markers (NeuN). Immature cultures are sensitive to glutamate/L-homocysteic acid (HCA)-induced ferroptosis. This cell death is independent of ionotropic glutamate receptors, which do not fully develop until much later *in vitro* (> 10 days). HCA-induced death in immature neuronal cultures is insensitive to MK801 (an ionic glutamate receptor antagonist; Sigma Aldrich) but is rescued by supplemental cyst(e)ine. Cells were plated at a density of 1 million cells/ml.

Mature primary cortical neuronal cultures

For mature cultures, cortices from E15 CD1 mice (mixed gender) were processed the same as immature cultures and plated on PDL coated plates in Neurobasal media (Life Technologies) containing 1x GS21 (MTI-Globalstem), 1x Glutamax (Life Technologies) and 5% BSA. Every three days 50% media was changed and cells were allowed to mature for 13 days before experimentation. Neurons were identified from visual morphology. Mature neurons were sensitive to glutamate-induced excitotoxicity as cell death was completely inhibited by MK801 treatment. Cells were plated at a density of 100,000 cells/ml.

Cultured cell lines

HT22 murine hippocampal cells were immortalized from embryos of unknown sex via expression of a SV40 T-antigen. These cells were cultured at 37°C with 5% CO₂ in Dulbecco's modified Eagle's medium (DMEM), 10% FBS, and 1% penicillin/streptomycin (4 mg/ml; Sigma Aldrich). HT1080 human fibrosarcoma cells (Male) were cultured at 37°C in DMEM, 10% FBS, 10% MEM non-essential amino acids (Thermo Fisher Scientific) and 1% penicillin/streptomycin. Experiments were conducted at a cell density of 60%–80%. Both cell lines were authenticated by visual morphology and sensitivity to HCA (HT22) and Erastin (HT1080)-induced toxicity. Cell lines used for experiments were passaged no more than 25 times. Plates used for culturing both cell lines were uncoated.

METHOD DETAILS

Collagenase-induced mouse model of ICH

All surgeries were conducted under aseptic conditions by a skilled animal surgeon. To induce a hemorrhagic stroke model in mice, male C57BL/6 mice (8 to 10 weeks of age) were anesthetized with isoflurane (2 to 5%) and placed on a stereotaxic frame. During the procedure, the animal's body temperature was maintained at 37°C with a homeothermic blanket. Using a nanomite syringe pump (Harvard Apparatus) and a Hamilton syringe, 1 μ L of collagenase (0.075 IU; Sigma Aldrich) was infused into the right striatum at a flow rate of 0.120 μ L/min. Relative to the bregma point, the stereotaxic coordinates of the injection were as follows: lateral, -0.20 ; anteroposterior, 0.62 ; and dorsoventral, -0.40 . In control animals, 1 μ L of saline was infused. The animals were randomized to saline volume control (APP Pharmaceuticals) or collagenase (ICH) groups. The identity of the mice that received vehicle or Se was masked to surgeons who performed the ICH. The identity was revealed after all the data was collected on all animals and the code revealed by a member of the team not involved in surgeries or drug preparation. Proper postoperative care was observed until the animals were completely recovered, specifically placing the animals in a heated cage (37°C) for 1–3 hours post injury and providing soft pellets in the home cage (Grossetete and Rosenberg, 2008; Tang et al., 2004; Karuppagounder et al., 2016).

Intracerebroventricular injection of sodium selenite

Using a nanomite syringe pump and Hamilton syringe, 3 μ L of either sodium selenite treatment (1–5 μ M; Sigma Aldrich; dissolved in saline) or vehicle control (saline only) was infused directly into the ventricles at a rate of 0.120 μ L/min 2 hours after collagenase infusion. The injection site relative to the bregma point was lateral, -0.05 ; anteroposterior, 0.12 and dorsoventral, -0.25 . Surgeon was blinded to treatment and control groups.

Intraperitoneal injection for tat peptides

Treatment groups of saline, Tat or Tat SelPep (dissolved in saline) was given to mice 2–6 hours after ICH and every day for 7 days by intraperitoneal injection at a total volume of 0.1 ml per animal. Peptides were given in a blinded manner at doses of 4–12 μ g/g.

Stereotaxic administration of adeno-associated viral vectors into the striatum

All surgeries were conducted under aseptic conditions by a surgeon skilled in mouse operation. For each mouse, 2 μ L of AAV8 [1×10^{13} genomic copies (GCs)] was injected into the right striatum at a flow rate of 0.120 μ L/min using a nanomite syringe pump through a Hamilton syringe. By contrast, control mice received 2 μ L injections (1×10^{13} GCs) of AAV8-eGFP or AAV8 CMV Null (Vector Biolabs). All mice received two injections at the following stereotaxic coordinates (all positions are relative to bregma): injection 1: posterior, 0.10 ; lateral, -0.15 ; dorsoventral, -0.35 ; injection 2: posterior, 0.03 ; lateral, -0.25 ; dorsoventral, -0.33 . The needle was left in place for 5 min after the injection was complete and withdrawn at a rate of 1 mm/min. All mice injected with either AAV8 were subjected to collagenase-induced ICH 14 days later (following the ICH procedure described). Proper postoperative care was taken until the animals recovered completely.

Behavioral analysis

The corner task assessed the integrated sensorimotor function in both stimulation of vibrissae (sensory neglect) and rearing (motor response; Schallert et al., 2000; Karuppagounder et al., 2016). Mice were placed between two cardboard pieces forming a corner with a 30° angle. While maintaining the 30° angle, the boards were gradually moved toward the mouse until the mouse approached the corner, reared upward, and turned 180° to face the open end. The direction (left or right) in which the mouse turned around was recorded for each trial. Ten trials were performed for each mouse. The adhesive tape removal task in mice was performed by placing adhesive tape on the planter region of the forward paw (right and left) of mice. The mouse was placed in a novel cage. The time from which the tape was applied to when the mouse successfully removed it was recorded for each paw. A maximum of 300 seconds for each paw was allowed. Behavior testing was done for 16 independent animals per study group, based on power calculations of 0.99 power (two-tailed test). Between experiments, animals were housed in home cages in pathogen-free facility.

Experimental ischemic model (filament MCAO method)

All surgeries were conducted under aseptic conditions by a skilled, mouse surgeon. Male mice were anesthetized with isoflurane (5% induction, and 2% maintenance). A 2 cm incision was opened in the middle of the anterior neck. The right common carotid was temporarily ligated with 6–0 silk (Ethicon Inc.). Right unilateral MCAO was accomplished by inserting a Silicon rubber-coated monofilament (Doccol Corporation) into the internal carotid artery via the external carotid artery stump. Adequacy of MCAO was

confirmed by monitoring cortical blood flow at the onset of the occlusion with a laser Doppler flowmetry probe affixed to the skull (Periflux System 5010; Perimed, Sweden). Animals were excluded if mean intra-ischemic laser Doppler flowmetry was > 30% pre-ischemic baseline. Transient focal cerebral ischemia was induced in mice for 45 minutes by reversible MCAO in the right brain hemisphere under isoflurane anesthesia followed by 24 hours of reperfusion following the procedure established in [Bodhankar et al. \(2015\)](#). Body temperature was controlled at $36.5 \pm 0.5^\circ\text{C}$ throughout MCAO surgery with warm water pads and a heating lamp. After 45 minutes of occlusion, the occluding filament was withdrawn to allow for reperfusion and the incision was closed with 6-0 surgical sutures (ETHICON, Inc). 0.5 mL prewarmed normal saline was given subcutaneously to each mouse after surgery. Mice were then allowed to recover from anesthesia and were survived for 24 hours after initiation of reperfusion. Following 2 hours of reperfusion, animals were given either saline, Tat or Tat SelPep (dissolved in saline) by intraperitoneal injection. The surgeon was blinded to treatment groups.

Infarct Volume Analysis

The individual performing the infarct volume analysis was blinded to treatment group. Mice were euthanized, and brains were collected at 24 hours of reperfusion for 2,3,5-triphenyltetrazolium chloride histology (Sigma, St. Louis, MO). The 2-mm brain sections were incubated in 1.2% 2,3,5-triphenyltetrazolium chloride (TTC) for 15 minutes at 37°C , and then fixed in 10% formalin for 24 hours. Infarction volume was measured using digital imaging and images were analyzed using Sigma Scan Pro 5.0 Software (Systat, Inc, Point Richmond, CA). To control for edema, infarct volume (cortex, striatum, and hemisphere) was determined by subtraction of the ipsilateral noninfarcted regional volume from the contralateral regional volume. This value was then divided by the contralateral regional volume and multiplied by 100 to yield regional infarction volume as a percent of the contralateral. Infarct volume was conducted on 12 independent brains per treatment group.

Immunocytochemistry

For immunocytochemical experiments in the brain, appropriate numbers of control mice with unilateral hemorrhagic stroke and selenium-treated mice with induced unilateral hemorrhagic stroke were perfused with 4% paraformaldehyde (PFA; Sigma Aldrich) in PBS for 15 minutes to fix their brains. The brains were isolated and post-fixed for 1h in 4% PFA at 7 days post ICH. After cryoprotection in a sucrose gradient, coronal sections were cut at $30\ \mu\text{m}$. For cell cultures, HT22 cells were plated on an 8 well glass slide and were fixed with 4% PFA 24 hours after treatment (siRNA, adenovirus or sodium selenite). Immunocytochemistry was conducted on > 3 independent brains per group and > 3 independent cultures per group.

Free-floating brain sections or cell cultures were blocked for 1h in a PBS solution containing 3% bovine serum albumin (Sigma Aldrich), and 0.5% Triton X-100 (Bio-Rad Laboratories). Primary antibodies were diluted in a PBS solution containing 3% bovine serum albumin (Sigma Aldrich) and applied for 12 hours at 4°C and followed by three washes with PBS. Tissue was then incubated for 1 hour in the appropriate secondary antibody, conjugated to Alexa 488 (1:1000; green fluorescence, Life Technologies), Alexa 568 (1:1000; red fluorescence, Life Technologies); for nuclear labeling ToPro was added to the mixture (1:15000, far red fluorescence, Invitrogen) in a PBS solution containing 3% bovine serum albumin (Sigma Aldrich). In multi-labeling experiments, sections were incubated in a mixture of primary antibodies, followed by a mixture of secondary antibodies under same conditions as above. After staining, the sections were flat mounted on a superfrost plus microscope slide (Thermo Fisher Scientific) and coverslipped using Vectashield mounting medium (H-1000, Vector Laboratories). The coverslip was sealed in place with nail polish.

The primary antibodies used in this study were the following: rabbit anti-GPX4 (1:800, LSBio), rabbit anti-Sp1 (1:300, EMD Millipore), and mouse anti-NeuN (1:1000, EMD Millipore). The samples were processed in the same mixtures of antibodies and imaged under Nikon Eclipse Ti-U confocal microscope using with a 20x water objective (0.75N.A.) and 60x oil objective (1.4N.A.). All sections were imaged under identical acquisition conditions, including: laser intensity, photomultiplier amplification, and Z stack step size. All images were processed and analyzed using ImageJ software. Fluorescence quantification were taken only from NeuN positive cells. Treatment conditions were masked during imaging and treatments were only revealed after completion of analysis.

TUNEL staining

Slice or culture preparation (fixation), and imaging was similar to what was described in antibody treatment. In this study we used DeadEnd Fluorometric TUNEL staining (Promega) using the protocol described by manufacturer. Briefly, following fixation, tissue and cell cultures were permeabilized with 0.2% Triton-X in PBS for 5 minutes and washed 5 times with PBS. Tissue/cultures were equilibrated for 5 minutes at room temperature in equilibration buffer (provided in kit). Slides were then labeled with TdT reaction mix (containing TdT nucleotide) for 60 min at 37°C . The TdT reaction was then stopped and slides were washed and counterstained with ToPro. TUNEL staining was conducted on 3 independent brains per group and 3 independent cultures per treatment group.

Fluoro-jade Staining

Neurodegeneration in mice following collagenase-induced intracerebral hemorrhage was assessed by staining with Fluoro-jade B (EMD Millipore) and carried out according to supplier's protocol. Briefly, control mice and ICH mice ($\pm\text{ICV Se}$) were sacrificed 7 days post ICH and brains processed according to the same protocol as the immunocytochemical experiments. Floating brain sections were immersed in a graded series of alcohol (50%, 70% and 100% ethanol for 5 min each; Sigma Aldrich) solutions. Floating sections are then immersed in a 0.06% potassium permanganate (KMnO₄ in distilled water) solution for 15 minutes. Sections were washed with double distilled (ddH₂O) before being immersed in a 0.001% Fluoro-jade staining solution (Fluoro-jade B in ddH₂O) for 20 minutes with gently shaking in the dark. Sections were then washed with ddH₂O and mounted on coated slides (TruBond 380; Fisher Scientific) and dried at room temperature overnight in the dark. Fluoro-jade B staining was examined within perihematoma

or hematoma regions using a fluorescence microscope (Zeiss Axiovert). Quantitation of Fluoro-jade B staining was performed using ImageJ software. Fluoro-jade staining was conducted on a minimum of 12 independent brains per group and Fluoro-jade positive cells were counted in the entire brain.

Hematoma Volume Measurement

To determine if treatments reduced hematoma volume mice (\pm ICV Se) were sacrificed 24h after ICH; the brains were removed and flash frozen in Freeze' IT (Fisher Scientific). Coronal sections were sliced at 30 μ m and placed directly on a glass slide. To quantify hematoma volume, sections were digitized at standardized coronal levels. A blinded user would measure the contours and hematoma from left and right hemisphere from each section. Hematoma volume and swelling were measured and calculated using Axiovision software (Carl Zeiss). Hematoma measurements were conducted on at least 5 independent brains per group and hematoma volume was measured throughout the brain.

Quantitative real-time PCR

Total RNA was prepared from either cell cultures or tissue using the NucleoSpin RNA II kit (Clontech) according to the manufacturer's protocol. Duplex real-time PCR reactions were performed with gene expression assays using 6-carboxyfluorescein-labeled probes (Applied Biosystems) for genes of interest. Primers used were: CAT, SOD2, GPX1, GPX4 (Exon 1a, 1b); SELP, TXNRD1, GPX3, SELK, MSRB1, SELW, GIT1, EIF3c, URB2, ATF4, NSMF and Sp1 (exon 2-3 and exon 5-6; Thermo Fisher Scientific). All expression levels were normalized to β -actin gene expression, which was determined with a VIC-labeled probe (Applied Biosystems). Probes with sample mRNA were prepared with TaqMan RNA to Ct 1-step kit (Applied Biosystems) in accordance to manufacturer's instructions. All experiments were performed using a Quant 6 Real-Time PCR System (Applied Biosystems) and up to 40 cycles in accordance to the 1-step qPCR protocol (Applied Biosystems). Replications from minimum 4 independent tissue samples or cell cultures were used for qPCR.

In vitro ICH model

Cell death was induced in primary cortical neurons and hippocampal HT22 cells by treatment with hemin (dose response 10 to 250 μ M at 16 hours; Sigma Aldrich). Stock solution for hemin was dissolved in 0.1M NaOH. For the neuroprotection studies, cells were treated with 80 μ M hemin (LD₅₀) in the presence of designated agents or sodium selenite (Sigma Aldrich) dissolved in ddH₂O. Cell viability was analyzed 16 hours after treatment. Cells were then washed in pre-warmed PBS (37°C) and assessed by MTT assay as per manufacturer's instructions (Promega). Briefly, neuronal cells are incubated for 2h in MTT reagent (5 μ l per 100 μ l media; 1 hour for mature cortical cultures, HT22 and HT1080). This was followed by 1 hour incubation on a shaker of detergent reagent (5 μ l per 100 μ l media; Stop Solution) in the dark at room temperature. The fidelity of MTT assays in measuring viability was verified by calcein-AM/ethidium homodimer-1 staining in PBS (Live/Dead assay, Thermo Fisher scientific) as per the manufacturer's instructions. The transcription inhibitor actinomycin-D (Sigma Aldrich) was dissolved in Dimethyl sulfoxide (DMSO; Sigma Aldrich) and used in immature neuron studies only. A minimum of 3 independent cell cultures were used for *in vitro* ICH.

In vitro model of ferroptosis in neurons

Primary cortical neurons, and HT22 hippocampal neuroblast cells were exposed to 5mM L-homocysteic acid (HCA; Sigma Aldrich) dissolved in MEM no phenol (Thermo Fisher Scientific), a structural analog of glutamate, to induce oxidative stress-induced cell death by blocking the X_C- transporter as previously described (Ratan et al., 1994b). Sodium selenite (Sigma Aldrich), dissolved in ddH₂O was applied to the media at varying concentrations. The time of addition of glutamate or HCA varied depending on experimental design; 24 hours after treatment with HCA, the cells were rinsed with warm PBS, and cell viability was assessed by MTT assay (Promega) or calcein-AM/ethidium homodimer-1 staining (Live/Dead assay, Thermo Fisher Scientific). Similarly, other known ferroptosis inducers, RSL3 (Cayman Chemical), FIN56 (Sigma Aldrich) or erastin (Selleck Chemicals) dissolved in DMSO, were used to induce cell death in primary cortical neurons and HT1080 cells (erastin only). A minimum of 3 independent cell culture experiments were performed with studies involving ferroptosis of cells *in vitro*.

In vitro model of excitotoxicity

Excitotoxicity was induced by glutamate (Sigma Aldrich) treatment in media at 100 μ M in HBSS buffer for 1 hour at 37°C, followed by a restoration of the media at 37°C for 24 hours. The glutamate receptor antagonist, MK801 (10 μ M; Sigma Aldrich) was used as a positive control and added immediately after glutamate treatment (similarly with Se treatment). Cell viability was assessed by MTT assay (Promega). Excitotoxicity studies were conducted on 3 independent cultures.

In vitro model of ER stress-induced death

Mouse primary cortical neurons were cultured as previously described. Thapsigargin (Sigma Aldrich) or Tunicamycin (Sigma Aldrich) were dissolved in DMSO to a stock concentration of 1mM. Final concentrations of 1 μ M of thapsigargin or 3 μ M of tunicamycin were added to immature primary cortical neurons 24 hours after they were plated and cell death was assessed (by MTT assay) 24 hours after thapsigargin or tunicamycin treatment. The non-selective caspase inhibitor, Z-VAD-FMK (0.01-100 μ M; Enzo Life Sciences) was added with ER stressors to verify that cell death was caspase dependent. ER stress studies were replicated in 4 independent cultures.

In vitro cell death time-lapse measurements

Mouse primary cortical neurons were cultured in glass bottom optically optimized plates. After 24 hours incubation cells were treated with erastin (5 μ M) or hemin (100 μ M) to induce ferroptosis. Imaging of individual neurons was performed sequentially over time. Prior to imaging, neurons were treated with ethidium homodimer to detect cells whose plasma membrane had been breached. Ethidium homodimer only fluoresces when it interacts with DNA. Neurons were maintained in a 37°C with 5% CO₂ chamber during imaging. Imaging was conducted on 4 independent cell cultures. Dead cells were imaged using a Zeiss LSM880 confocal microscope with a non-contact 10x/0.45NA objective using Zen Black/Blue software (Carl Zeiss). Each well was imaged at 3 locations every 30 minutes, for 16 hours. Cells were excited with a 561 nm laser, and Ethidium homodimer fluorescence was detected within a bandpass of 570 – 758 nm. The same laser line was also used to acquire Differential Interference Contrast (DIC) images on the transmitted light path, in order to capture the morphology of the cells over the imaging period. Imaging was conducted at Microscopy and Image Analysis Core of Weill Cornell Medicine.

Using ethidium homodimer as a cell death marker, blinded counting of cells were done at each time point and combined into a Kaplan Meier survival curve (ImageJ for counts and Graphpad Prism for curve). Curves were compared statistically using Log-Rank (Mantel-Cox test) to determine significant changes in survival.

Chromatin immunoprecipitation

The ChIP assays were performed with the EZ-Magna ChIP assay kit (Millipore) as per the manufacturer's instructions. For each condition 40 million cells were used and replicated in 4 independent cell cultures. Primary cortical cells were cross-linked with 1% PFA (in PBS) at 37°C for 7 minutes and then washed with glycine stop solution (125mM glycine in PBS) and PBS alone. Cells are scraped in a solution of ice cold PBS with protease inhibitors (Roche, 1 tablet/50ml) and phenylmethylsulfonyl fluoride (PMSF; 100mM; Sigma Aldrich). Samples are then sonicated using the Bioruptor (Diagenode) at 4°C for 30 seconds on and 30 seconds off for 1 hour. Genomic targets were immunoprecipitated with 5mg of rabbit Sp1 (Millipore), TFAP2c (Santa Cruz) or rabbit IgG (Santa Cruz, Sc-2027) antibody. Quantitation of immunoprecipitated genomic DNA regions was performed with real-time PCR using the SYBR Green Master Mix kit (QIAGEN) on a Quant 6 Real-Time PCR System (Applied Biosystems) with primers specific to the promoter region of GPX4 were:

Human: Forward 5'- CTGTACAGGGGTCAAAGTCCA-3' and Reverse 5'- CCCACATCTTGGCTTCCAAC-3'
Mouse: Forward 5'-CTGCTCTCCAGAGGCCTG-3' and Reverse 5'-GAGGTGTCCACCAGAGAAGC-3'.

Plasmid amplification

Agar plates were made by adding 1 packet of LB Broth with agar (Sigma Aldrich) to 500mL of ddH₂O and then sterilized by autoclave. After autoclaving, broth was allowed to cool to 55°C and 500 μ L of 50mg/mL carbenicillin was added (Sigma Aldrich). LB broth without agar (Sigma Aldrich; L7658) was prepared in a similar manner with the exception that it was divided in 250ml aliquots and stored in liquid form.

Plasmids from DNA were generated and amplified according to the following protocol. Approximately 4 μ L of plasmid DNA plus 50 μ L of competent cells (New England Biolabs or Invitrogen) were mixed on ice for 30 minutes, followed by heat shock at 42°C for 30 seconds, and then back to ice for 2 minutes. SOC medium (New England Biolabs) was added to the cells and shaken 37°C for 1 hour at 750 rpm. Under sterile conditions 5 μ L of carbenicillin (Sigma Aldrich) was added to the surface of the agar plates, followed by spreading of the competent cells with plasmid of interest (with ampicillin resistance). Plates were incubated overnight at 37°C and colonies collected the next day.

Colonies were mixed thoroughly in 5ml LB broth without agar (but with carbenicillin) for 1hr and then transferred to 250ml LB Broth (without agar) plus carbenicillin. LB Broth (without agar) was placed on a shaker at 200 rpm at 37°C overnight. Samples were centrifuged and 5 α E.coli cells were processed for maxiprep. For maxiprep, we followed the protocol described in Fast Ion Plasmid Maxi Kit (IBI Scientific). All plasmid amplification experiments were conducted under sterile conditions to avoid contamination.

Response Element Screening

To determine region of the promoter region required for regulation of GPX4 by ferroptotic stimuli with or without selenium exposure, a –1 to –4000bp promoter region of GPX4 was cloned in to the pGL3basic (Promega) luciferase backbone (Viraquest). Restriction enzyme sites were added as part of the sequence or added to the sequence roughly 1000 base pairs apart. Restriction enzymes were used (New England Biolabs; NdeI R0111S; BamHI R0136S; HindIII R0104s) to cut various sizes of the promoter region and then these varying sizes were ligated to the luciferase backbone in the pGL3basic vector (Figure S5A). The resulting promoter-reporter plasmids were incubated for 1 hour with NEBuffer (New England Biolabs) and specific restriction enzymes to cut at the site of interest. Samples were separated on electrophoresis gel and the sequence of interest (determined by predicted size) was extracted using Qiaquick gel extraction kit (QIAGEN), following the recommended protocol. The plasmid of interest was then blunted using blunting buffer, blunting enzyme and DNTP (New England Biolabs) and incubated for 15min followed by 10min inactivation at 70°C. The ends of the plasmid construct of interest was ligated using Quick T4 DNA ligase kit (New England Biolabs) and plasmid was amplified via maxiprep. Region –1763 to –1189bp of the GPX4 promoter was cloned in to pGL3basic backbone. At –1468 there is a XbaI restriction

enzyme site (NEB, R0145T). Mutations in promoter region were developed by synthesizing this region with G/C to A/T mutations in the binding region of binding site 1, 4, and 5; and then ligating that region to the luciferase. All sequences were verified by DNA sequencing either at Cornell University's sequencing core or at Viraquest, Inc.

Cell based luciferase Assays

HT22 neuroblasts were co-transfected using Lipofectamine 2000 kit (Life Technologies) as per the manufacturer's instructions, with GPX4 promoter-reporter sequences and a pTK-renilla plasmid (Promega) to control for transfection efficiency. Transfected cells were incubated for 24 hours prior to exposure to pharmacological or molecular manipulations. Control luciferase activity was measured using a pTK-PGL3 backbone construct. Luciferase activity was quantified after 12 hours of treatment (treatment procedures described earlier) using a dual luciferase assay kit (Promega) and bioluminometer (MDS Analytical Technologies). Each luciferase construct was experimentally examined in 4 independent, parallel cultures.

Use of adenovirus infection for modulating gene expression

Primary cortical neurons or HT22 were infected with adenovirus by replacing media with warm HBSS at a multiplicity of infection (MOI) of 60 for 1 hour. After infection, HBSS was replaced with warm media. Cells were examined for changes in gene expression 12 hours after transduction. Adenovirus vectors encoding a CMV promoter followed by ddGPX4, GPX4 alone (adGPX4), Sp1 (adSp1), mutant (mSp1), Catalase (CAT) or superoxide dismutase 2 (SOD2) genes were engineered by Viraquest, Inc. The mSp1 construct had 3 zinc finger DNA binding site deletions from the native Sp1 gene (Lee et al., 1997). Adenoviral TFAP2c (adTFAP2c) was engineered by the viral core at University of Iowa. ddGPX4 sequence contains a previously published destabilization domain (Iwamoto et al., 2010) bound to GPX4. ddGPX4 is stabilized in cells by applying Trimethoprim (TMP; Sigma Aldrich, dissolved in DMSO) to the bathing media.

siRNA to reduce levels of target genes

Molecular depletion of GPX4 was achieved using lipofectamine RNAiMax (Thermo Fisher Scientific) transfection of specific siRNAs against GPX4 into primary cortical neurons. Transfection was done via modifications of the RNAiMax protocol. Briefly, siRNA and RNAiMax lipofectamine were incubated in Opti-MEM (Thermo Fisher Scientific). The siRNA concentrations used for cortical neurons were 6-fold greater than what the industry protocol recommended, however, the lipofectamine concentration remained the same. Cells were treated with siRNA plus lipofectamine mixture for 12-24 hours before treatment or collection for verification of message reduction. Three distinct sequences of siRNAs were used independently to validate target specificity of effects (Thermo Fisher Scientific; GPX4 Exon 5,6; Exon 4; Exon 3). Sp1 siRNA was used to validate specificity of Sp1 antibody staining for immunofluorescence studies (Thermo Fisher Scientific). Scrambled siRNA was used as a control (Thermo Fisher Scientific). Molecular depletion was validated by both qPCR or immunoblot in 3 independent cultures. 50 μ M of N-acetyl-cysteine (NAC; Sigma Aldrich), which has no effect on steady-state GPX4 mRNA levels, was used to ensure survival of siGPX4 transfected cells so protein and mRNA could be collected. MTT and live/dead assays were also conducted in 3 independent cultures.

Protein extraction and immunoblotting

Whole Cell Protein Extraction

Prior to protein collection, primary cortical neuronal cultures were washed with 4°C PBS and collected in 4°C PBS. Cells were centrifuged at 1000xg and PBS was removed. Under cold conditions triton 1% Triton X-100 lysis buffer was added in the presence of the protease inhibitors (Sigma Aldrich), PMSF, MG132 (Sigma Aldrich), and sodium orthovanadate (Sigma Aldrich) according to the manufacturer's protocol. Cells were incubated for 10 minutes on ice, while also lightly shaken every 5 minutes. Cells were then centrifuged at 21,000 x g and supernatant containing soluble cell protein was used for immunoblotting.

Nuclear Extraction

Primary cortical neurons were collected in 4°C PBS and centrifuged as described in whole cell extraction. Cytoplasmic buffer (10mM HEPES, 10mM KCl, 2mM MgCl₂ and 0.1 mM EDTA in ddH₂O; all reagents from Sigma Aldrich) with protein degradation inhibitors was added to the cell pellet and incubated on ice for 20 minutes; with light tapping of the tube every 5 minutes. Then 10% of nonidet p40 substitute (Affymetrix) was added to the cytoplasmic buffer (25 μ l per 200 μ l of buffer) and incubated on ice for 5 minutes. Following incubation, samples were centrifuged at 4°C at 3000 x g for 5 minutes to separate cytoplasmic component from nuclei. Supernatant was then removed and pellet containing nuclei were lysed in nuclear buffer (50mM HEPES, 50mM KCl, 300mM MgCl₂, 0.1 mM EDTA and 10% glycerol by volume in ddH₂O) with protein degradation inhibitors. Samples were then rocked at 4°C for 30 minutes and then centrifuged at 10,000xg for 10 minutes. Supernatant was used for nuclear fraction.

Mitochondrial Extraction

Using the cytoplasmic supernatant collected from the nuclear extraction described earlier, supernatant was centrifuged at 12,500xg for 8 minutes at 4°C to obtain crude mitochondria (pellet) and cytoplasm (supernatant). Crude mitochondria was then resuspended in 3% Ficoll PM 400 (Sigma Aldrich), layered in to 6% Ficoll PM 400 (Lai and Clark, 1979) and centrifuged at 11,500xg for 30 minutes at 4°C. The pellet was suspended in isolation buffer (0.25M sucrose, 1mM EGTA, 10mM Tris-HCl, pH7.4) with protein degradation inhibitors and centrifuged at 11,500xg for 10 minutes at 4°C. Pellet was resuspended in small amount of resuspension buffer and this was used as pure mitochondria.

Immunoblotting

Protein concentrations of samples were quantified using Bradford (whole cell extraction; Bio-Rad Laboratories) or DC assay (fractions; Bio-Rad Laboratories). Protein samples were diluted in Laemmli buffer (Boston Bioproducts) and heated to 95°C for 5 minutes. All samples were electrophoresed under reducing conditions on NuPAGE Novex 4%–12% Bis-Tris polyacrylamide gels (Invitrogen) before being transferred onto a nitrocellulose membrane (Bio-Rad). Membranes were immersed in blocking media (LI-COR Odyssey blocking buffer) for 1 hour. Primary antibodies were treated overnight in blocking media (LI-COR Biosciences). The primary antibodies used in this study were the following: rabbit anti-GPX4 (1:1000, LSBio); rabbit anti-Sp1 (1:1000, EMD Millipore); mouse anti-TFAP2c (1:500, Santa Cruz); mouse TFAP2d (1:500, Abcam); rabbit TFAP2a (1:500, Cell Signaling Technology); rabbit histone H3 (1:1000, Cell Signaling Technology; mouse, cell signaling technology); mouse histone H4 (1:1000, Cell Signaling Technology); rabbit Cox IV (1:1000, Cell Signaling Technology); mouse anti-actin (1:10000, Sigma Aldrich), and rabbit anti-actin (1:10000, Sigma Aldrich). Secondary antibodies were mixed in blocking buffer and treated on membrane for 1 hour incubation at room temperature on a shaker. Secondary antibodies used in this study were IRDye-680 or IRDye-800 (LI-COR Biosciences; 1:10,000 dilution). All proteins were detected using an Odyssey infrared imaging system (LI-COR Biosciences). Densitometry was measured on Image Studio ver. 5.2 (LI-COR Biosciences). Samples for immunoblotting were obtained from > 3 independent animals or cell cultures.

RNA Sequencing and Weighted Gene Co-Expression Network Analysis

Library Preparation, Alignment and Quantification

Primary cortical neurons were collected following 6 hours of treatments with control (no treatment), 5mM HCA and/or 1μM Se from 4 independent cultures. Approximately 50–100μg of RNA was isolated from each sample using the miRNeasy kit with no modifications (QIAGEN). For each RNA sample, RNA quality was initially quantified using the RNA Integrity Number (RIN) on an Agilent Bioanalyzer (Agilent Genomics). We used rRNA depletion with the RiboZero Gold kit (Illumina) to prepare the library. RNA was depleted from 500ng total RNA with the Ribo-Zero Gold kit (Epicenter). Subsequent steps followed the Illumina Stranded TruSeq protocol to generate standard fragment sizes (100–300bp, mean 150bp). After this protocol was followed, libraries were quantified with the Quant-iT PicoGreen assay (Life Technologies) and validated on an Agilent 2200 TapeStation system. Libraries were prepared at the core facility at UCLA and sequenced on HiSeq 4000 platform. 100bp paired-end reads were mapped to mouse GRCm38 genome build using Gencode M10 (Ensembl v85) annotations using rna-STAR (Dobin et al., 2013). We used bias-aware quantification of genes and transcripts using Salmon (Patro et al., 2017). RNA-seq data generated in this study is available on NCBI GEO (GSE126787).

Differential Gene Expression

DGE expression analysis was performed with expression levels normalized for gene length, library size, and G+C content (referred to as ‘normalized FPKM’) using the CQN package in R. A linear model framework was used to assess differential expression in $\log_2[-\text{normalized FPKM}]$ values for each gene between the selenium/HCA treated and untreated samples accounting for RIN, RNA concentration and sequencing biases in each sample. Significant results are reported at FDR < 0.05.

WGCNA

The R package weighted gene co-expression network analysis (WGCNA) was used to construct co-expression networks using normalized data after adjustment to remove variability from technical covariates. We used the biweight midcorrelation to assess correlations between $\log_2[\text{adjusted FPKM}]$ and parameters for network analysis are previously described (Parikhshak et al., 2016). For supervised WGCNA, protein encoding transcripts of GPX4 were taken from Ensemble v85 and each transcript was compared between control and Se treated. Consensus networks were formed based on genes correlated with GPX4-001 transcript (mitochondrial transcript) at absolute correlation > 0.5. GO term enrichment analysis was performed using GO elite (v1.2.5; Zambon et al., 2012), with 10,000 permutation and results are presented as enrichment Z scores. We presented all the top molecular and biological functions for the supervised WGCNA.

Inductively coupled plasma mass spectrometry

Approximately 24 hours after Se and/or Hemin treatment *in vitro* (8 independent cultures per group) or ICH and/or Se injection *in vivo* (3 independent animals per group), primary neuronal cells or whole striatum were washed 3 times in PBS for optimal removal of the contaminating elements before acid digestion and inductively coupled plasma mass spectrometry (ICP-MS) analysis. A sample of 10% of the total cells were taken for protein quantification by Bradford assay (Bio-Rad Laboratories). The remaining sample was frozen at –80°C and sent to the University of Nebraska-Lincoln Spectroscopy core facility for ICP-MS. Samples were digested with 70% w/v nitric acid overnight and loaded onto a 96-well plate after 20-fold dilution with 2% nitric acid containing 50 ppb Ga as internal standard. The elemental analysis was carried out by ICP-MS with an Agilent Technologies ICP-MS 7500cx (Santa Clara, CA) coupled to an SC/DX-4 high-throughput autosampler (Elemental Scientific Inc., Omaha, NE). The SC-Fast sample introduction system was modified to allow analysis of 100μl samples by using a microperipump (MP-2) to push the carrier/chase solution (2% nitric acid)

A second microperipump (MP-1) was used to rinse the sample loop and load the samples onto the injection loop within 8–10 seconds. The instrument operated in Collision/reaction mode with a 3.5 ml/min flow of hydrogen gas and 1.5ml/min of helium gas for elimination of polyatomic and Ar derived interferences. The argon carrier flow was set at 0.9L/min and argon make-up flow at 0.15L/min, RF power of 1,500W, sample depth = 8mm. The analysis method was optimized for 18 elements (7Li, 11B, 23Na,

24Mg, 31P, 34S, 39K, 40Ca, 55Mn, 56Fe, 59Co, 60Ni, 63Cu, 66Zn, 75As, 78Se, 95Mo and 111Cd) also with 71Ga as the internal standard. Calibrations were performed prior to and after analyzing the samples. The instrument performance during the runs was verified by spiking a blank with 10% of the standard stock mix (QCS 10).

HIV-Tat Peptide Synthesis for Drug Delivery

Materials

Solvents for peptide synthesis were purchased from Fisher Scientific (Pittsburgh, PA). Fmoc-amino acids were purchased from RS Synthesis (Louisville, KY). 2-Chlorotrityl chloride resin SS (100-200 mesh) and 1-hydroxy-7-azabenzotriazole (HOAt) were purchased from Advanced ChemTech (Louisville, KY). Triisopropylsilane (98%) was purchased from Acros Organics (Pittsburgh, PA). *N,N'*-diisopropylcarbodiimide was purchased from Chem-Impex Int'l Inc. (Wood Dale, IL). 1-[Bis(dimethylamino)methylene]-1*H*-1,2,3-triazolo[4,5-*b*]pyridinium 3-oxid hexafluorophosphate (HATU) was purchased from Oakwood Chemical (N. Estill, SC). All other chemicals were purchased from either Sigma Aldrich (Milwaukee, WI) or Fisher Scientific (Pittsburgh, PA). Mass spectral analysis was performed on an Applied Biosystems QTrap 4000 hybrid triple-quadrupole/linear ion trap liquid chromatograph-mass spectrometer (SciEx, Framingham, MA).

Peptide Syntheses

Fmoc-Selenocysteine(pMeOBzl)-OH was synthesized as reported previously (Hondal and Raines, 2002) and used to synthesize the Sec-containing peptide: Gly-Arg-Lys-Lys-Arg-Arg-Gln-Arg-Arg-Arg-Pro-Gln-Sec-Lys-Sec-Asn-Leu-Asn (GRKKRRQRRRPQKUNLN). Fmoc-amino acids were used to synthesize the following control peptide: Gly-Arg-Lys-Lys-Arg-Arg-Gln-Arg-Arg-Arg-Pro-Gln (GRKKRRQRRRPQ). Both peptides were synthesized using solid-phase synthesis as described below. Peptides were synthesized on a 0.1 mmol scale using a glass vessel that was shaken with a model 75 Burrell wrist action shaker. Each batch used 300 mg of 2-chlorotrityl chloride resin SS (100-200 mesh, AdvancedChemtech). The first amino acid in the sequence was added directly to the resin via shaking for 1 hour at room temp in 10 mL of 2% *N*-methylmorpholine and 98% dichloromethane. Unreacted resin was successively capped using methanol; 10 mL of 80% dichloromethane/10% methanol/10% *N*-methylmorpholine, shaken 15 minutes at room temperature. Subsequent amino acid couplings were performed using a 2-fold excess of both Fmoc-amino acid and HOAt, and 2% v/v *N*-methylmorpholine (for all amino acids except Sec), or 2-fold excess of both Fmoc-Sec(pMeOBzl)-OH and HATU, and 1% v/v *N,N'*-diisopropylcarbodiimide (for Sec only), in 10 mL of dichloromethane or dimethylformamide (DMF) solvent. Preactivation of the amino acid was not performed to minimize the racemization of L-selenocysteine. These coupling conditions are essentially the same as those of Barany and co-workers, which were likewise used to minimize racemization of cysteine (Han et al., 1997). Couplings were deemed complete by ninhydrin testing after allowing the reaction to proceed for 1 hour. Removal of the Fmoc group between couplings was achieved via two 10 min agitations with a 20% piperidine/80% DMF mixture, fully covering the resin and rinsing between each deblocking step four times with DMF. Success of deblocking was monitored qualitatively using a ninhydrin test (Kaiser et al., 1970). Removal of the final Fmoc protecting group completed the peptide synthesis.

Cleavage of the peptides from resin, along with deprotection of the side chain protecting groups, was done via a 2 hour reaction using a cleavage cocktail consisting of a 96% trifluoroacetic acid (TFA)/2% triisopropylsilane/2% water mixture (Harris et al., 2007; Schroll et al., 2012). For the selenocysteine containing peptide, 0.4 mmol 2,2'-Dithiobis(5-nitropyridine) (DTNP) was included in the cleavage cocktail. This reaction mixture with DTNP removes the pMeOBzl protecting group from selenocysteine, replacing it with 5-nitropyridine (Harris et al., 2007; Schroll et al., 2012). Following cleavage and deprotection, the resin was washed with TFA and DCM to remove any additional peptide, after which the volume of the cleavage solution was reduced by evaporation with nitrogen gas. The cleavage filtrate was then pipetted into cold, anhydrous diethyl ether, where the peptides were observed to precipitate. Centrifugation at 3000rpm on a clinical centrifuge (International Equipment Co., Boston, MA) for 10 minute pelleted the peptide, which was followed by two additional wash-precipitation cycles using TFA to dissolve the pellet and diethyl ether for precipitation. Peptides were then dissolved in a minimal amount of water and lyophilized. Stock solutions of peptides were dissolved in ddH₂O and applied to media *in vitro* or given via intraperitoneal injection *in vivo*.

Tat Cys synthesis

Tat Cys (GRKKRRQRRRPQCKCNLN) was synthesized by Bachem.

Analysis by Mass Spectrometry

Peptides were directly infused with a guard column at 10 μ L /min into a 100 μ L /min mobile phase flow consisting of 50/50 water/ acetonitrile with 0.1% formic acid. The mobile phase flow was introduced into an Applied Biosystems QTrap 4000 hybrid triple-quadrupole/linear ion trap liquid chromatograph-mass spectrometer operating in positive ESI mode. Mass spectra were collected in linear ion trap mode, scanning from *m/z* 200–1500.

QUANTIFICATION AND STATISTICAL ANALYSIS

Data in figure legends are presented as mean \pm SEM values. The exact value of the sample size (*n*) are given in each figure legends and represents either the number of animals used *in vivo* or the number of cell clones/numbers of separate cultures used *in vitro*. In cell viability (MTT assay) experiments each replicate (*n* value in figure legends represent each replicate) was done in 3 wells (of a 96 well plate) for the purposes of reproducibility and lowering variation. Power calculations for experiments were conducted using G*Power Calculator (University of Dusseldorf). GraphPad Prism 6 and Microsoft excel 2016 were used for all statistical

analyses. We evaluated normality by Kolmogorov-Smirnov test and variance by homogeneity using Levene test. For normally distributed data with homogeneous variance, we used Student's t test if 2 groups were compared or one-way analysis of variance (ANOVA) followed by bonferroni posthoc test if two independent variables were compared. For not normally distributed results and or non-homogeneous variance, we used the Kruskal-Wallis test followed by Dunns post hoc test.

DATA AND SOFTWARE AVAILABILITY

RNA-sequencing data are available under Gene Expression Omnibus ID GEO: GSE126787 (<https://www.ncbi.nlm.nih.gov/geo/query/acc.cgi?acc=GSE126787>). Unaltered immunoblots, complete WGCNA, differential gene expression, synchronized cell death videos, siRNA data, additional TUNEL staining, Z-VAD-FMK data and scatterplots for all behavioral data are available at Mendeley data repository <https://doi.org/10.17632/2jsgwzh3zz.1> (<https://doi.org/10.17632/2jsgwzh3zz.1>).

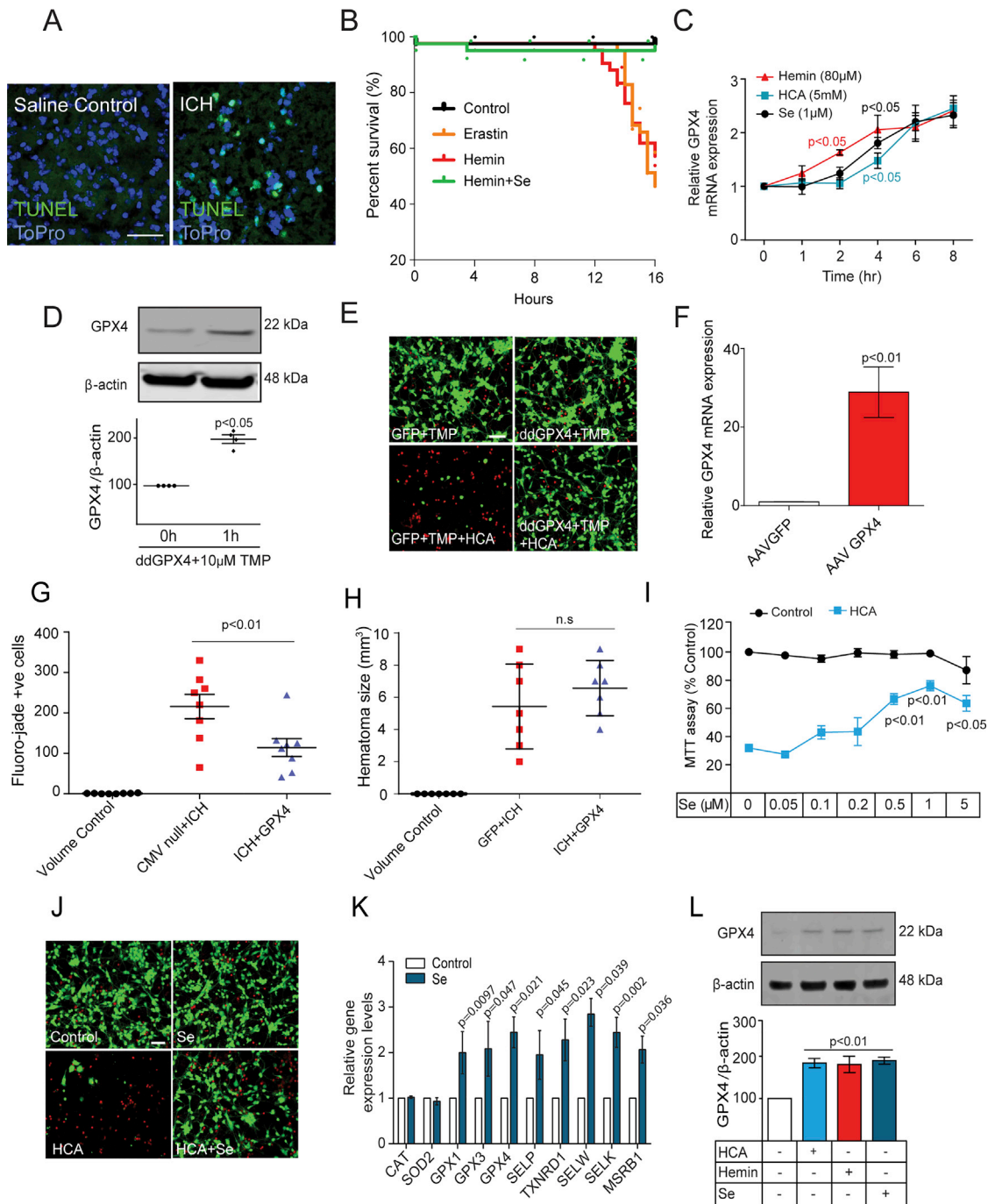


Figure S1. Forced Expression of GPX4 or Addition of Se Protects Neurons from Ferroptotic Stressors, Related to Figures 1 and 2

(A) ICH modeling *in vivo* shows TUNEL labeling, one feature of ferroptosis. TUNEL staining (green) of brain section from a mouse 7 days after collagenase injection into the striatum (ICH model). Insert shows ToPro (blue) and/or TUNEL positive cells (green). Scale bar 50μm.

(B) Kaplan-Meier curve of individual neuron death up to 16 h following hemin or erastin treatment, which both induce ferroptosis *in vitro* (n = 4; Mantel-Cox test; p < 0.05).

(C) Time course of changes in GPX4 mRNA expression (measured by qPCR) in cortical neurons following exposure to Hemin (80μM), HCA (5mM) or Se (1μM). P values indicate the time when GPX4 mRNA is significantly increased (n = 3; p < 0.05; t test; data shown as mean ± SEM).

(D and E) Validation that ddGPX4 levels can be stabilized by varying concentrations of trimethoprim, which neutralizes the destabilization domain. Increased ddGPX4 protein levels can protect neurons from HCA-induced ferroptosis. (D) Quantification of GPX4 protein levels as measured by immunoblot in neurons infected with the adenovirus encoding ddGPX4 1h after TMP (10μM) treatment (n = 4; p < 0.05; t test; mean ± SEM). (E) Live(green)/Dead (red) imaging of GFP (control) or (ddGPX4) treated with TMP (10μM) following exposure to 5mM HCA (n = 3). Scale bar, 50μm.

(legend continued on next page)

(F) GPX4 message can be increased in striatum by using an AAV8 encoding GPX4 under the control of the synapsin 1 promoter. Relative GPX4 mRNA expression from qPCR of mouse striatum collected 14 days after transduction with AAV8-synapsin-GFP or AAV8-synapsin-GPX4 (n = 4; p < 0.01; t test; mean ± SEM).

(G) Forced expression of GPX4 *in vivo* decreases degenerating neurons following ICH. Quantification of number of Fluoro-jade positive cells in or near the hematoma at 14 days post ICH in mice infected with AAV8-synapsin-GFP or AAV8-synapsin-GPX4. Expression was driven selectively in neurons via a portion of the synapsin promoter encoded in AAV8 (n = 12; p < 0.01; t test; mean ± SEM).

(H) Forced expression of GPX4 *in vivo* has no effect on hematoma size. Quantitation of hematoma size 24 hours after ICH in mice infected with AAV8 GFP or GPX4 in the striatum reveals that GPX4 does not inhibit collagenase activity (n = 7; p > 0.05; t test; mean ± SEM).

(I and J) Selenium (Se) protects against HCA-induced ferroptosis in primary cortical neurons. (I) Viability measured by MTT reduction 24h following exposure to 5mM HCA and varying concentrations of Se (n = 8; p < 0.05; t test; mean ± SEM). (J) Live(green)/dead (red) assay of primary cortical neurons following 24h HCA (5mM) treatment ± 1μM Se (n = 3). Scale bar, 50μm.

(K and L) Se increases selenoprotein mRNA expression and GPX4 expression in primary cortical neurons. (K) qPCR measurements of mRNAs for select selenoproteins from neurons treated ± Se (1μM) for 6h (n = 4; p < 0.05; t test; mean ± SEM). (L) Immunoblot of GPX4 protein following 8h HCA (5mM), hemin (80μM) or Se (1μM) treatment (n = 3; p < 0.05; ANOVA; mean ± SEM).

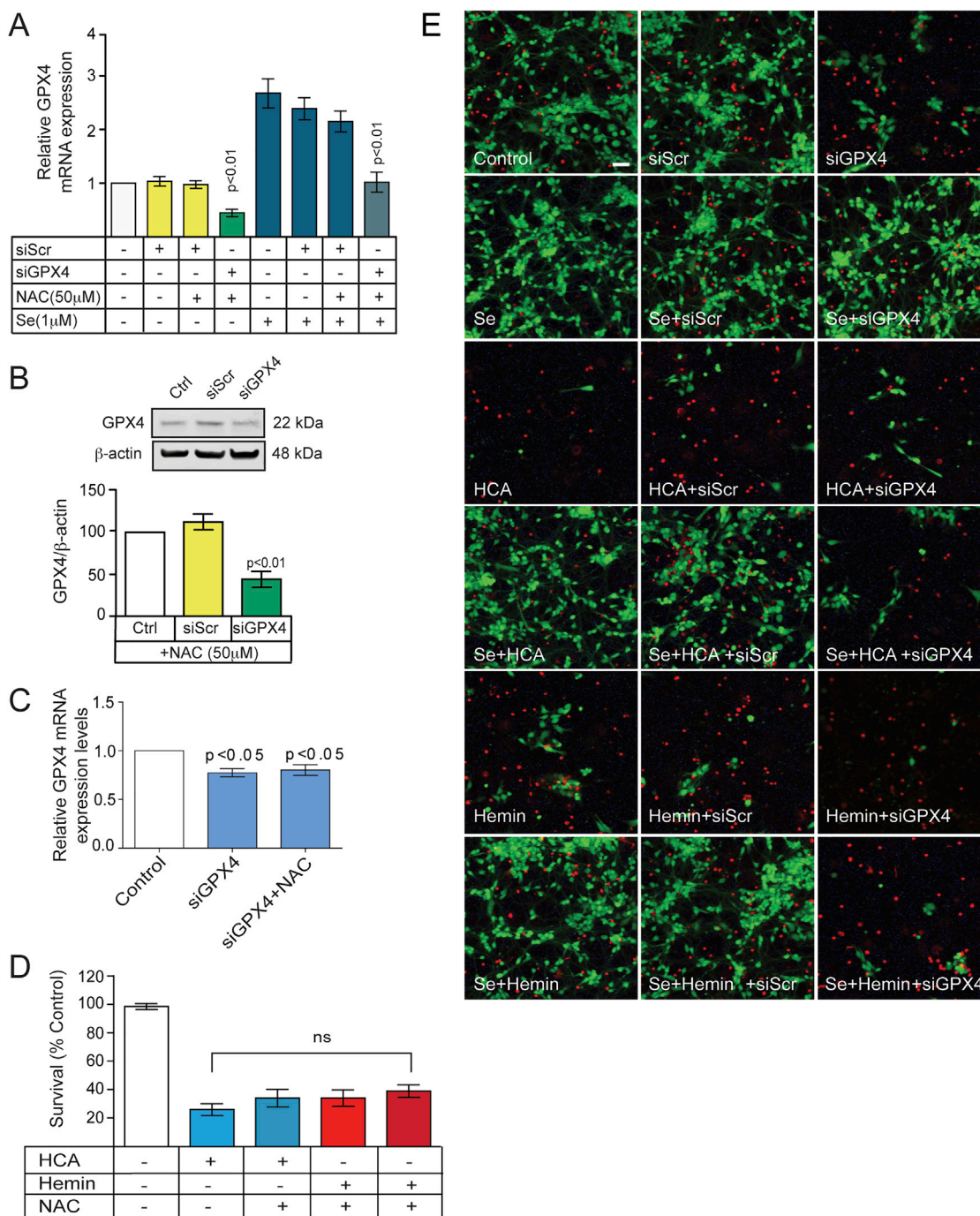


Figure S2. Molecular Depletion of GPX4 (via siRNA Targeting exon 3) Inhibits Se-Dependent Protection following HCA or hemin Treatment, Both of which Lead to Cell Death with Features of Ferroptosis, and These Results Demonstrate that GPX4 Is Required for Se-Dependent Protection against Cell Death, Related to Figure 2

(A and B) Validation of GPX4 siRNA. Short interfering RNAs were used to deplete GPX4 mRNA (siGPX4, measured by qPCR; $n = 4$; $p < 0.01$; ANOVA; mean \pm SEM) and protein (immunoblot, $n = 3$; $p < 0.01$; ANOVA; mean \pm SEM). siScr represents control scrambled siRNA. Cells were exposed to 50 μ M NAC which prevents steady-state cell death due to GPX4 reduction, but does not affect susceptibility to HCA or hemin-induced death. Data for additional targeted exons shared on Mendeley data repository <https://doi.org/10.17632/2jsgwzh3zz.1>

(C) NAC (50 μ M) does not interfere with siGPX4 (exon 3). Relative GPX4 mRNA expression (measured by qPCR) at 8 hours following Si GPX4 ($n = 3$; $p < 0.01$; ANOVA; mean \pm SEM).

(legend continued on next page)

(D) NAC (50 μ M) blocks steady state cell death but does not protect against ferroptosis. Viability (MTT assay) of neurons treated with NAC (50 μ M) HCA (5mM) or Hemin (80 μ M) for 24 and 16h, respectively (n = 3; p > 0.05; ANOVA; mean \pm SEM).

(E) Live (green)/dead (red) assay of primary cortical neurons showed that Se-induced protection from hemin (80 μ M) or HCA (5mM)-induced death was abrogated by reduction in GPX4 levels. Scale bar = 50 μ m (n = 3 independent cultures). siRNA to GPX4 targets sequences in exon 3.

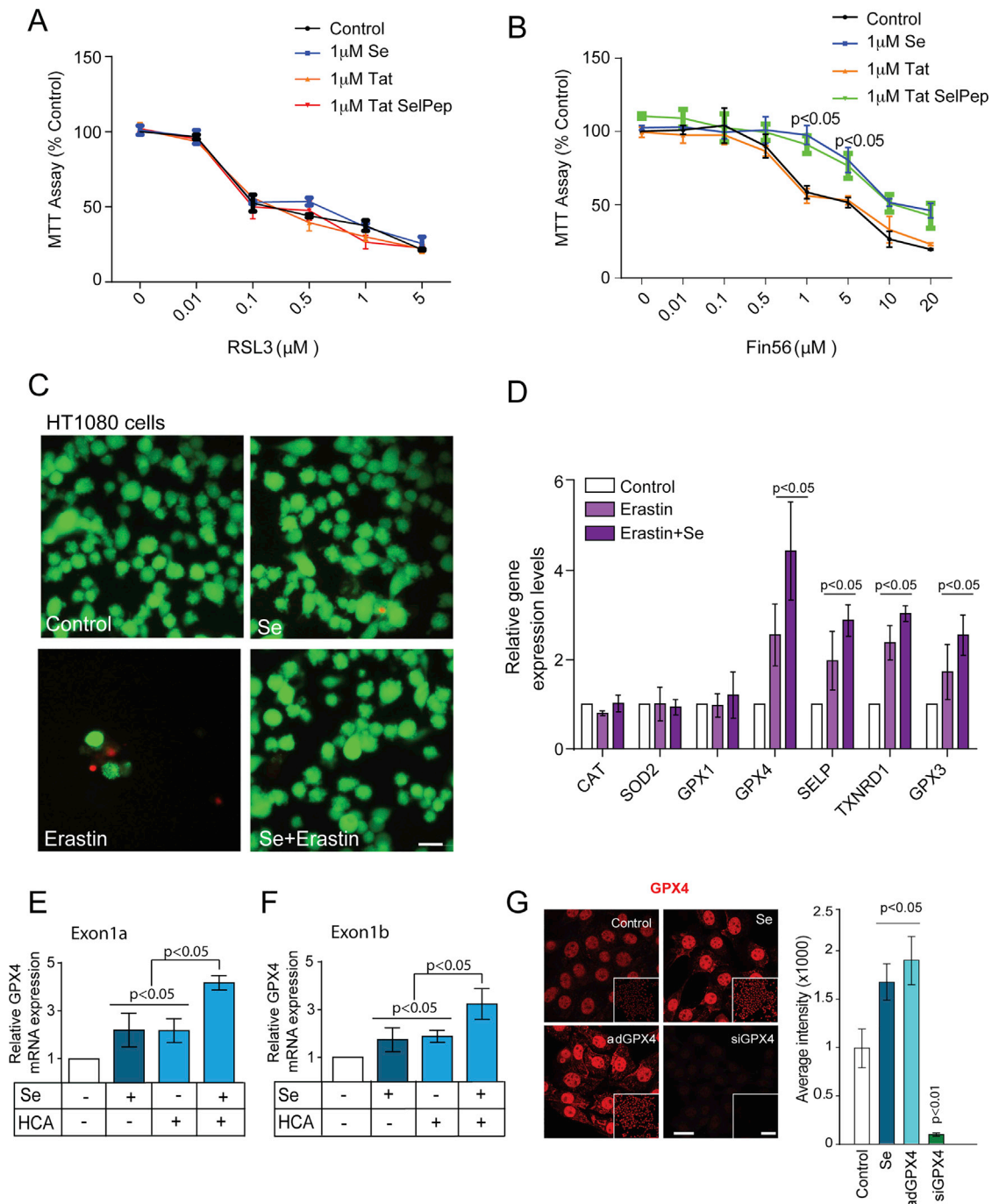


Figure S3. Selenium Does Not Protect against GPX4 Inhibitor RSL3 but Does Protect against FIN56, which Targets GPX4 or Squalene Synthetase (related to Figure 2), and Se Drives Transcription of GPX4 in HT1080 Cancer Cells and Protects against Erastin-Induced Ferroptosis, Related to Figure 3

(A) Selenium fails to protect against GPX4 inhibitor RSL3. Viability measured in cortical neurons (by MTT reduction) with various concentrations of the GPX4 inhibitor, RSL3 (0-5 μ M), with Se (1 μ M), Tat (1 μ M) or Tat SelPep (1 μ M; $n = 3$; $p > 0.05$; ANOVA; mean \pm SEM).

(B) Selenium protects against FIN56, an inhibitor of squalene synthetase and GPX4 activity. Viability (MTT assay) measured in cortical neurons (MTT reduction) of various concentrations of ferroptosis inducer Fin56 (0-5 μ M), treated with Se (1 μ M), Tat (1 μ M) or Tat SelPep. Se/Tat SelPep can protect between 1-5 μ M of FIN56 ($n = 3$; $p < 0.05$; ANOVA; mean \pm SEM).

(C) Live(green)/Dead(red) assay of fibrosarcoma cell line (HT1080) treated 24h with erastin (1 μ M) with or without Se (1 μ M; $n = 3$ independent cultures). Scale bar, 20 μ m.

(legend continued on next page)

(D) Levels of a spectrum of mRNAs for putative antioxidant enzymes (measured by qPCR) in neurons following 6h treatment with vehicle or erastin (5 μ M) with or without Se (1 μ M; n = 3; p < 0.05; ANOVA; mean \pm SEM).

(E and F) Selenium plus HCA or selenium plus hemin increases message of mitochondrial and nuclear isoforms of GPX4. Levels of GPX4 transcript including exon 1a (containing a mitochondrial targeting sequence) or exon 1b (containing nuclear targeting sequence) of GPX4 (qPCR) following 6h treatment of HCA (5mM) with or without Se (1 μ M; n = 3; p < 0.05; ANOVA; mean \pm SEM).

(G) GPX4 expression in cells is highest in the nucleus and the perinuclear area. Immunofluorescence of GPX4 protein (red) following 8 hours of vehicle, Se (1 μ M), 24h adenoviral GPX4 (ad; 50 MOI) or 24h GPX4 siRNA + Nac (50 μ M) treated HT22 cells. Scale bar, 25 μ m; inset, 200 μ m (n = 3 independent cultures). Graph depicts quantitation of fluorescence (n = 100 cells; p < 0.05; ANOVA; mean \pm SEM).

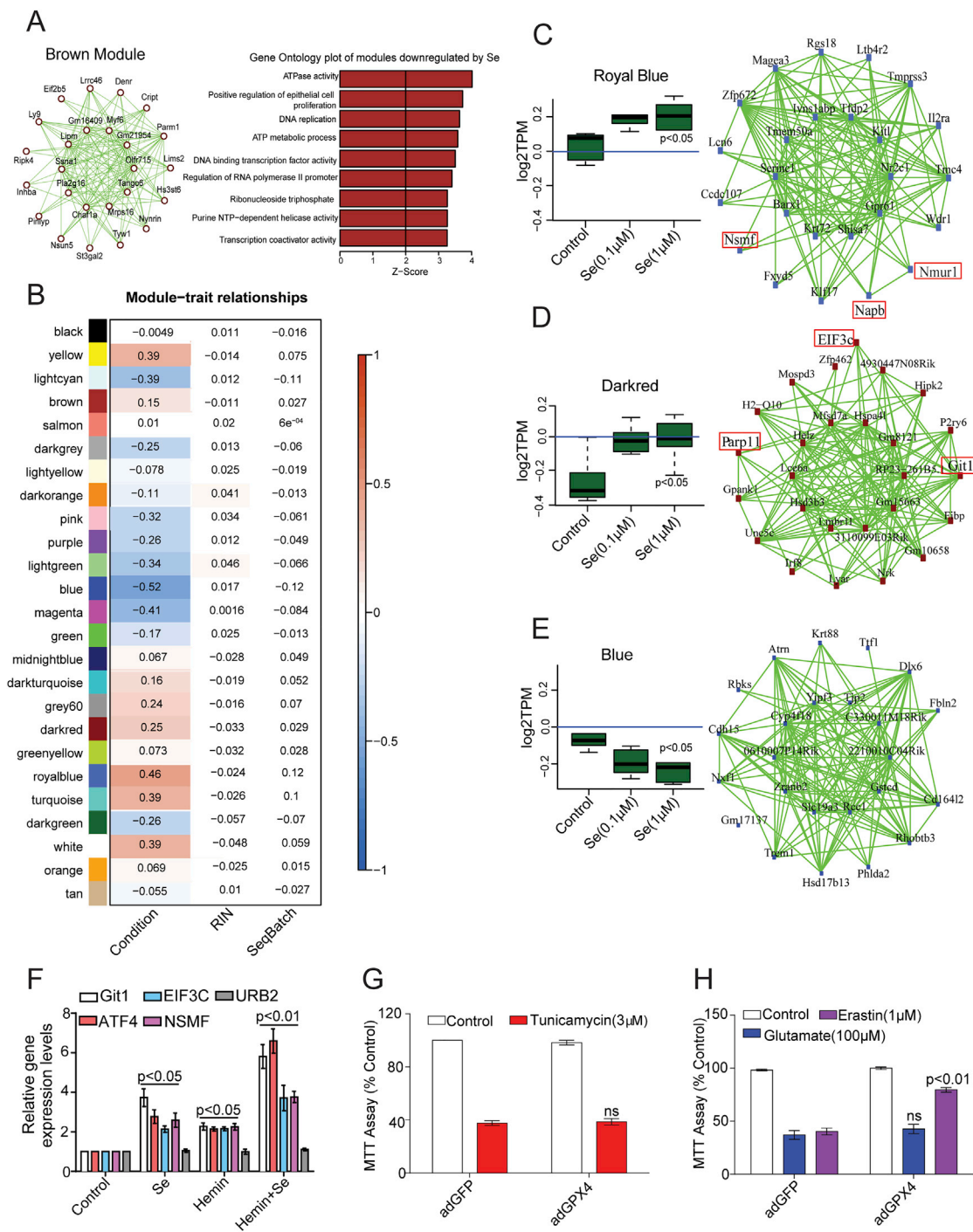


Figure S4. Se Induces a Broad Transcriptional Response Leading to GPX4-Independent Protection from ER Stress-Induced Apoptosis or Excitotoxicity, Related to Figure 3

(A) Hub genes in brown module from unsupervised WGCNA analysis, which was most downregulated by Se from supervised WGCNA analysis. (B) Heatmap of module eigengene-traits upregulated and downregulated by 6h Se treatment in cortical neurons based on unsupervised WGCNA analysis. (C-F) Modules significantly upregulated and downregulated used to identify genes involved in ER stress and excitotoxicity. (C-D) Module eigengene and networks significantly upregulated by Se (Royal Blue and Dark Red) based on unsupervised WGCNA. Genes linked to protection from ER stress (apoptosis) or excitotoxicity highlighted in red ($n = 4$). (E) Module eigengene and network (Blue) are significantly downregulated by Se ($n = 4$). (F) qPCR validation of genes potentially involved in ferroptosis, excitotoxicity and ER stress (apoptosis) that are upregulated by 6h Se ($1\mu\text{M}$) in primary cortical neurons ($n = 4$; $p < 0.05$; t test; mean \pm SEM). URB2 is negative control.

(legend continued on next page)

(G and H) Forced expression of GPX4 fails to protect against ER stress or excitotoxicity. (C) Survival (MTT) assay of immature primary cortical neurons (2 DIV) overexpressing GFP (control) or GPX4 via adenoviral transduction following 16h of tunicamycin (3 μ M; ER stress) treatment (n = 4; p > 0.05; t test; mean \pm SEM). (D) Survival (MTT) assay of mature cortical neurons (13 DIV) infected with adenovirus encoding GFP (control) or GPX4 following 24h of glutamate (100 μ M; excitotoxicity) or erastin (1 μ M; ferroptosis) treatment (n = 4 p > 0.05 for glutamate, p < 0.01 for erastin; t test; mean \pm SEM).

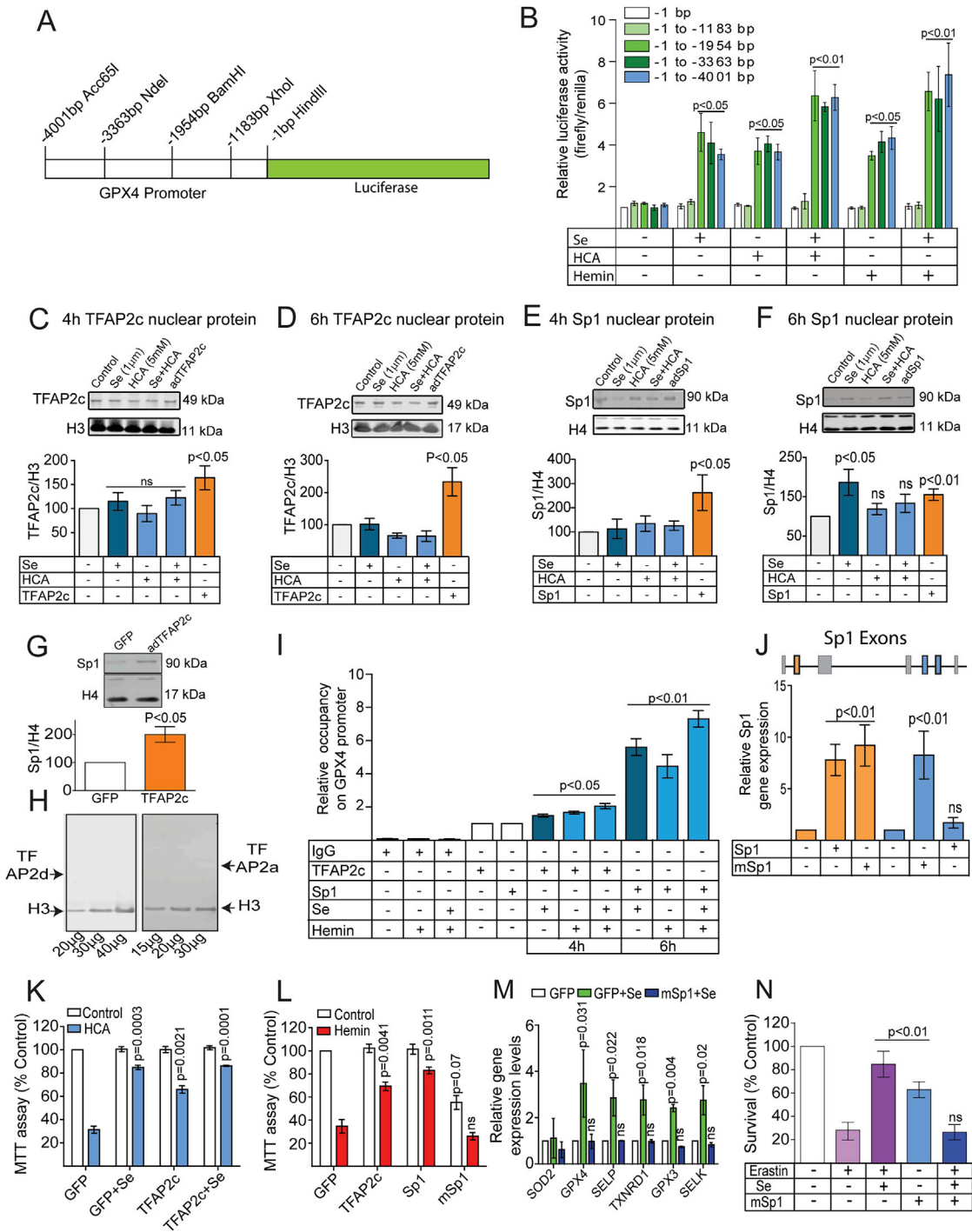


Figure S5. Se Induces a Transcriptional Response Mediated by TFAP2c and Sp1 to Regulate GPX4, Related to Figure 4

(A and B) Unbiased identification of transcription factors controlling GPX4. (A) Restriction enzyme sites for GPX4 promoter-reporter constructs. (B) Luciferase activity from distinct promoter-reporter constructs of the GPX4 gene following 6h of HCA (5mM) or Hemin (80µM) with or without Se (1µM) treatment (n = 5; p < 0.05; ANOVA; mean ± SEM).

(C–F) Immunoblot of Sp1 and TFAP2c from nuclear extracts of primary cortical neurons at 4h and 6h post HCA (5mM) and/or Se (1µM; n = 4; ANOVA; mean ± SEM) exposure. Infection of cortical neurons with an adenovirus encoding TFAP2c or Sp1 for 24 hours was used as positive control.

(G) TFAP2c overexpression increases protein levels of Sp1 in the nuclear fraction of a population of cortical neurons. Immunoblot of Sp1 expression in nuclear extracts from cortical neurons 24h after adenoviral overexpression of GFP or TFAP2c (n = 3; p < 0.05; t test; mean ± SEM).

(legend continued on next page)

(H) TFAP2 isoforms (a,b,d) are not expressed in neurons. Immunoblot to verify absence of expression of TFAP2a or TFAP2d over a wide dynamic range of protein loading in neurons. Arrows point to expected migration site for these isoforms, which cannot be detected at protein level (n = 3).

(I) Chromatin Immunoprecipitation (ChIP) using an antibody to TFAP2c or Sp1 to monitor occupancy at the GPX4 promoter after exposure to hemin (80 μ M) with or without Se (1 μ M) treatment (n = 3; p < 0.05; ANOVA; mean \pm SEM).

(J) Validation of expression of Sp1 or DNA binding mutant of Sp1 (mSp1; lacking DNA binding domain in exon 5) (measured by qPCR, n = 4; p < 0.05; ANOVA; mean \pm SEM).

(K and L) TFAP2c or Sp1 overexpression protects against HCA or hemin toxicity. (K) Viability (MTT assay) in neurons with forced expression of TFAP2c following 24h HCA (5mM) treatment (n = 4; p < 0.05; t test; mean \pm SEM). (L) Viability (MTT assay) of neurons with forced expression of TFAP2c, Sp1 or mSp1 following 16h of hemin (80 μ M) exposure (n = 4; p < 0.05; t test; mean \pm SEM).

(M) RNA levels of putative antioxidant genes from cortical neurons (measured by qPCR) with forced expression of GFP or mSp1 following 6h Se (1 μ M) treatment (n = 3; ANOVA; mean \pm SEM).

(N) Viability (measured by MTT assay) 24h after erastin (5 μ M) exposure with or without Se (1 μ M) treatment in neurons with forced expression of GFP (Control) or mSp1 (n = 4; p < 0.01; ANOVA; mean \pm SEM).

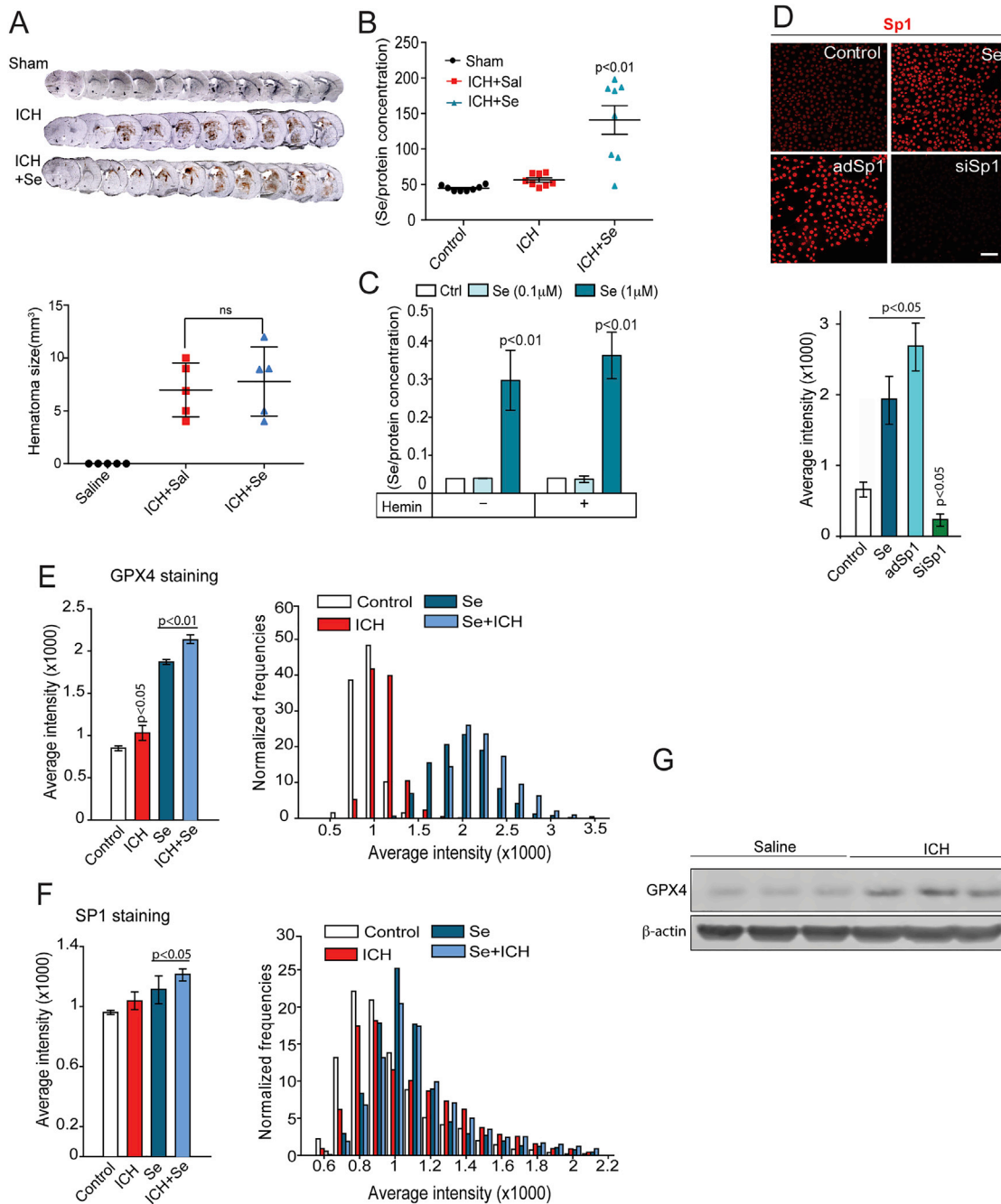


Figure S6. ICV Injection of Se Improves Recovery following Brain Hemorrhage without Inhibiting Collagenase Activity and Initial Hematoma Size, Related to Figure 5

(A) ICV injection of Se does not influence the size of the hematoma induced by collagenase injection. Light microscopy of brain sections 24h following ICH with or without Se (2.5μM; top) and (bottom) quantification of hematoma size (n = 5; p > 0.01; ANOVA; mean ± SEM).

(B and C) ICH does not reduce steady-state selenium levels. (B) ICP-MS measurements of selenium levels in saline volume control or ICH mice with or without 2.5μM Se injection in striatum 24 hours following injury onset (n = 8; p < 0.01; ANOVA; mean ± SEM). (C) ICP-MS measurements of selenium levels normalized to protein concentration in cortical neurons treated with or without 80μM hemin and/or Se (n = 3; p < 0.01; ANOVA; mean ± SEM).

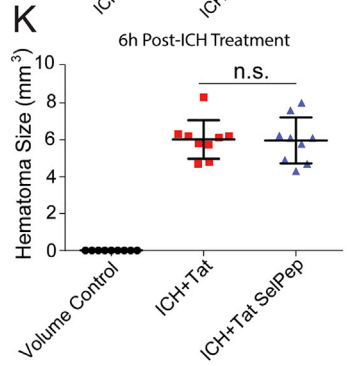
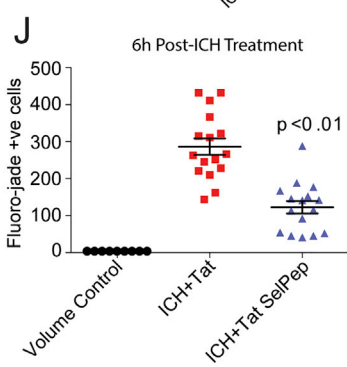
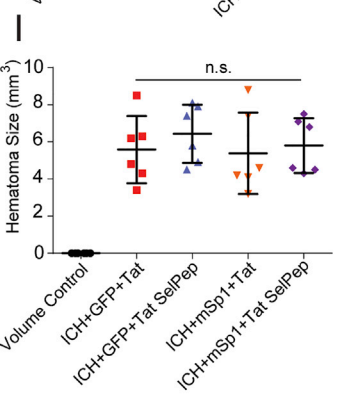
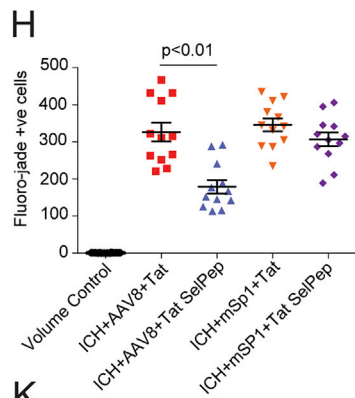
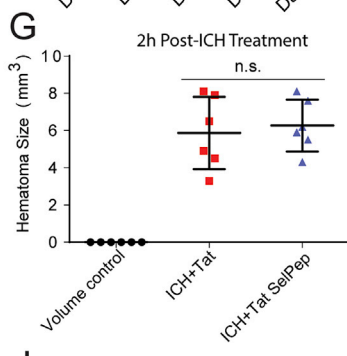
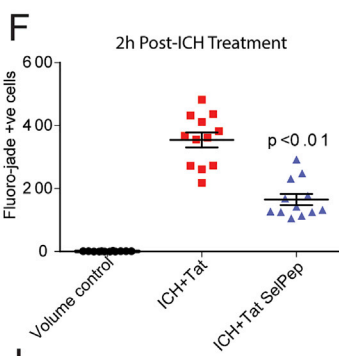
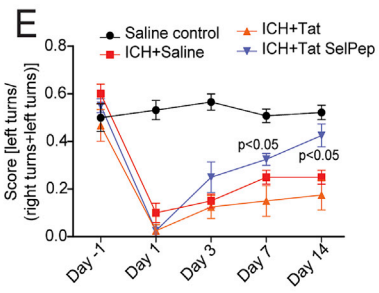
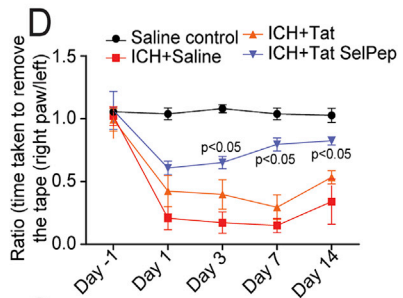
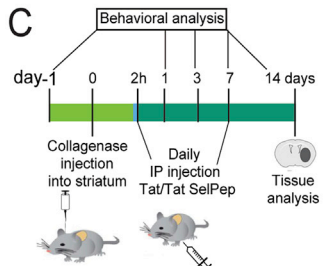
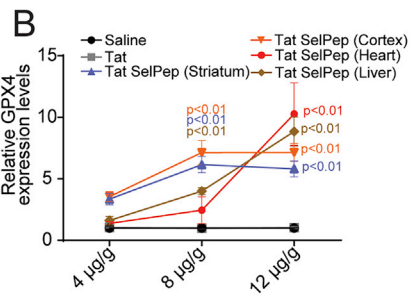
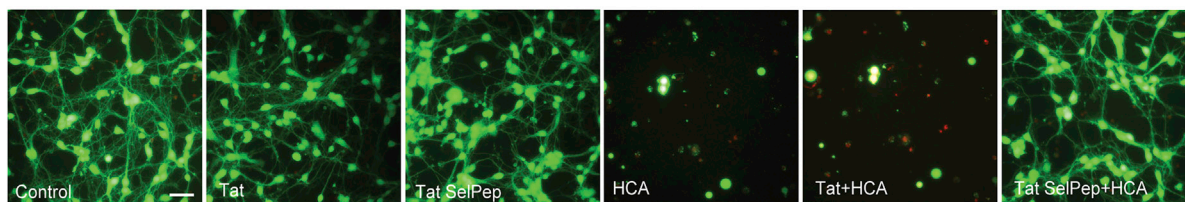
(D) Validation of Sp1 antibody for immunofluorescence studies (red) in HTT22 cells; vehicle, 6h Se treated, infected with adenovirus encoding Sp1 or exposed for 24h with Sp1 siRNA (n = 3 independent cultures). Scale bar, 100μm. Quantified immunofluorescence intensity shown in panel below (n = 100 cells; p < 0.01; ANOVA; mean ± SEM).

(E and F) Quantification of changes in GPX4 and Sp1 in neurons after ICH *in vivo* in the presence and absence of selenium. (E) Quantification of GPX4 immunofluorescence intensity in slices from mouse brain 7 days post ICH with or without Se (2.5μM) ICV injection (left panel). Binned normalized frequency of

(legend continued on next page)

distribution of neurons based on intensity level (right panel; $n = 3$ animals & 100 neurons; $p < 0.01$; ANOVA; mean \pm SEM). (F) Quantitation of Sp1 immunofluorescence intensity in neurons (excluding Sp1 expression in non-neuronal cells) from slices of mouse brain 7 days post ICH with or without Se ($2.5\mu\text{M}$) ICV injection (left panel) and binned normalized frequency of neurons expressing Sp1 (right panel; $n = 3$ animals & 100 neurons; $p < 0.01$; ANOVA; mean \pm SEM). (G) GPX4 protein is induced following ICH. Immunoblots from brain lysates of animals injected with vehicle control or collagenase into the striatum. Striatal lysates were collected 24h after ICH ($n = 3$).

A



(legend on next page)

Figure S7. Systemic Injection of Tat SelPep Is Sp1 Dependent and Has a Therapeutic Window of 6 h, Related to Figure 6

(A) Live(green)/Dead (red) assay of primary cortical neurons following HCA (5mM) treatment with or without 1 μ M Tat SelPep (n = 3 independent cultures). Scale bar, 75 μ m.

(B) Systemic injection of Tat SelPep increases GPX4 message in multiple organs. Striatum (Brain), cortex (Brain), heart or liver GPX4 mRNA (measured by qPCR) 24h following IP injection of Tat SelPep (4-12 μ g/g; n = 5; p < 0.01; t test; mean \pm SEM).

(C–G) Tat SelPep improves outcomes when given systemically 2h after ICH. (C) Collagenase-induced ICH followed at 2h by intraperitoneal injection of Tat (12 μ g/g) or Tat SelPep (12 μ g/g) and then every day for 7 days post injury. Saline volume control was also injected in a group instead of collagenase. Behavioral measurements were made prior to and 1, 3, 7 and 14 days after hemorrhagic stroke and tissue was collected and processed at 14 days for analysis. (D–E) Tat SelPep, but not Tat alone reduced sensory neglect (D; n = 16; p < 0.05; ANOVA; mean \pm SEM) and spatial neglect (E; n = 16; ; p < 0.01; ANOVA; mean \pm SEM). (F–G) Tat SelPep reduces number of degenerating neurons when given 2h post ICH with no effect on hematoma size. (F) Quantification of Fluoro-jade positive cells near hematoma at 14 days post ICH in mice given intraperitoneal injections of Tat or Tat SelPep 2 hour post injury, followed by daily injections for 7 days (12 μ g/g; n = 12; p < 0.01; ANOVA; mean \pm SEM). (G) Quantification of hematoma size 24 hours after ICH, with Tat or Tat SelPep given 2 hours after ICH (n = 6; p > 0.05; ANOVA; mean \pm SEM).

(H and I) Tat SelPep protection given systemically 2 hours post ICH is Sp1-dependent. (H) Quantification of fluoro-jade positive cells near hematoma at 14 days post ICH in mice given daily injections of Tat or Tat SelPep with overexpression of mSp1 or CMV Null in striatum by AAV8 transduction (12 μ g/g; n = 12; p < 0.01; ANOVA; mean \pm SEM). (I) Quantitation of hematoma size 24h after ICH in mice overexpressing GFP or mSp1 in striatum and given IP injection of Tat or Tat SelPep (12 μ g/g) 2h after ICH (n = 6; p > 0.05; ANOVA; mean \pm SEM).

(J and K) Tat SelPep given systemically up to 6h ICH reduces number of degenerating neurons. (J) Quantification of fluoro-jade positive cells near hematoma at 14 days post ICH in mice given intraperitoneal injections of Tat or Tat SelPep 6h post injury, followed by daily injections for 7 days (12 μ g/g; n = 16; p < 0.01; ANOVA; mean \pm SEM). (K) Quantitation of hematoma size 24h after ICH in mice given IP injection of Tat or Tat SelPep 6h after ICH (n = 9; p > 0.05; ANOVA; mean \pm SEM).